EVANESCENT FIELD COUPLING THEORY OF A D– FIBRE

A Thesis

submitted to the Faculty of Engineering

of the University of Glasgow

for the degree of

Master of Science in Electronics

by

Mélanie Lydie Marie Pralong,

DIPL. EPFL

January, 1989.

ProQuest LLC.
789 East Eisenhower Parkway
P.O. Box 1346
Ann Arbor, MI 48106 – 1346

A Mary et Patrick,

A ma famille.

ACKNOWLEDGEMENTS

I would like to acknowledge Professor Lamb, Head of the Department of Electronics and Electrical Engineering at Glasgow University. Sincere thanks go to my supervisor Dr. J. Arnold, Senior Lecturer, for proposing the research topic and for his invaluable and resourceful suggestions.

I am also grateful to the Royal Society and the British Council, whose scholarship enabled me to study at Glasgow University. It is hoped that more British and Swiss students will benefit from the exchange program funded by the Royal Society and the Fonds National Suisse.

I am also indebted to the computing staff, in particular Miss A. MacKinnon and Mr. D. Muir. Special thanks go to Mary Brown for her boundless enthusiasm in correcting and editing the manuscipt, and for her assistance in drafting the many figures.

Lastly, I would like to thank all those who made my stay in Glasgow such a pleasure, in particular Tahar and my flat mates Ragnhild, Björn and Kenny.

CONTENTS

SUMMARY

This thesis describes theoretically the evanescent coupling of a D− fibre, with the aim of calculating the propagation constants of the transverse modes. Both analytical and numerical methods are considered for the study of coupling situations involving a fibre.

The first analytical method, Coupled Mode Theory (CMT), provides an understanding of the coupling phenomenon which occurs between two similar guides. In this situation, for example, for two fibres/guides with a similar range of propagation constants, coupling does not occur between a guided mode of the first guide and a radiation mode of the second. However, plane wave analysis is preferred to CMT for its simplicity and adequacy in prism coupling application.

Secondly, the GF method is selected as the appropriate numerical method for the case of a D− fibre coupled to a semi− infinite dielectric medium, in preference to the point matching and finite elements methods. The GF method (a semi− numerical method) leads to an eigenvalue problem, with the propagation constant as the only unknown.

The behaviour of the GF is dependent on the refractive index of the medium surrounding the fibre, the distance from the core to the flat surface of the cladding, and the possible effective refractive indices of the guided modes. A program is developed to calculate the GF as a function of these variables. By defining these parameters, it enables the testing of several routines which could be later introduced into a final program calculating the different propagation constants of the guiding structure.

Finally, the analytical study has been extended to allow direct application in the final program.

LIST OF ABBREVIATIONS AND SYMBOLS

GF	Green function
PDC	Polished Directional Coupler
CMT	Coupled Mode Theory
BC	boundary conditions
E,H	vector fields
γ	scalar field
β	propagation constant of a mode
n_1	refractive index of the core
n_2	refractive index of the cladding
n_3	refractive index of the surrounding medium
n_e	effective refractive index of a guided mode
α_s	skew angle of a local plane wave
α_e	elevation angle
θ_c	critical angle of total reflection
$G_{11,..}$	vector GF
$g(r,r')$	scalar GF
r	vector position of the observation point
r'	vector position of the source point
$\beta_{a,b}$	propagation constant of local modes
$\Gamma^{\pm}$	propagation constant of coupled or normal modes
$C_{a,b}$	coupling coefficients
$A\pm$	amplitude of the symmetrical and antisymmetrical coupled modes
$E_{a,b}$ $H_{a,b}$	mode fields of a local modes

CHAPTER ONE INTRODUCTION

Recent technical developments have considerably improved the characteristics of optical fibres, and in particular of monomode fibres. These fibres are characterized by a very high data rate handling capacity, with a bandwidth potential of several GHz over 1km, and hundreds of MHz over 10km. However, their electrical counterpart: the co-axial cable, limits the transmission of a communication system to a few hundred MHz at a distance of the order of 1km.

The unique properties of these fibres have also stimulated considerable interest in a broad range of other applications including interferometers, optical signal processors, and optical sensors. In particular, some basic functions required in any optical systems such as: polarization controllers, modulators, power dividers, and passive filters, all previously performed in bulk materials, are now successfully achieved by in-line optical fibre components. One of the first important functions that was considered, was the transfer of signal power between two optical fibres. Thus, the fibre to fibre coupler became a basic component of a 'fibre-based' device, which operates on the principle of evanescent coupling, as further explained in chapter 3.

Concurrently, important developments were taking place in integrated optics, particularly in modulators [Pp], integrated lasers [Nk], deflectors [Hm], and detectors [Os]. Thus, other optical functions previously elaborated in bulk materials, are replaced by their integrated optics equivalents. The main advantage of an integrated system comes from its small size, and therefore such a device is thermally and mechanically more stable than its bulk counterpart. What is more, the high electrical and optical densities possible in integrated optics lead to very efficient and compact devices.

However, the advance in integrated optics, is of use only if an efficient method of coupling optical circuits to optical fibres acting mainly as a data link, exists. Therefore, efficient coupling of optical fibres to integrated waveguides is the basis for the development of all guided optics systems.

Note that, the replacement of an 'electronics system' by optical circuitry based on fibre and integrated optics devices, is an attractive solution only if its

performance is superior and its cost acceptable [K] . However, the positional and dimensional tolerances imposed by the small fibre core diameter ($\simeq$ 8 μm) are tight, and progress has not been spectacular in the domain of coupling from a fibre to a slab waveguide. Consequently, this problem is still of great interest, especially that of finding a half–coupler based on a fibre, involving a simple, low cost manufacturing process. For this purpose the D–fibre was elaborated, and the study of its evanescent field coupling behaviour was chosen as the basis of this thesis. Nevertheless, let us first introduce the different possible solutions for a fibre to slab waveguide coupler.

1.1 FIBRE–SLAB WAVEGUIDE COUPLER

The various fibre–slab waveguide couplers can be classified into two principal categories:

1. the end–fire or butt coupler.
2. the transverse, directional or evanescent coupler.

1.1.1. End–fire coupling

The end–fire coupler is the most common coupler, and is used as an input or output coupler. A schematic description of a fibre–film coupler is shown in fig. 1.1.a. The fibre–end is cleaved or polished, and set up so that the beam coming or merging from the fibre is normal to the polished side of the film. Different methods are used for the alignment and fixation of the fibre [Aj, Mp, Nt]. Thus, the light leaving the end–face of the first guide is radiated directly into the end–face of the second. One difficulty with this technique, is that any loss or misalignment results in a degradation of the primary optical signal. A second source of loss comes from the Fresnel losses, due to the reflection at the fibre/air and air/waveguide interfaces.

The butt–joint approach, although dependent on very tight alignment and geometrically matching conditions, can be satisfactorily achieved in numerous applications. Komatsu et al. [Km], for example, reported a loss from fibre to

(a) end-fire coupling

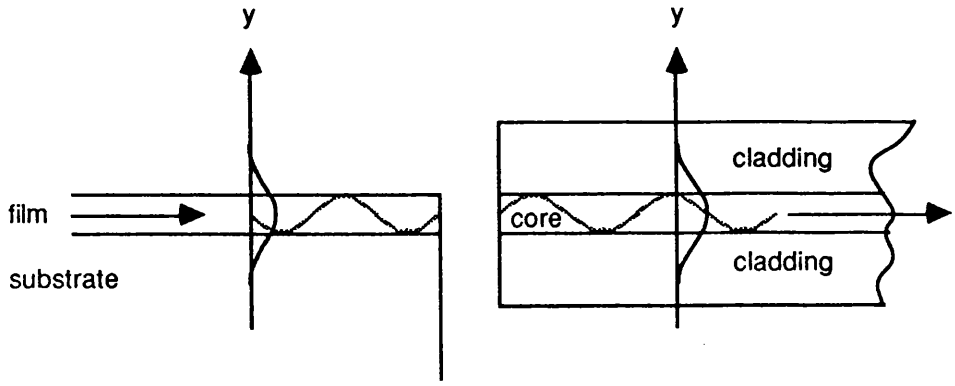

(b) transverse coupling

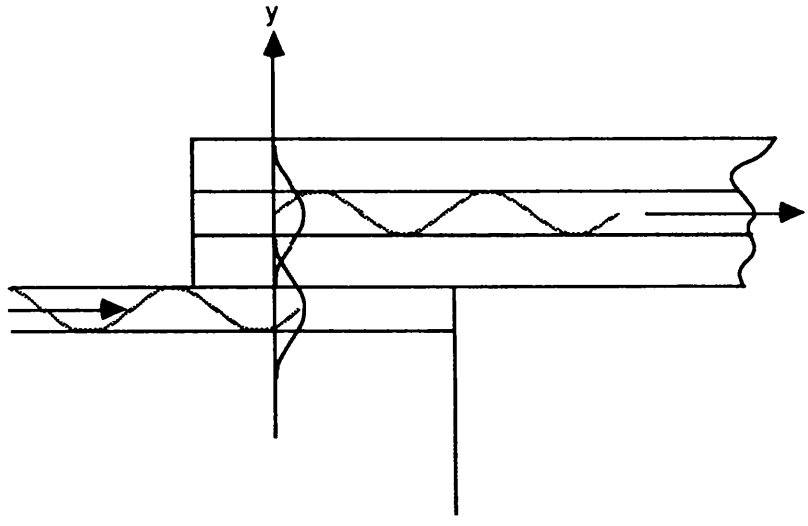

FIGURE 1.1

a. End– fire coupling from a fibre to a film waveguide.
The arrows represent the direction of propagation of the guided light.

b. Evanescent coupling between a fibre and a film waveguide

waveguide to fibre coupler of only 0.5 dB. Furthermore, it is simpler to manufacture an end–fire coupler than an evanescent coupler. Thus, the former is often preferred to evanescent coupling. However, end–fire coupling is not a flexible solution, and it would be advantageous if the fibre could be coupled at any part of an integrated circuit, and not only at the film edge. What is more, it does not allow selective coupling in terms of power, polarization, mode or wavelength, which can be succesfully achieved by the directional coupling method described below.

1.1.2. Directional coupling

This coupling method is a second approach to the fibre to slab waveguide coupling problem. The coupling of optical power is made possible by a perturbation of the evanescent field which extends outside the core and the film, for the guided mode of the fibre and the slab waveguide, respectively, as shown in fig. 1.1.b. A theoretical explanation of directional coupling is given in chapter 3.

However, we shall mention the main advantages to be gained from this coupling technique in comparison with end–fire coupling:

a. Firstly, the relative cross–section of the waveguides to be coupled does not need to be the same or similar.

b. Secondly, coupling can take place at any point on the thin film.

c. Thirdly, thanks to the evanescent coupling properties, some functions can be directly executed through a selective coupler in terms of the modes, power, polarization or wavelength.

d. Finally, the power transfer can reach a theoretical and maximum value of 100%. However, a successful total power transfer has not yet been reported in the literature. The fabrication tolerances and the complexity of the half–fibre coupler, constitute the main difficulties of the method. A fibre–film–fibre loss of 2dB has been reported [Br2], at a wavelength of 1.35 and 1.54 microns, which correspond to the region of minimum loss and dispersion in optical fibres, and thus is of great interest for telecommunication applications.

It is interesting to note that many analogies can be drawn from the well–established microwave technology of directional and distributed couplers [H]. The technique applied in microwave couplers can in principle be applied to higher optical frequencies. However, because of the much shorter wavelengths of light, the dimensional and positional tolerances of such couplers decrease. Thus, further difficulties are introduced, although realization is still within the framework of our present–day technology.

In conclusion, despite higher losses than a corresponding end–fire coupler (due to the manufacturing process), the directional coupler is the appropriate and complementary coupling technique in many cases, due to the particular properties it exhibits.

1.2 HALF–FIBRE COUPLER

Optical fibres have thick cladding layers, specifically chosen so that the evanescent field at the outer cladding surface is negligibly small for all well–guided modes. To enable directional coupling, much of the cladding must be removed locally, thus allowing a perturbation of the evanescent field of the fibre by the other half–coupler (i.e., to cause sufficient overlap of the evanescent fields of the two half–couplers). There are two basic approaches:

1. to use a conventional fibre polished locally.
2. to use a D–fibre.

1.2.1. Use of a conventional fibre.

The first use of a fibre in a directional coupler was proposed by Hsu in 1876 [Hs]. He demonstrated coupling from a single–mode fibre to a prism. The fibre was disposed in a preferentially etched silicon v–groove and polished to within a few microns of the core. A high index prism was then used to remove the fundamental mode power (see sect. 3.2).

However, the most common method using a polished fibre, was developed by Bergh et al. [Bg]. They achieved a tunable fibre–fibre coupler, giving any desired

coupling ratio with very low insertion loss or cross– talk. This coupler is known as the 'Stanford coupler' or polished 'directional coupler' (PDC) (see fig. 1.2). The fibre in each coupler was bonded into a groove cut into a silica substrate block. The groove had a radius of curvature of typically 25cm, and was formed using a wire saw. The surface of the substrate containing the fibre was polished to remove the excess cladding.

The main inconvenience of this method, is that extreme care is necessary to maintain an accurate radius of curvature. Afterwards, other similar techniques were used to set up the fibre [Pr,Ny,Zh]. However, each technique involves fastidious polishing of the whole half fibre– coupler. In order to give access to the evanescent field of a half– coupler, most of the cladding must be removed to within a few microns of the core. Hence, this operation implies the removal of nearly 60μm for a conventional single mode fibre (core radius of 4μm and overall diameter of 125μm).

Finally, for flatness of the polished area of the fibre, and a reproductibility of the core/flat distance, the silica substrate block and the epoxy were chosen because of the polishing hardness rather than the optical index matching.

1.2.2. Use of a D– fibre.

Before the use of the D– fibre, another method avoiding fastidious polishing was used in a fibre–fibre SMDC. The two fibres were etched [Sh] to locally remove most of the cladding around the core. The remaining fibre was locally very thin, and susceptible to mechanical damage. However, this method is not applicable to a fibre– film coupler.

A coupler using a D– fibre is another interesting alternative which avoids the polishing process of the polished directional coupler. The first application of a D– fibre using the evanescent coupling effect was published by Shöner et al. [Sc,Hn,Dy], who manufactured a single mode directional coupler (SMDC) between two D– fibres.

(a)

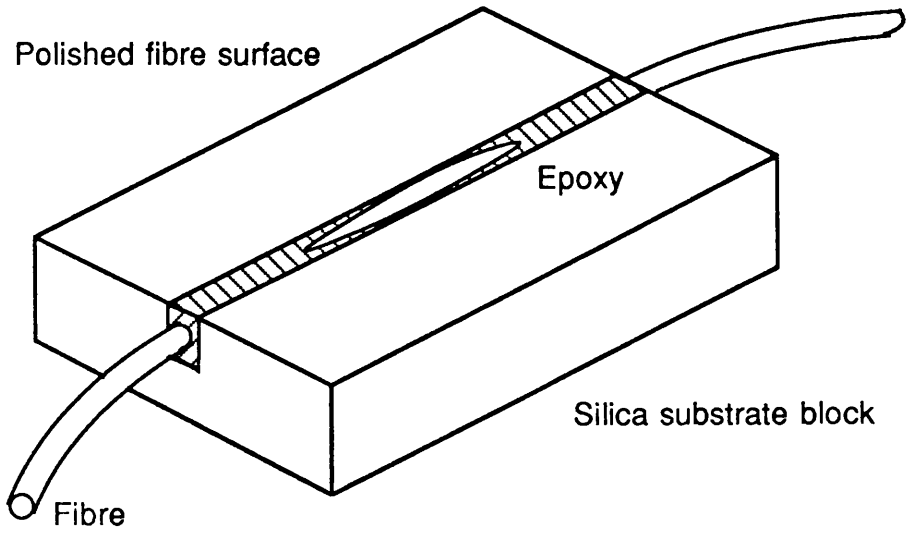

(b)

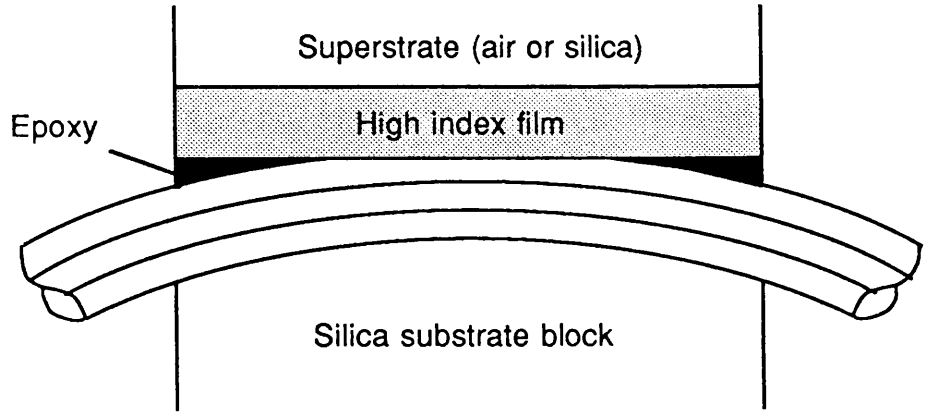

FIGURE 1.2

a. Geometry of a half–Stanford coupler, also called polished directional coupler (PDC), showing set–up in silica substrate block.

b. Cross–section of fibre–film coupler using PDC.

a. Fabrication

Now, let us briefly describe the fabrication of a D− fibre, the geometry of which is shown in fig. 1.3. First of all, a flat is cut and polished parallel to the core of a standard single mode preform. This modified preform is then pulled by the usual process for the fabrication of the fibre. By this means, a fibre with an approximately semicircular cross− section, called an SCCS− fibre or D− fibre was manufactured.

Note, that a preform was previously manufactured to build a directional coupler, based on a double core fibre pulled from two appended partial preforms [Sf]. The main advantage of this method is that the core alignment is carried out directly on the fibre's preform. However, it is difficult to splice or couple two single mode fibres at each extremity of the double core fibre, the two cores of the fibre being close enough to enable evanescent coupling (the spacing was approximately 10μm for a fibre monomode at 633μm). To overcome this difficulty the D− fibre was drawn.

b. Characterisation

In their article 'Fabrication and Characterisation of D− fibres with a Range of Accurate Controlled Core/Flat Distance', Millar et al. [Ml] at BRTL defined the first study of the fundamental optical properties of D− fibres drawn from a standard quasi− step− index type 'B' single mode design preform. This is probably the most important class of D− fibres, owing to their compatibility with main stream single mode fibres.

First of all, in order to characterize the D− fibres, one preform was cut and polished at an angle to the longitudinal axis. This choice of polished preform, should therefore allow the full range of fibre samples which could possibly be used in evanescent field coupling situations.

Precautions were taken to keep the circular cross− section of the fibre core constant, and to reproduce the D− shape by minimizing the rounding effects due to surface tension. Numerical values of these characteristics are given in the article previously mentioned.

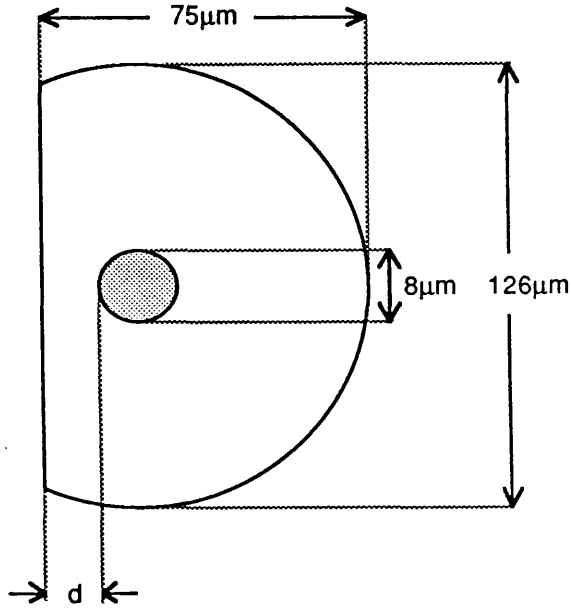

FIGURE 1.3

Typical D− fibre with core/flat distance: d, of 4 μm, and variation between the core and cladding refractive indices: $\Delta n = 0.005$.

Transverse coupling behaviour was then investigated by measuring the input prism coupling efficiency (see section 3.2.1), as a function of the core/flat distance (d), at a wavelength of 633nm. Repeatable input coupling measurements (±0.8dB), were achieved, using the curved surface of a 5cm glass rod to push the fibre against the prism. At this chosen wavelength, the fibre was supporting at least three sets of degenerate modes, which were identified by their far field pattern and synchronous coupling angle. Figure 1.4 shows the plot of coupled power against the core/flat distance, for the fundamental mode (LP01), and the first order mode (LP11).

The fundamental mode is better confined in the core than the LP11 mode, i.e., its evanescent field does not extend into the cladding as far as that of the higher order mode. This implies, that the evanescent input coupling power, which propagates along 20cm of fibre, decreases more rapidly for the fundamental mode than for the first order mode.

The lesser confinement of the higher order mode, induces important perturbation of the evanescent field for small core/flat distances. Therefore, some power from the guided mode radiates during its propagation along the fibre to the detector, resulting in an apparent decrease in coupling efficiency as 'd' diminishes.

c. Conclusion

Consequently from the above characterisation, the alternative method of building a half fibre–coupler with a D–fibre becomes quite interesting, especially as it avoids partial or total polishing of the half–fibre set–up, and therefore simplifies the manufacturing procedure of the coupler. It also allows the advance determination of the appropriate core/flat distance for efficient coupling. Additionally, long coupling lengths are possible, allowing weak interactions over extensive propagation distances ($10^4 - 10^5$ wavelengths), and thus leading to high Q–factor devices.

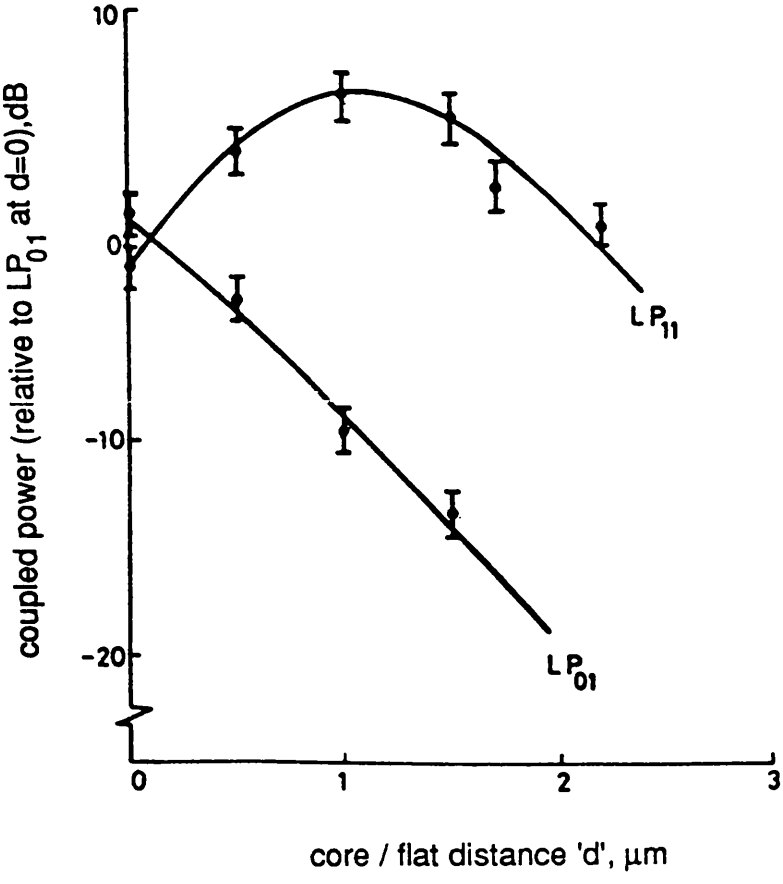

FIGURE 1.4

Normalised coupled power into LP_{01} and LP_{11} modes at $\lambda = 633$ nm using a prism coupler, as a function of core/flat distance (from [Ml]).

1.3 Review of the content of the thesis

The background information on the two principal coupling methods: transverse and directional coupling, have previously been introduced. We have also given the motivation for the use of a D– fibre in a half– fibre coupler.

The second chapter on waveguide theory introduces the parameters and definitions used in the following chapters.

Next, in the third chapter we give two analytical approaches to the coupling problem:

- Coupled Mode Theory (CMT) applied to two similar waveguides,
- plane wave analysis of a prism coupler.

Both analyses give a basic understanding of the evanescent coupling phenomenon.

Thereafter, in chapter 4 we try to formulate the perturbation theory for transverse modes in a coupling structure formed by a D– fibre and a semi– infinite dielectric medium. Thus we want to calculate the propagation constants of the mode of the perturbed D– fibre. We first introduce the assumptions of the problem. Then, a review of the theory of the GF is given before the definition of the Kirchhoff– Huygens integral, having this GF as one of its elements. Finally, we justify the selection of the GF method (which is in fact a semi– numerical method), for these particular applications.

In chapter 5, we first develop the analytical calculation of the first and second parts of the GF. Then, starting from the Kirchhoff– Huygens integral, we derive an eigenvalue problem with the propagation constants as the only variables.

However, programming application involves further analytical developments as described in chapter 6.

The results of the GF are reported in chapter 7. Finally, we give the further development leading to a total definition of the evanescent field coupling of a D– fibre to a prism.

Fibres, planar waveguides, and prisms constitute a group of guides between which evanescent coupling may occur. Therefore, in the following paragraph let us give a brief description of these different guides, which is not exhaustive but which aims to introduce the parameters and the definitions used in the following chapters.

2.1 FUNDAMENTAL PROPERTIES OF THE MODES

The electric and magnetic field vectors $E(x,y)$ and $H(x,y)$ are each separated into two parts: one part representing the power guided without attenuation along the guide, the other representing the power radiated away from the waveguide. For a simple guide (fibre, slab waveguide, rib waveguide for example), it is possible to calculate a finite number of guided modes and a continuum of radiation modes.

2.1.1 Modal expansion of the guided or bound modes

Let us consider an ideal guide supporting forward propagating modes only. Thus, the field vectors satisfying the homogeneous vector wave equations ([S1] equ. 30.18) are expanded as a finite sum of the modal electric or magnetic fields, $E_n(x,y,z)$, $H_n(x,y,z)$ as in:

$$E(x,y,z) = \sum a_n E_n(x,y,z) \qquad \text{with } n = 1,2,..,N \qquad (2.1)$$

$$H(x,y,z) = \sum a_n H_n(x,y,z)$$

where a_n are the modal amplitudes, which depend on the source of excitation, and where the time dependence $\exp(-i\omega t)$ of the modal fields is assumed implicit.

Note, that the decomposition in series is a general form of fitting boundaries and satisfying a partial differential equation, for example in our case the wave equation. However, the application of this method requires the separation of the partial differential equation into coordinates, ξ_n, so that a boundary corresponds to one or more constant coordinate values, i.e., ξ_1 = constant ([Mf] sect. 6.3). Consequently, this method is applicable to guides with simple geometry, and we will consider only the two main ones: the slab waveguide and the fibre.

2.1.2 Translational invariance and propagation constant

a. Translational invariance:

The cylindrical symmetry or translational invariance of a guide enables us to express the modal fields in the separable form, as in:

$$E_j(x,y,z) = e_j(x,y) \exp i(\beta_j z - \omega t) \qquad (2.2)$$

$$H_j(x,y,z) = h_j(x,y) \exp i(\beta_j z - \omega t)$$

where β_j is called the propagation constant or eigenvalue of the j^{th} mode. Furthermore, the translational invariance in conjunction with the homogeneity of the guide, implies that no coupling occurs between the modes.

b. β for guided modes:

The decomposition of the fields in series of eigenfunctions ([Mw] sect.9, [Mf] sect. 6.3), has the different propagation constants: β_j as eigenvalues. As a result of these different eigenvalues, the boundary conditions are satisfied for each mode. There is a distinct β_j per mode, unless two modes are degenerate. Such modes have equal phase velocity, but their transverse field distributions do not need to be identical. From a ray approach ([Sl] part 1, [Tm] sect. 2.1), or a modal treatment ([Sl] sect. 31, [Tm] sect. 2.2.6), the range of all possible values of the propagation constants for the guided modes is limited within the interval:

$$kn_3 \leq kn_2 \leq \beta \leq kn_1 \qquad (2.3)$$

where n_1, n_2, and n_3 are the refractive indices of respectively, the film, the substrate, and the superstrate, and where $k = 2\pi/\lambda$ is the wave number in free space. If we consider a fibre, the relation (2.3) becomes:

$$kn_{cl} \leq \beta \leq kn_{co} \qquad (b)$$

where n_{co} and n_{cl} are the core and the cladding of a fibre, respectively.

c. Cutoff condition:

If the propagation constant of a mode satisfies the following relation:

$$\beta = kn_2 \quad \text{or} \quad \beta = kn_{cl} \qquad (2.4)$$

the mode is said to be cutoff. In the ray picture, this situation corresponds to the loss of total internal reflection, and in the modal analysis, to the loss of optical confinement and field spreading from the guiding region throughout the surrounding medium (substrate or cladding).

Consequently, over the cutoff value, the guide supports radiation modes only, i.e.,

$$\text{for } \beta > kn_2 \quad \text{or} \quad \beta > kn_{c1} \tag{2.5}$$

2.1.3 Helmholtz equation

There are only a few guides which have an exact analytical solution of their modal fields. Planar guides, circular symmetric and elliptical fibres, all with a step index profile, for example, have an exact solution. A step index fibre has a core and cladding of uniform refractive index, with the cladding being assumed infinite. Thus, the only variation in profile is a step discontinuity at the core/cladding interface.

This characteristic implies, that the analytical solution of a waveguide with a step index profile, can be calculated from a simplification of the homogeneous vector wave equation (^{SI} equ. 12.2). Each cartesian coordinate of the electromagnetic field satisfies the Helmholtz equation within each region of constant refractive index, i.e.,

$$\{ \nabla^2 + n^2k^2 - \beta_j^2 \} e_{nj} = 0 \qquad \text{with } n = x,y,z \ , \tag{2.6}$$

but not at the interface between two different regions. This equation is sometimes called the scalar wave equation, and is the appropriate equation for a uniform electric medium.

2.1.4 TE, TM and hybrid modes

In general, modes of an optical waveguide satisfying the homogeneous vector wave equation, have both e_{zj} and h_{zj} components, and are called hybrid modes. These modes are usually called EH and HE modes for reasons discussed elsewhere SI.

However, in special situations depending on the geometry of the cross-section and the profile variation of the guide, the modes can be separated into two linearly

independent sets [Jh]: one with $h_{zj} = 0$ everywhere, called transverse magnetic mode (TM); the other with $e_{zj} = 0$ everywhere, called transverse electric mode (TE).
The simplest example is the planar waveguide, where all modes can be expressed as either TE or TM modes. Another example is provided by the modes with azimuthal symmetric fields on circular fibres. In these two special cases, the transverse electric field components: e_{tj}, with $t = x,y$, satisfy the scalar wave equation given below in (2.7).

The last and trivial case is the one occuring in an infinite uniform medium, with $e_{zj} = h_{zj} = 0$ everywhere. In this situation, the modal fields are called TEM waves, and satisfy the following scalar wave equation:

$$\{ \nabla_t^2 + n^2k^2 - \beta^2 \} \psi = 0 \qquad (2.7)$$

where the scalar field: ψ, represents any one of the following transverse components: e_x or e_y, h_x or h_y .
Remember, that β is supposed to be the propagation constant of one particular mode, and its subscript: j, defined in the previous section is omitted, unless it is necessary.
To conclude, note that a TEM mode induces a wave phenomenon, possessing a phase constant identical to that of a uniform wave propagating in an unbounded medium, and is expressed by the following equation:

$$\psi = \psi_0 \exp\{i(kx - \omega t)\} \qquad (b)$$

where **x** is the unit vector in the direction of propagation of the wave,
and where ψ_0 is the scalar field amplitude at $\mathbf{x} = 0$.

2.1.5 Weak guidance approximation (or paraxial approximation)

Let us consider a cylindrical guide with a core and an infinite cladding region of refractive indices n_{co} and n_{cl}, respectively. By the term 'weakly guiding' (Gloge 1971 [Gl]), we mean that the refractive indices of the two regions are not too dissimilar, or to be more specific that $n_{co} - n_{cl} \ll n_{co}$.
Thus, if the different refractive indices are almost equal, the profile height, defined by:

$$\Delta = (n_{co}^2 - n_{cl}^2)/\, 2n_{co}^2 \ll 1 \qquad (2.8)$$

is small. It follows, that the range of propagation constants of the bound modes becomes narrow. Consequently, we may assume that:

$$\beta_j \cong n_{co} \cong n_{cl} \qquad (2.9)$$

Thereby, this slight non-uniformity maintains total internal reflection inside the guide, but the medium is virtually homogeneous as far as the polarization effects are concerned. Thus, the modal fields of a weakly guiding waveguide are nearly TEM waves, since the direction of propagation of a ray is almost parallel to the z-axis (i.e., $e_{zj} \cong h_{zj} \cong 0$), with only a weak dependence on the polarization properties of the waveguide.

It follows that, the tranverse electromagnetic fields satisfy the following simple relation:

$$h_t = (\epsilon_0/\mu_0)^{1/2}\, n_{co}\, z \times e_t \qquad (2.10)$$

with the transverse components expressed as in:

$$h_t = h_x(x,y)\, x + h_y(x,y)\, y \qquad (2.11)$$

$$e_t = e_x(x,y)\, x + e_y(x,y)\, y \qquad (2.12)$$

Thereafter, if we know e_t, the electromagnetic field is specified. This is done by solving the scalar wave equation (2.7) for e_x and e_y, with the appropriate boundary conditions at the interfaces defining the field amplitudes.

Note, that the scalar wave equation gives no information about the electric field polarization, i.e., its vector field direction. Thus, this direction must be determined from the polarization or symmetry properties of the waveguide.

2.2 SLAB WAVEGUIDE AND WEAK GUIDANCE APPROXIMATION

The slab waveguide has been extensively studied [Ad], and its behaviour is well known. However, let us recall some of its properties.

2.2.1 Mode field shape

From the geometry of the slab waveguide defined in figure 2.1, a guided mode propagates in the z-direction, with the assumption of a z-dependence of the form

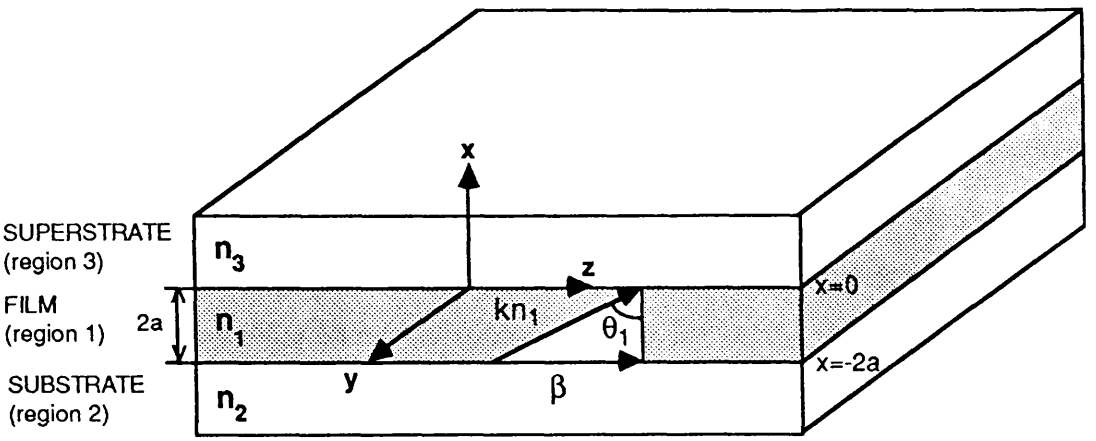

n_1 : refractive index of the film/guide

n_2 : refractive index of the substrate

n_3 : refractive index of the superstrate

θ_1 : incidence angle of ray

β : propagation constant of guided mode

k : free space wave number

FIGURE 2.1

Geometry of a slab waveguide with conditions of guidance of the waves inside the film defined by: $n_1 > n_2 \geq n_3$ and $\theta_1 < \theta_c$.

$\exp(i\beta z)$. Secondly, a guided mode has no variation along its y– axis, i.e., $\partial/\partial y = 0$. Finally, this mode is confined in the x– direction, and thus the guide has a confinement of order one. Thus, a phase front of a mode lies in the xy– plane and extends at infinity in the y– direction.

The above invariance assumption in the y– direction, implies (via Maxwell's equations) that the only nonzero field components are, respectively: E_y, H_x, H_z for a TE mode and H_y, E_x, E_z for a TM mode. This implies that, starting from the solution of the Helmholtz equation (2.6), the magnetic field of a TE mode can be written in terms of the electric field, as in:

$$h_x = \beta/\omega\mu_0 \; e_y \qquad (2.13)$$

$$h_z = -i/\omega\mu_0 \; \partial e_y/\partial x$$

with $h_x(x,y)$, $h_y(x,y)$, and $e_y(x,y)$ as defined in (2.2).

Then, as we want a guidance of the modal power to be largely confined inside the guiding layer of the planar waveguide (see fig. 2.1), the solution of the wave equation must be oscillatory in region 1. The previous condition associated with the assumption of a finite guided energy inside the guide, implies an exponential decay of the fields towards $\pm\infty$ in the x– direction. Consequently, the fields have an evanescent 'tail' in the substrate (region 2), and in the superstrate (region 3). From the above consideration, and the inequation concerning the propagation constant in (2.3), we write the solution for the electric field of a TE mode for the three regions of the guide, in the y– direction, in the following form:

$$A\, e^{-(\beta^2 - n_3^2 k^2)^{1/2} x} \qquad (2.14)$$

$$\text{with } x > 0 \text{ and } \beta^2 > n_3^2 k^2$$

$$B \cos(n_1^2 k^2 - \beta^2) + C \sin(n_1^2 k^2 - \beta^2) \qquad (b)$$

$$\text{with } 0 > x > 2a \text{ and } \beta^2 < n_1^2 k^2$$

$$D\, e^{-(\beta^2 - n_2^2 k^2)^{1/2}(x + 2a)}$$

$$\text{with } -2a > x \text{ and } \beta^2 > n_2^2 k^2 \qquad (c)$$

where A,B,C,D are constants to be determined.

As the tangential field components (i.e., e_y and $h_z \simeq \partial e_y/\partial x$) must be continuous

across a boundary between two different regions, we obtain four equations from which the unknowns of (2.14) will be calculated.

2.2.2 Eigenvalue equation

We assume that the slab waveguide is symmetric, i.e., the refractive index of the substrate equals that of the superstrate (i.e., $n_2 = n_3 = n_{cl}$). By elimination of the constants A,B,C,D in equation 2.14, and by satisfying the continuity conditions at the interfaces, i.e., by using the modal approach, or by means of the ray approach, the eigenvalue equation (also called the characteristic equation) for a TE mode of a weakly guiding step index slab waveguide, becomes:

$$\tan(2u) = 2u(v^2 - u^2)^{1/2} / (2u^2 - v^2) \qquad (2.15)$$

The normalized variables u, v, b are given by:

$$v = ak(n_1^2 - n_2^2)^{1/2} \qquad (2.16)$$

$$u = a^2(k^2 n_1^2 - \beta^2)^{1/2} \qquad (b)$$

$$b = 1 - u^2/v^2 \qquad (c)$$

where 2a is the width of the guiding layer.

Using u and b as the dependent variables, and v as the independent variable, the eigenvalue equation may be rewritten as:

$$2v(1 - b)^{1/2} = \tan^{-1}\left[\frac{2b^{1/2}(1 - b)^{1/2}}{1 - 2b}\right] + j\pi \qquad (2.17)$$

where $j = 0,1,2,..J$ is the mode number.

Therefore, the numerical resolution of the above transcendental equation leads to the values of the propagation constants, β_j, of the particular TE_j modes.

Furthermore, from the above characteristic equation, we define the normalized frequency at cutoff, v_c, for a symmetric slab waveguide, as in:

$$v_c = j\pi/2 \qquad \text{with } j = 0,1,..,J \qquad (2.18)$$

Thus, the corresponding expression for the number of propagating modes, M, in a guide of normalized frequency v, is:

$$M \leq 2v/\pi \qquad (2.19)$$

where M is the lowest integer satisfying the above inequality.

Finally, from the characteristic equation (2.17), we deduce that higher order modes have a smaller β_j than the fundamental mode (with j = 0). Then, thanks to the expression of the mode field in the guiding layer (2.14.b), we can also tell that higher modes have more field turning points, which affect the evanescent coupling between two modes of two parallel waveguides (see sect. 3.1.6).

2.2.3 Confinement of the modal power inside the core

The time average power flow, P, of a mode in a waveguide, is given by the integral over the guide cross-section of the z-component of the Pointing vector, S_z, as in:

$$P = \int_{-\infty}^{+\infty} S_z \, dx = 1/2 \int_{-\infty}^{+\infty} \mathrm{Re}(E_j \times H_j^*) \, z \, dx \qquad (2.20)$$

where Re means that the real part of the complex number is used, and where the superscript * defines the complex conjugate.

After some calculation, the proportion of modal power in the guiding region, P_{film}, versus the total modal power, P, is expressed as:

$$\frac{P_{film}}{P} = \frac{v\, b^{1/2} + b}{v\, b^{1/2} + 1} \qquad (2.21)$$

for the case of a weakly symmetric slab waveguide. Thus, the power in the cladding region, P_{clad}, versus the total modal power, is given by:

$$\frac{P_{clad}}{P} = 1 - \frac{P_{film}}{P} \qquad (2.22)$$

Now, if we introduce the cutoff value of the propagation constant ($\beta = n_{cl}$) inside the normalized variables in (2.21), we see that the power in the guiding layer is zero. If β is close to the propagation constant of a wave in an unbounded medium of refractive index n_1 (i.e., $\beta^2 = n_1^2 k^2$), nearly all the power is in the guiding region, and the mode has a strong confinement inside that region. Thereby, the equivalent refractive index:

$$n_e = \beta / k \qquad (2.23)$$

leads to an intuitive understanding of how strongly a mode is guided. An effective index close to n_1 indicates that the corresponding mode is well confined inside the guide. However, the extent of the evanescent field is greater for a mode with an effective index close to that of the cladding.

Finally, as the low order modes have higher β values than the higher order modes (see previous sect.), we deduce that the fundamental mode has the highest confinement inside the guide.

2.3 MODE SINKS

In order to give an intuitive understanding of mode sinks, we first of all consider a planar symmetric guide. Then, we increase the thickness of the guiding layer of width equal to 2a. This also implies an increase in the number of guiding modes defined in (2.19), which is rewritten explicitly as in:

$$M \leqslant \frac{2a\ k(n_1^2 - n_2^2)^{1/2}}{\pi} \qquad (2.24)$$

When the guiding layer is extremely thick, i.e., 1000's of wavelengths, the mode density is so high, that it can be considered as continuous. This mode continuum is known as a mode sink. The prism is one example of this, and has a confinement of order zero.

Observe, that a mode sink situation comes from the loss of at least one order of confinement, which is also the case for a coupling structure formed by a fibre and a slab waveguide.

Note finally, that this approach using an increasing thickness of guide, will be used to calculate the weak coupling between a planar guide and a semi– infinite substrate or a prism (see sect. 3.1.8).

2.4 WEAKLY GUIDING OPTICAL FIBRE

Now we consider the properties of a weakly guiding fibre, where its geometry implies a confinement of order two.

2.4.1 The equivalent step index fibre

The only optical fibres which have an exact analytical solution are the step index fibre and some graded index fibres ([Sl] chap. 14, [Tm] sect. 2.4). The solution of the mode fields of a step index fibre is mathematically more involved than the slab waveguide analysis, since it is stated in terms of circular functions, and its modes are a solution of the vector wave equation.

However, ultra low loss single mode fibres used in telecommunication, as described for example by Miya et al. [My] and Linke et al. [Ln], have a graded index profile. What is more, very few graded index profile fibres are amenable to exact analytical solution, for example, fibres with smoothly varying profiles. Nevertheless, the other fibres are approximated by numerical methods. Very accurate solutions have been obtained by the variational technique [Ok], and by the beam propagation method [Ft]. Another technique, known as the 'equivalent step index' method (ESI) [Bl,Ml2], has been demonstrated to a sufficient accuracy to explain the fibre–film coupling behaviour [Br]. From an index profile measurement the corresponding ESI profile is calculated, and thus the equivalent index difference and the ESI core radius are determined. Consequently, the step index fibre will be considered in the coupling theory, in the situation where a fibre is one element of the coupler.

2.4.2 Weakly guiding step index fibre

Most monomode fibres, for example those used in telecommunication, are weakly guiding. The weak guidance, as defined in sect. 2.15, allows the use of the scalar wave equation (2.7). It follows that, the mode fields are nearly TEM, i.e., $E_z \cong H_z \cong 0$.

As a result of the above approximation, it is possible to define linearly polarized modes or 'pseudo–modes': LP_{lm} modes. Several approaches have been used to build these LP modes and their approximate eigenvalue equation. Adams ([Ad] sect. 7.2.2) started from the exact eigenvalue equation and field components. However, Gloge [Gl] derived his results by assuming linearly polarized modes. Arnaud [Ar] then pointed out that these results can also be simply achieved by scalar analysis, so that the

approximation relies on the solution of the scalar wave equation, rather than on vector solution of the vector wave equation.

a. Fundamental LP_{01} mode

Several authors used the same approach as Arnaud, in particular Snyder ([Sn,Sl] sect. 13), who defined the modal parameters in the case of a weak guidance approximation as:

$$\tilde{U} = \rho(n_{co}^2 k^2 - \tilde{\beta}^2) \tag{2.26}$$

$$\tilde{W} = \rho(\tilde{\beta}^2 - n_{cl}^2 k^2) \tag{2.27}$$

$$V = (\tilde{U}^2 + \tilde{V}^2) = k\rho(n_{co}^2 - n_{cl}^2)^{1/2} \tag{2.28}$$

where $\tilde{U}$ is the core parameter,

$\tilde{W}$ is the cladding parameter,

V is the waveguide or fibre parameter,

and $\tilde{\beta}$ is the scalar propagation constant.

As a result of his calculation, the eigenvalue equation derived from the scalar wave equation for the fundamental mode of a weakly guiding step index fibre is:

$$\frac{\tilde{U}\, J_1(\tilde{U})}{J_0(\tilde{U})} = \frac{\tilde{W}\, K_1(\tilde{W})}{K_0(\tilde{W})} \tag{2.29}$$

where the range of single mode operations is given by $0 < V < 2.405$. With this convention, the fundamental modes HE_{11}, i.e., the two polarizations, are degenerated into the LP_{01} mode. The degeneracy of the LP modes is of course exact only when the profile height is equal to zero (i.e., $\Delta = 0$ as defined in (2.15)).

Then, to improve the accuracy of the LP modes, Snyder ([Sl] table 14−3) gives a polarization correction, $\partial\beta$, to the scalar propagation constant. If we compare the corrected mode parameters:

$$\tilde{U} + \partial\tilde{U}$$

with the exact solution: U, of the fundamental mode, we find that the maximum relative error has a magnitude of less than 0.005% for $\Delta = 0.005$. Note, that this profile height is a typical value for the low loss fibre used in telecommunication or

for a D− fibre.

b. LP designation for $l \geq 1$

The construction of the remaining LP_{lm} modes degenerate the four even $HE_{l+1,m}$ and odd $EH_{l-1,m}$ modes, the latter denoting TM_{0m} and TE_{0m} when $l=1$. However, unlike the fundamental and other LP_{0m} modes, all the LP_{lm} modes with $l \geq 1$ are not plane polarized. Instead, due to fibre polarization effects, the direction of the field depends on the position in the fibre cross− section.

Accordingly, the LP designation of the fundamental mode is applicable if we ignore the polarization properties of the fibre. Thus, all degenerate modes have the same propagation constant (see fig.2.2). Nevertheless, such a description will lead to more significant errors for the higher order modes. In practice, even for a small profile height, the $HE_{l+1,m}$ and $EH_{l-1,m}$ modes have slightly different propagation constants. Only after a distance of a beat wavelength, i.e., $2\pi/(\beta_1-\beta_2)$, are the two constituant hybrid modes exactly in phase, so that a linear polarization is achieved. This means, that a LP_{lm} or 'pseudo− mode' will change its field distribution during its propagation.

Despite its disadvantages, the LP mode treatment of the weakly guiding fibre has provided useful results for fibre design.

2.4.3 Birefringence of a D− fibre

Consider a D− fibre pulled from a weakly guiding single mode fibre. If the core/flat distance, d, (see fig. 2.3a) is sufficiently small, i.e., if d is smaller than the effective penetration of the fundamental mode of an equivalent unperturbed fibre, then the cladding cannot be considered everywhere as infinite. The circular symmetry of the fibre cross− section is broken and the D− fibre becomes birefringent. Thus, the propagation constants, β_y and β_x, differ along the axes of symmetry (see fig. 2.3b) defining the principal axes of birefringence.

However, in a first approximation, we consider that the modes are far from cutoff and well confined in the core region, so that $\beta_x \simeq \beta_y$. Thus, we also ignore

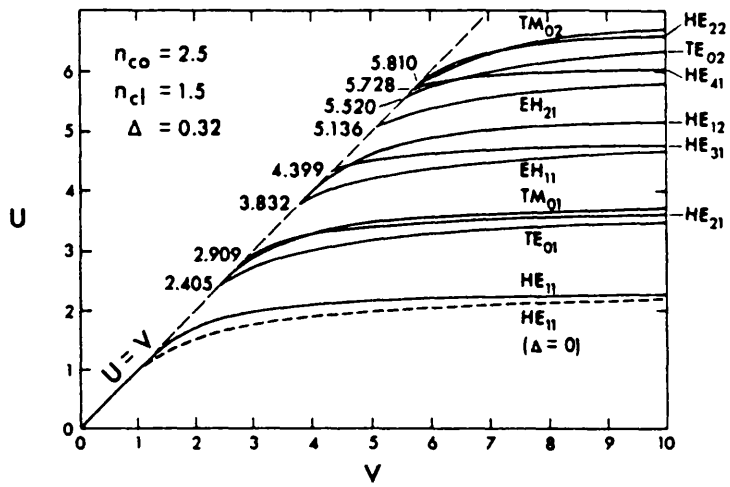

FIGURE 2.2

Numerical solutions of the eigenvalue equation (from [S1] p. 320), showing the mode labelling and the corresponding values of l and m. The values along the dashed lines are the cutoff values, v_c (one for each mode).

the radiation leakage due to a small coupling effect between the two polarization states, and the resulting slight difference of propagation constant ([SI] sect. 13.13), and therefore β_x and β_y remain constant during the propagation of a mode of a D– fibre.

(a)

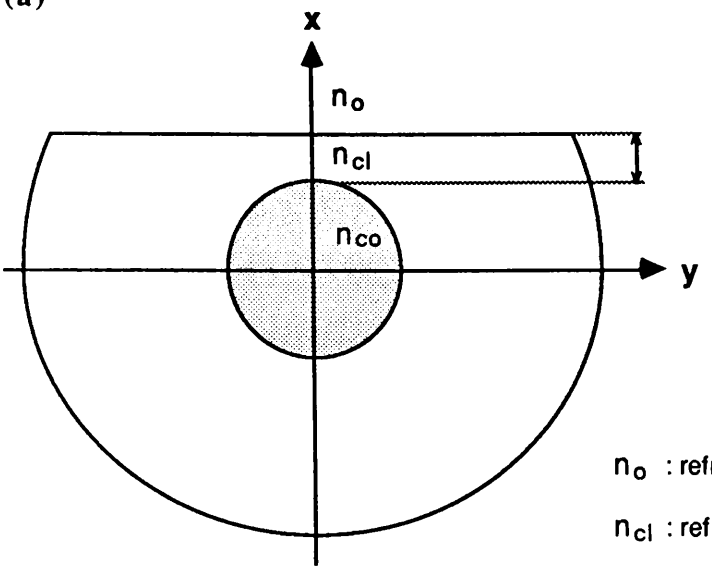

n_o : refractive index of the air

n_{cl} : refractive index of the core

n_{co} : refractive index of the cladding

d : core/flat distance

x,y : axes of birefringence

(b)

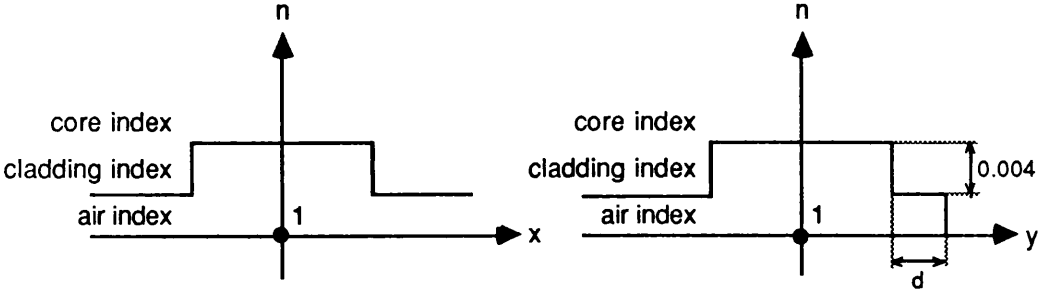

n : refractive index
x,y : axes of birefringence centred on the core
d : distance core/flat surface

FIGURE 2.3

a. Geometry of a D− fibre showing the main axes of birefringence: x and y, and the core/flat distance: d, on which depends the anisotropy of the fibre.

b. Schematic refractive index profiles of a D− fibre along the main axis of birefringence.

3.1 COUPLED MODE THEORY (CMT)

Solving electromagnetic problems by the eigenvector or modal expansion approach (see sect. 2.2.2), where fields are expanded into modes that individually satisfy the boundary conditions, is both mathematically powerful and physically intuitive in special situations, where separation of variables is possible. However, for complicated boundary conditions, in which separation of variables is no longer possible, the modal approach must be abandoned, as it is not possible to define some of them.

Couple mode theory (CMT) attempts to preserve the mode concept in some situations in which the modes cannot be easily found by analytical calculation, but where they remain physically intuitive. However, CMT is applicable to weak perturbation, for example, to slightly irregular or lossy fibres, or in our case, to a two– waveguide structure with a weak coupling between them. By weak perturbation, in a coupling situation for example, we mean that the modal fields of the guiding structure are nearly the modes of each guide.

3.1.1 Perturbation assumption of CMT

CMT is accomplished by expanding the fields of a complicated system, in terms of a complete set of known and local modes for simpler subsystems. In the case of a directional coupler, the subsystems are formed by the two guides in isolation. However, in this theoretical approach, we will consider the coupling between two similar monomode guides. Thereafter, we will briefly extend our study to the case of guides supporting several modes.

Therefore, let us first consider two dielectric waveguides placed alongside each other. The introduction of the second guide distorts the field distribution of the first one. In order to solve the theoretical problem, CMT uses a perturbation formalism to approximate the solution. This approximation Mr,Yr,Ty involves the assumption of

a weak perturbation caused by the coupling situation, so that each waveguide mode distribution remains unaffected by the presence of the other guide. Consequently the fields of the two waveguide system: E and H, are expressed as a linear combination of the unperturbed fields of each guide. It follows, that the total fields: E and H at the plane $z=0$ (see fig. 3.1), are assumed as the sum of the fields of the two waveguides in isolation, so that:

$$E = E_a + E_b \qquad (3.1)$$

$$H = H_a + H_b \qquad (b)$$

where E_a,H_a, and E_b,H_b are respectively, the local mode fields in the two guides a and b.

However, the field coefficients of the local modes now depend on their position along the $z-$axis. Consequently, they can no longer be obtained directly from orthogonality properties (see [S1] sect. 31.3), as the local modes do not satisfy the boundary conditions of the whole structure. Instead, they are found by solving a set of first order differential equations, called coupled line equations.

3.1.2 Coupled line equations

First of all, we consider a coupler formed by two parallel single mode guides, i.e., with a non-absorbing, uniform dielectric structure along their length. We also set the two guides to have equal confinement (for example two fibres), and to support guided modes.

To begin our study, we consider the two guides in isolation. The fields of the local forward propagating modes in guides a and b, can be written as follows:

$$E_a = A\, e_a(x,y)\, \exp(i\beta_a z) \qquad E_b = B\, e_b(x,y)\, \exp(i\beta_b z) \qquad (3.2)$$

$$H_a = A\, h_a(x,y)\, \exp(i\beta_a z) \qquad H_b = B\, h_b(x,y)\, \exp(i\beta_b z) \qquad (b)$$

where the subscripts a,b refer to guides a and b, respectively,

e_a, h_a, and e_b, h_b are the transverse field distributions,

A, B are the modal amplitudes at $t=0$ (or modal field coefficients),

β_a, β_b are the propagation constants of the two modes to be coupled.

Now, we can write the phase change of the electric field, according to the following

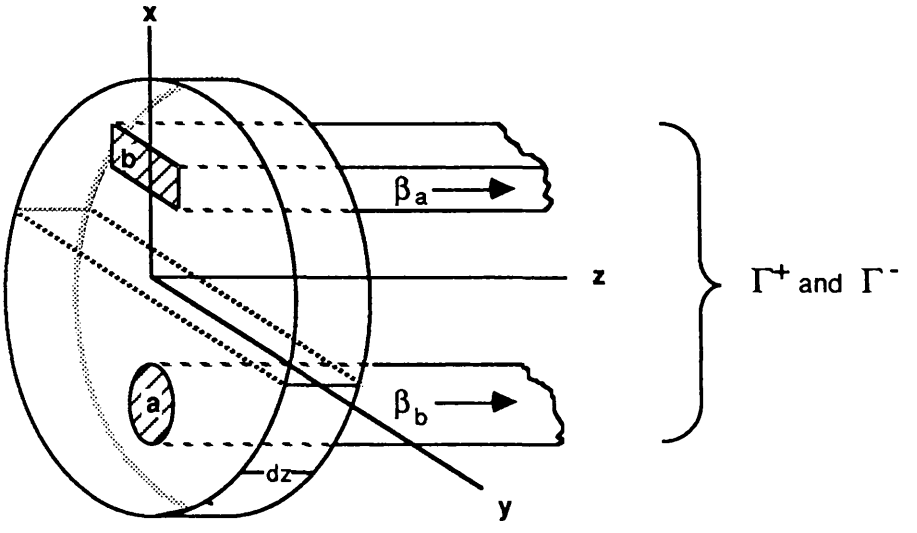

β_a : propagation constant of guide a in isolation

β_b : propagation constant of guide b in isolation

Γ^+, Γ^- : propagation constants of the coupled mode of the whole structure

FIGURE 3.1

Geometry of a directional coupler formed by two guides of equal confinement. The arrows represent the direction of propagation of the local modes, β_a and β_b, to be coupled between guides a and b.

differential equations:

$$dE_a/dz = i\ \beta_a\ E_a \qquad (3.3)$$

$$dE_b/dz = i\ \beta_b\ E_b \qquad (b)$$

Next we suppose the modes to be coupled together by some means, so that E_a is affected by the amplitude of E_b and vice– versa. Therefore, in the presence of a coupling effect, we can write the general coupled line equations of the two modes ^{Mr}, as in:

$$dE_a/dz = i\ \beta_a\ E_a + C_{ab}\ E_b \qquad (3.4)$$

$$dE_b/dz = i\ \beta_b\ E_b + C_{ba}\ E_a \qquad (b)$$

where the coupling coefficients which quantify the effect of guide b on guide a, and vice– versa, are C_{ab} and C_{ba}, respectively.

β, C_{ab} and C_{ba}, may be complex since we want to include the case of lossy modes.

Note finally, that similar equations as in (3.3) and (3.4) can be written for the magnetic field.

3.1.3 Coupled modes

We consider the coupling between two modes only. As demonstrated in the following section, efficient directional coupling is possible, only if the propagation constants of one mode in each guide are identical, i.e. $\beta_a = \beta_b = \beta$, and these modes (also called local modes) are said to be degenerate. Note that the coupling coefficients are allowed to be different, since the two modes can be different though degenerate.

Now let us assume that, the two guides constuting the coupler would support forward propagating modes only, if uncoupled. Thus, if the waveguides are lossless, conservation of power in a co–directional coupler imposes the following relation between their two coupling coefficients ^{Mi}, such that:

$$C_{ab} = -C_{ba}^{*} \qquad (3.5)$$

The asterisk indicates complex conjugation.

Since we consider the coupling of two degenerate local modes with β, C_{ab}, and C_{ba}

constant, the solution of the coupled line equation for synchronous guides has the following form:

$$E_a(z) = 1/2\left\{A\left[e^{+iT^+z} + e^{+iT^-z}\right] + (C_{ab}/C_{ba})^{1/2}\, B\left[e^{+iT^+z} - e^{+iT^-z}\right]\right\} \tag{3.6}$$

$$E_b(z) = 1/2\left\{B\left[e^{+iT^+z} + e^{+iT^-z}\right] + (C_{ba}/C_{ab})^{1/2}\, A\left[e^{+iT^+z} - e^{+iT^-z}\right]\right\} \tag{b}$$

$$\text{with } \Delta\beta = i(C_{ab}\, C_{ba})^{1/2}, \tag{3.7}$$

$$T^+ = \beta + \Delta\beta, \text{ and } T^- = \beta - \Delta\beta. \tag{3.8}$$

Consequently, the modal amplitude in each guide appears as the superpositon of two new modes, called coupled or normal modes, with new propagation constants, T+ and T^-, as described in fig. 3.1. The degeneracy of the two modes of the isolated waveguides is removed by coupling. The amount of mode splitting of the two coupled modes depends on the coupling strength, i.e., on the coupling coefficients: C_{ab}, C_{ba}.

Next, from a linear combination of E_a and E_b of two identical fibres, the normal mode amplitudes, which satisfy the boundary conditions of the whole structure, can be defined as in:

$$A^+ = E_a(z) + E_b(z) = (A + B)\, e^{+iT^+z} \tag{3.9}$$

$$A^- = E_a(z) - E_b(z) = (A + B)\, e^{+iT^-z} \tag{b}$$

where A^+ and A^- define the amplitudes of the symmetrical and anti-symmetrical coupled modes, also known as normal modes. Due to their differing propagation constant ($\Delta\beta$), the two coupled modes beat with each other in a distance, l, satisfying the relation: $l = \pi/\Delta\beta$. This gives the appearance of an interchange of power from the local mode of one fibre to the local mode of the other fibre.

3.1.4 Power transfer between two single mode guides

From the solution of the coupled line equations (3.6), let us study the

cross-talk of power in a co-directional coupler with two single mode guides of equal confinement. To start, we consider that the modes are lossless (i.e., $C_{ab}= C_{ba}^{*}$ and $\Delta\beta$), and that all the power is initially in the first guide. Therefore, the power in each guide can be written as a function of the distance z, as in:

$$P_a(z) = A^2 \cos^2(\Delta\beta) \qquad (3.10)$$

$$P_b(z) = B^2 \sin^2(\Delta\beta) \qquad (b)$$

From the above equations, it follows that the two waveguides exchange power after a distance, D, given by:

$$D = \pi/2\Delta\beta \qquad (3.11)$$

The previous equation also demonstrates, that the cross-talk between the two degenerate modes, is determined by the change in their propagation constants and not by their coupling coefficient. It follows that, with the perturbation assumption (3.1), it is sufficient to calculate $\Delta\beta$ to define the mode fields of the coupler formed by two similar single mode guides interacting weakly (see sect. 3.1.6).

Then, let the ideal guides have different propagation constants, i.e., $\beta_a \neq \beta_b$. It can therefore be demonstrated [Ls,Sn] that the distribution of power initially in guide a, satisfies the following relations:

$$P_a(z) = 1 - P_b(z) \qquad (3.12)$$

$$P_b(z) = F \sin^2 \left[((\beta_a - \beta_b)/2)^{1/2} + |C_{ab}|^2 z\right]^{1/2} \qquad (3.13)$$

where

$$F = \frac{1}{1 + ((\beta_a - \beta_b)/ 2|C_{ab}|^2)} \qquad (b)$$

is the maximum of power transfer (see fig. 3.3).

In conclusion, if the propagation constants are mismatched, little power is transferred between the modes, unless $\beta_a - \beta_b \ll |C_{ab}|^2$.
Therefore, a strong coupling (i.e., with a large $|C_{ab}|^2$), allows a relatively large propagation constant mismatch: $(\beta_a - \beta_b)$, for a given efficiency. However, in CMT we assume a weak coupling, so that significant power transfer occurs only between modes of nearly identical propagation constants, i.e. for $\beta_a \simeq \beta_b$.

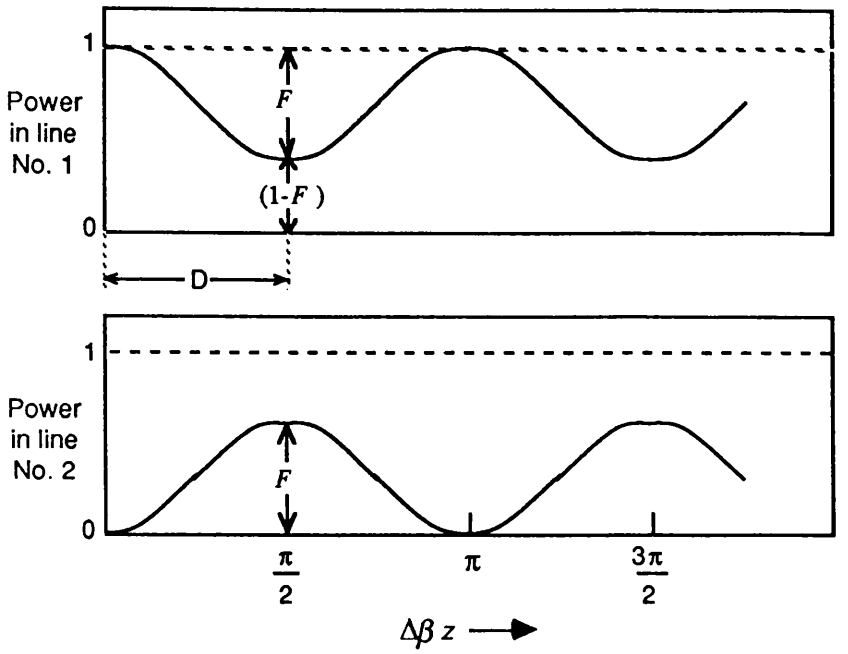

$D = \frac{\pi}{2\,\Delta\beta}$: distance of power exchange

$\Delta\beta$: difference of propagation constant between the local modes of the two coupled guides

F : maximum of power transfer

FIGURE 3.3

Power division between two coupled guides when propagation constants of the uncoupled guides (or local modes) are different. There is only partial power transfer, but it is periodic.

3.1.5 Other assumptions for CMT in use for single– mode couplers

The first simplification of CMT comes from the study of the coupling between forward nearly degenerate modes (i.e., $\Delta\beta \ll \beta_a, \beta_b$), of two similar guides. Thus, to couple efficiently with a weak perturbation condition, i.e., $|C_{ab}|$ being small, the power transfer from a forward mode of the first guide a, with a backward mode of the second guide b, is very small (see (3.13)) and can be neglected.

Note that:

$$\beta_{-b} = -\beta_b \tag{3.14}$$

Secondly, we can consider the coupling of a guided mode of one guide to a radiation mode of the second guide. As we have previously considered that the two guides are similar, they therefore have a similar range of bound modes, so that a propagation constant of a radiation mode, β_{ra}, β_{rb}, satisfies the following relation:

$$\begin{aligned} k^2\, n_{clmax}^2 &< \beta_a^2,\ \beta_b^2 \\ \beta_a^2,\ \beta_b^2 k^2 &< k^2\, n_{clmin}^2 \end{aligned} \tag{3.15}$$

with n_{clmax}, n_{clmin} being the maximal and minimal values of the refractive index of the cladding of both guides a and b.

This means, that except for discrete modes close to cutoff (see sect. 2.1.2), the propagation constant of a guided mode is much larger than that of a radiation mode, and can therefore be neglected. Nevertheless, starting with CMT applied to a coupler with one lossy guide, Arnaud [Ar2] demonstrated coupling to a mode sink, which supports radiation modes only (see sect. 2.3).

3.1.6 Perturbation theory for CMT

From the perturbation assumptions in (3.1) and the solution of the coupled line equations in sect. 3.3, we have seen that the coupling theory is based on finding the difference in propagation constant: $\Delta\beta$, between the two local modes and the coupled modes. Remember, that the local modes are those which propagate into the two guides in isolation and are supposed to be degenerate, whereas the coupled modes are valid for the whole coupling structure and were defined by (3.8). To calculate $\Delta\beta$, several perturbation formulae, all equivalent in accuracy, have been derived, for

example by Marcuse [Mr], Vanclooster [Vc], Yariv [Yr], Taylor [Ty], and Snyder ([Sl] sect. 26). However, we report the one proposed by Arnaud [Ar], which involves an integral along a contour located between the two waveguides (see fig. 2.1).

At first, Arnaud defined E_a, H_a, E_b, H_b, as being the modal fields of the local modes of the two waveguides in isolation, with the propagation constants: β_a, β_b.

Then, he let E^+, $H^+ \equiv (-E_z, E_t, H_z, -H_t)\exp(-iTz)$ be the adjoint field of a normal mode (E,H) of the two coupled waveguides.

Thus, his perturbation formula, based on Lorentz's reciprocity theorem, was expressed as in:

$$\int_{S_{a,b}} E_{a,b} \times H^+ - E^+ \times H_{a,b}\, ds = 0 \qquad (3.16)$$

where:

$S_{a,b}$ was the surface formed by $S_{a,b}$, $S'_{a,b} + C_{a,b}\, dz$ shown in fig. 3.1, and ds was a vector normal to the integration surface pointing outward, with a magnitude of unity.

Then, he let the spacing, dz, between S'_a and S_a tend towards zero, so that the above equation was reformulated so that:

$$(i\beta_a - iT)\int_{S_a} (E_a \times H^+ - E^+ \times H_a)\, dS_a = -\int_{C_a} (E_a \times H^+ - E^+ \times H_a)\, dC_a \qquad (3.17)$$

Then, by interchanging subscript a with b, a similar expression was written for the second guide, b.

From the perturbation assumption (2.1), he replaced the expression for the total field (E, H), by its approximation as a function of the local fields (E_a,H_a, and E_b,H_b). Thereafter, he chose the two contours, C_a and C_b, as being coincident with the y− axis, and closed at infinity where the field vanishes. Finally, after neglecting some second order terms in the development of (3.17), his perturbation formula [Al] was obtained, as in:

$$(T - \beta_a)(T - \beta_b) = C^2 / P_a P_b \qquad (3.18)$$

where C was the coupling coefficient dependent on the overlap between the fields in the two guides, such that:

$$C = 1/2 \int_{-\infty}^{+\infty} (E_{ay}H_{bz} + E_{az}H_{by} - E_{by}H_{az} + E_{bz}H_{ay})\, dy \qquad (b)$$

$$\text{where} \quad P_{a,b} = \iint_{-\infty}^{+\infty} (E_{a,b} \times H_{a,b})\, z\, dx\, dy \qquad (c)$$

with z denoting the unit vector along the z− axis.

If we assume now, that the local modes are degenerate, i.e., that $\beta_a = \beta_b = \beta$, the perturbation formula can be rewritten as in:

$$(T - \beta) = \pm(C^2 / (P_a P_b)) \qquad (3.19)$$

This equation leads to the two propagation constants for the two coupled modes defined in sect. 3.3, and expressed as:

$$T^{\pm} = \beta \pm \Delta\beta \qquad (3.20)$$

with the variation of propagation constant, or 'mode splitting': $\Delta\beta$, given explicitly as:

$$\Delta\beta = (C^2/P_a\, P_b) \qquad (b)$$

Consequently, if the guide separation is increased, the coupling strength is reduced, since the field intensity of each guide in the vicinity of the other would fall (i.e., also the coupling strength: C). Therefore, $T^{\pm}$ would converge towards the original value of the local modes of the two guides in isolation.

3.1.7 Extension of CMT to multimode guides

A strict analysis of the coupling between two multimode guides should include, for each mode of one guide, the effect of each mode on the second guide.

As demonstrated in sect. 3.4, the effect of the coupling between one mode, i, of the first guide, a, with one mode, j, in the second guide, b, is negligible, unless $\beta_i \simeq \beta_j$. This condition comes from the weak coupling assumption, which implies that $C_{ij} \ll \beta_i, \beta_j$. It does not imply that only like modes couple, unless the two guides are

identical. The coupling will occur between two degenerate modes, i and j, one in each guide. Coupling of the modes i,j to a third one is negligible, unless the third mode is nearly degenerate with the two others, i.e., $\beta_n \simeq \beta_i \simeq \beta_j$. Thus, in general, if m β_i's of the first guide have a corresponding nearly degenerate β_j in the other guide, m couple line equations as in (3.4) must be solved. Snyder [Sn] and Digonnet [Dg], for example, have shown that the total coupling coefficient, C, of the two weakly coupled and synchronous guides, is simply given by the spatial overlap of the interacting modes in the two guides, so that:

$$C = -\omega \epsilon_0/4P \iint_{-\infty}^{+\infty} (n(x,y)^2 - n_2^2)\ E_a^*\ E_b\ dx\ dy \qquad (3.21)$$

The variables of the previous equation are defined such that:

$n(x,y)$ is the refractive index profile of the guiding region,

n_2 is the refractive index of the cladding or substrate,

P is the total power carried by the waveguides at t= 0,

ω is the angular frequency, and

E_a, E_b are the transverse electric field distributions for the interacting modes expanded as in:

$$E_a = \sum_{i=1}^{m} a_i\ e_{ai}(x,y) \qquad (3.22)$$

$$E_b = \sum_{j=1}^{m} b_j\ e_{bj}(x,y) \qquad (b)$$

with a_i, b_j being the modal amplitude at t= 0,

and e_{ai}, e_{bj} being the modal transverse electric field distributions of guides a and b, respectively.

Consequently, if the two guides are not identical, their transverse fields will have a reduced overlap compared to the modes of identical guides, since positive and negative field contributions will cancel each other out as described in fig. 3.4. This implies, that the coupling coefficient is reduced and the coupling length increased.

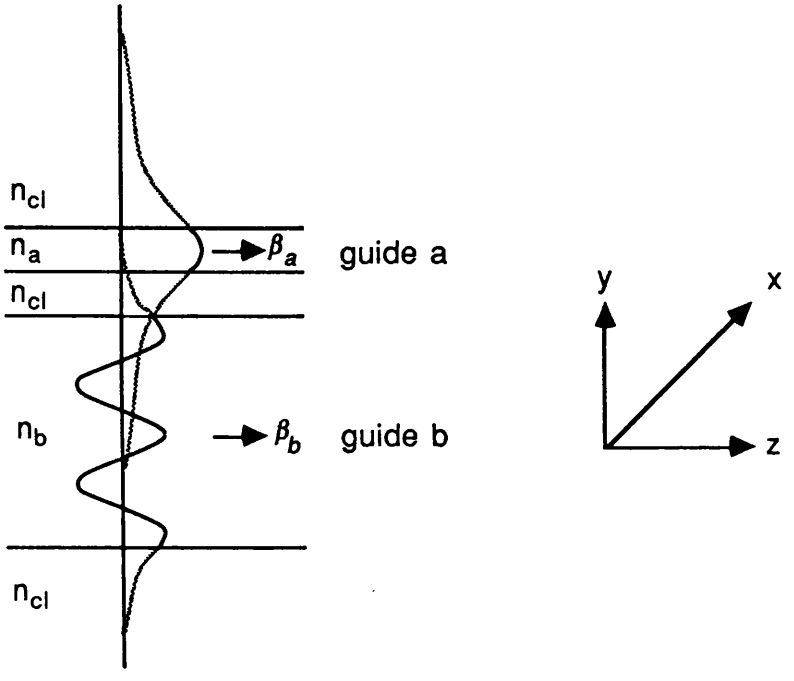

β_a , β_b : propagation constants of guides a and b, respectively

n_a, n_b: refractive indices of the guiding regions of guides a and b, respectively

n_{cl} : refractive index of the cladding region

→ : direction of propagation of the local modes

FIGURE 3.4

Field overlap of two different and degenerate modes of two multimode guides. The field overlap is reduced for local or uncoupled modes having different mode field distributions, by partial cancellation of positive and negative contributions.

3.1.8 Discussion

It follows from CMT, that the mode splitting $\Delta\beta$ can be calculated directly from the modal fields of the two guides in isolation, i.e., derived by using the same coordinate system for both guides [Ar]. Thus, the propagation constant of the coupled modes and the transfer of power between the two guides constituting the coupler, can be calculated. However, the results of CMT, even though intended for arbitrary waveguides, are accurate only in special cases of nearly identical guides with a weak coupling situation. Hardy and Streifer [Hr] have extended the accuracy of CMT by starting from the following perturbation assumption:

$$E = E_a + E_b + E_{residual} \qquad (3.23)$$

$$H = H_a + H_b + H_{residual} \qquad (b)$$

instead of the one defined in (3.1). This improves the accuracy of CMT by a few percent, and extends its applicability to stronger coupling, but in very strong coupling situations this approximation is still inaccurate.

Finally, note that CMT was used by Arnaud [Ar2] to demonstrate the coupling of a planar waveguide to a semi–infinite dielectric substrate acting as a mode sink, such as a prism, for example. At first he considered a substrate with a finite thickness and a complex propagation constant, the imaginary part being responsible for the radiation losses. Thus, the propagation constants of the coupled modes, T^+ and T^-, are still given by (3.18) for two guides of equal confinement. Now, by increasing the thickness of the substrate, the number of lossy guided modes increases, until a mode continuum (which characterizes a mode sink) is obtained. Therefore, by adding losses associated with each substrate mode, an expression for the total loss is obtained along with the coupling coefficient. However, as the method is valid for feeble coupling only, and as CMT for two similar guides has already provided an understanding of the weak coupling process, the full development is not given here. We will prefer a plane wave approach to prism coupling, which gives a simple and intuitive understanding of the parameters used in prism coupling application.

3.2 PLANE WAVE ANALYSIS OF PRISM COUPLING

As prism to fibre coupling is a development of the prism to thin film coupler, let us first describe the latter. The prism to thin film coupler was first described by Ulrich and Tien [Ul], and subsequently by numerous workers [Md,Ul2]. Its main application is the input coupler. A light beam coupled via the prism into the guide modes of the planar guide, is a basic problem for a group of optical signal processing devices [Mi,Sb] (e.g., modulators). The high power density obtainable in such films, and the inherent possibilities of phase matching conditions, make the prism to planar guide a suitable device for electro-optics and non-linear experiments.

A second important application of the prism to thin film coupler, is the determination of the characteristic propagation constant of the modes in a given film, by measuring the 'mode angles', which are also used to calculate the refractive index and the thickness of the film [Ul3].

3.2.1 Input coupler

First, we analyse the propagation constant in the half-space formed by the prism and the air-gap. There is total reflection (see fig.3.5), provided that the incident angle at the base of the prism satisfies Snell's law:

$$\theta_p > \theta_{cp} = \sin^{-1}(1/n_p) \qquad (3.24)$$

where θ_p and θ_{cp} are the incident and critical angles, respectively, at the base of the prism, and where n_p is the refractive index of the prism.

The superposition of the incident and reflective plane waves at the base of the prism/air interface, yields a standing wave along the vertical x-axis in the denser medium. Below the interface, the standing wave continues into an exponentially decreasing function, which is said to be evanescent, since it decreases rapidly in the air medium, and does not represent a free radiation.

The incoming wave in the prism has a wave vector of magnitude: kn_p, which can be decomposed into a vertical component, and a horizontal one of magnitude: $kn_p \sin\theta_p$, which is equal to the propagation contant, β_p, of a free wave in the

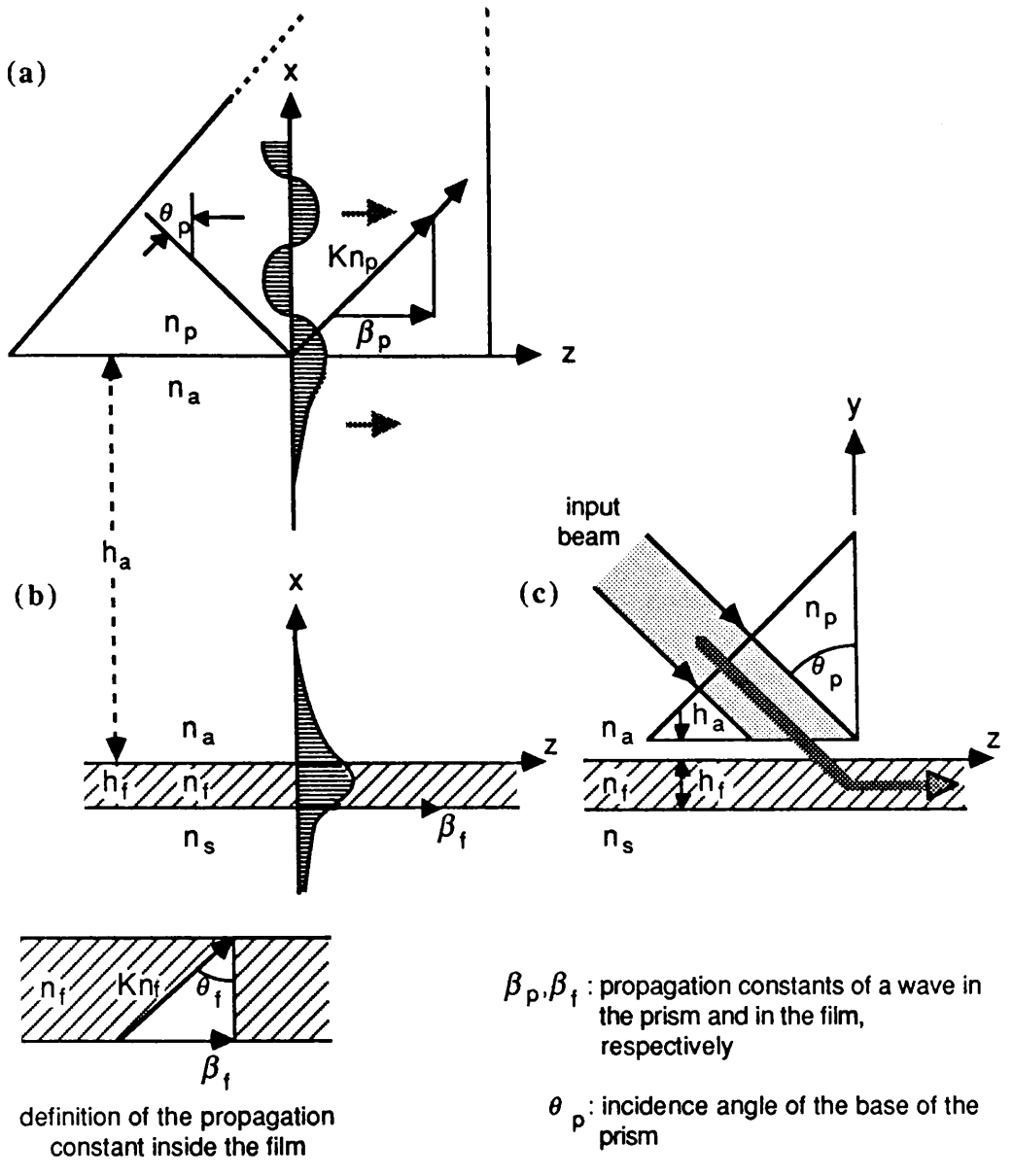

definition of the propagation constant inside the film

β_p, β_f : propagation constants of a wave in the prism and in the film, respectively

θ_p : incidence angle of the base of the prism

FIGURE 3.5

Coupled– mode description of prism coupler:

a. Field of a plane wave incident from a denser medium, undergoing total reflection at the interface to a rarer medium, i.e, $\theta > \theta_c = \sin^{-1}(n_a/n_b)$.

b. Field of a surface wave propagating along a thin film, with $n_f > n_a, n_c$.

c. The two preceding configurations can be brought together by letting h_a become very small, thus obtaining the prism– air– gap– thin– film structure shown here. The incident field now couples to the surface wave via the evanescent field in the air gap.

prism. The entire field can be regarded as a radiation mode in the half-space geometry, which propagates in the z-direction as a function of the form: $\exp(i\beta z)$.

Secondly, consider the second waveguide which is formed by a film on a substrate. With a similar ray approach, its corresponding propagation constant, β_f, of the plane wave becomes:

$$\beta_f = k\, n_f \sin\theta_f \tag{3.25}$$

Note that, β_f corresponds to one discrete mode. Therefore, the critical angle at the interface film/substrate is:

$$\theta_{cf} = \sin^{-1}(n_s/n_f) \tag{3.26}$$

with n_s and n_f being the refractive indices of the substrate and the film, respectively. It follows that the range of all possible guided modes is expressed by the following inequation:

$$kn_s < \beta_f < kn_f \tag{3.27}$$

Observe from fig. 3.5, that each guided mode has its own evanescent fields extending into the substrate and the air gap.

Finally, the whole structure formed by the prism on top of the film is considered. Provided the air gap between the prism and the film is sufficiently small (one eight to one fourth of the vacuum optical wavelength), the reflection at the base of the prism is no longer total, but frustrated by the presence of the guiding layer of the planar guide. If the radiation mode of the prism has the same propagation constant as one mode of the planar guide (i.e., $\beta_p = \beta_f = \beta$), some energy of the beam in the prism will tunnel through the air gap into the film. The optical tunnelling, which constitutes a leakage of energy, will be explained in sect. 3.2.6.

3.2.2 Phase matching conditions and design of the prism

The degeneracy of the propagation constants of the modes to be coupled is necessary to obtain an efficient evanescent coupling, as proved in sect. 3.3.2. This condition is equivalent to a phase matching condition, and is effectuated by changing the angle of the incoming light at the entrance of the prism, θ_i, and thus also the angle, θ_p, at the base of the prism, as described in fig. 3.6. Provided a refractive

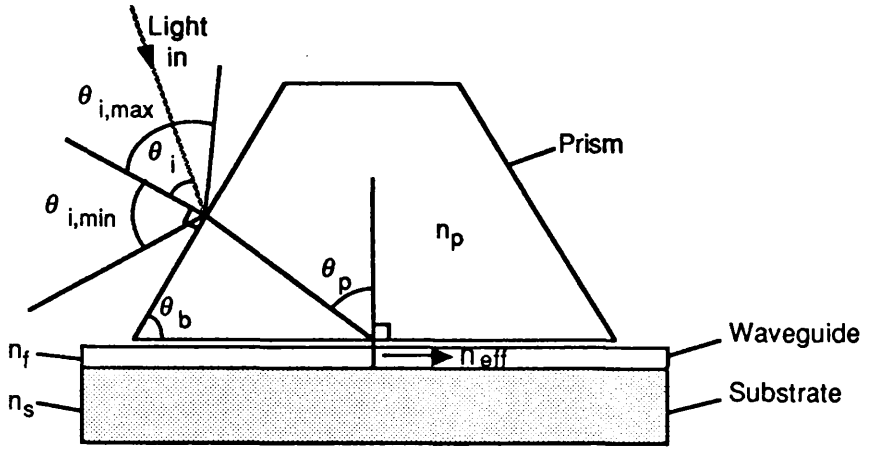

θ_b : base angle of the prism

θ_p : input angle of the light at the base of the prism

θ_i : input angle of the light at the entrance of the prism

$\theta_{i,max}, \theta_{i,min}$: maximum and minimum input angles

n_{eff} : effective index of the excited mode

n_p, n_f, n_s : refractive indices of the prism, the film, and the substrate

FIGURE 3.6

Geometry of the symmetrical prism on film waveguide, which defines the variables of the input coupler from a prism to a selected guided mode of effective index: n_{eff}, propagating inside the film.

index of a guided mode of the prism superior to the effective index of a guided mode of the film, it is possible to couple to any guided mode by selecting the suitable synchronous input angle: θ_i, of the light wave at the entrance of the prism. All the range of input angles comprised between the minimal value: $\theta_{i,max}$ and the maximal value: $\theta_{i,min}$, both chosen at grazing incidence, is defined by the following relation:

$$-\pi/2 < \theta_{i,min} < \theta_i < \theta_{i,max} < \pi/2 \qquad (3.28)$$

It follows that, all the guided modes can be excited only if the base angle of the prism satisfies the inequation:

$$\theta_b = \arcsin \frac{n_{eff}}{n_p} + \arcsin\left\{ \frac{1}{n_p} \sin\theta_i \right\} \qquad (3.29)$$

calculated by Snell's law.

The design considerations of the prism are well described by Seligson [Sg] and Ulrich [Ul3].

3.2.3 Coupling length

We have previously defined the necessary conditions for the transfer of light from the prism to the film. However, the energy transferred in the planar guide in the region $0 < z < L_p$, defined by fig. 3.7b, escapes back to the prism in the region $z > L_p$. This leakage of energy from the film is due to the frustrated reflection at the film/air gap interface, caused by the presence of the prism. In a first approximation, Tamir [Tm] described that the maximal coupling of a uniform beam occurs after a coupling length, L_p, defined as:

$$L_p = 2a / \cos\theta_p \qquad (3.30)$$

where 2a is the incident beam width and θ_p is the incidence angle at the base of the prism. It follows that, if the prism coupling is stopped after a coupling length, the coupled energy is trapped in the film and propagates. This is done by using a right angle prism as described in fig. 3.7b.

In more accurate analysis, Tien [Tn] for example, considered a uniform beam at the base of a right angle prism between $x = 0$ and $x = L$ satisfying the phase

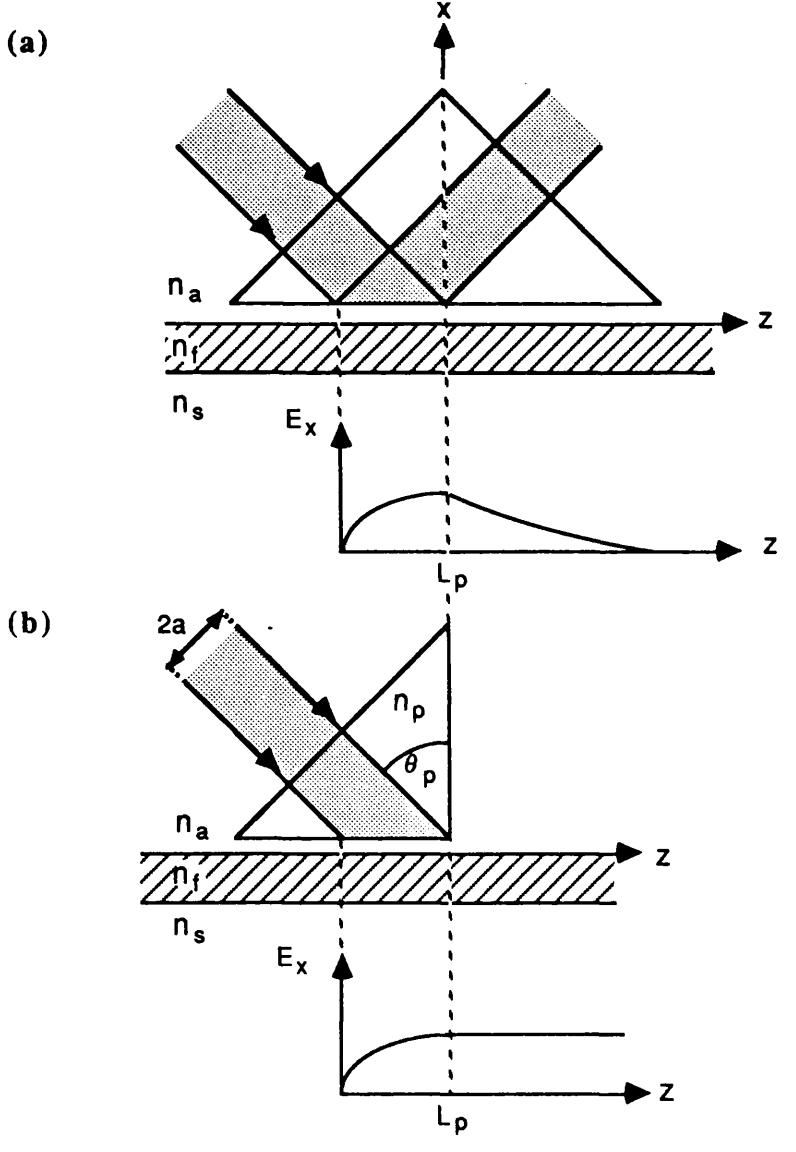

L_p : coupling length

2a : diameter of input beam

θ_p : incident angle at the base of the prism

FIGURE 3.7

Use of symmetrical and right angle prisms in an input coupling situation:

a. The light energy transferred from the symmetrical prism in the region $0 < z < L_p$ is returned to the prism in the region $z > L_p$. The net energy is therefore 0.

b. By using a right angle prism, coupling between the prism and the film stops in the region $z > L_p$. The light wave coupled into the film in the region $0 < z < Lp$ is therefore retained in the film and continues to propagate.

matching condition, and showed that the coupling efficiency, η, was:

$$\eta = 2/\ SL(1 - \exp(-SL))^2 \qquad (3.31)$$

where L was the interaction length.

By maximizing the above expression with respect to SL, he found the maximum coupling length:

$$SL = 1.25 \qquad (b)$$

where the coupling strength, S, was defined by equation 15 in reference [Tn].

In the coupling situation represented in fig. 3.7, complete transfer of energy from the beam surface wave cannot occur even if all the media are lossless. This is due to the fact that the amplitude variation within the beam cross-section has been neglected. Tien also showed that a maximum energy of about 80% can be coupled in the case of an incident beam having a uniform or Gaussian profile, with a constant air-gap between the prism and the film. Nevertheless, a perfect input coupler (100% efficient) could be realised, if the input light would be properly distributed along the coupling gap, since the uncoupled light is immediately lost upon being reflected at the base of the prism. This implies that, the field distribution of the output coupler has to match the field distribution of an equivalent output coupler with the same coupling conditions, where the amplitude leakage of the light in the right angle of the prism could be described by:

$$b_p(x) = b_p(0)\ \exp(-Sx),\ x>0 \qquad (3.32)$$

$$b_p(x) = 0 \qquad ,\ x<0 \qquad (b)$$

A better field distribution can be achieved, for example, by varying the air-gap between the planar waveguide and the prism ([Tm] sect. 3.1.5).

3.2.4 m-lines

Nevertheless, the symmetrical prism is used for the determination of mode angles. As seen in the previous section, the energy fed into the film is returned after one coupling length. However, as the film in practice is not perfect and scatters light, a more complex phenomenon occurs. Since the incident angle of the beam is chosen to match the propagation constant of one mode, the energy is

coupled to that selected mode. Then, some of the energy in the film is rapidly scattered into other waveguide modes. It follows, that the light wave coupled back to the prism consists of many waveguide modes. The reflection of each mode onto a screen appears as an m− line, as described in fig. 3.8. The angle of reflection allows us to calculate the corresponding propagation constant. The reflected main beam is on the m− line which corresponds to the excited mode.

Therefore, by measuring the deviation angle of the different m− lines, it is possible to calculate the propagation constant of the modes by means of the ray approach.

3.2.5 Output coupler

By reciprocity relations, the behaviour of a plane wave propagating in the film and then coupled out into the prism, can be deduced. However, as the prism supports only radiation modes, the light is not coupled back to the prism. Note, that the energy of each mode is coupled out into the m− lines.

3.2.6 Leaky wave theory of beam coupler

a. Inhomogeneous plane wave

We first recall that the solution of the Helmholtz equation in the guiding region of a step index slab waveguide, can be expressed in terms of plane waves, as in:

$$\psi = \psi_0 \exp\{i(k_x x + k_z z)\} \tag{3.33}$$

where $(k_x^2 + k_z^2)^{1/2} = k$ is the wave number in free space, and

ψ stands for the scalar field.

Note that, we assume a two dimensional situation ($\partial/\partial y$) and a time dependence of the form $\exp(-i\omega t)$, as in sect. 2.1.2, with the solution of the fields expressed in rectangular coordinates.

If the wave vector components: k_x and k_z, satisfying the following relations:

$$k_x = k \cos\varphi \tag{3.33b}$$

$$k_z = k \sin\varphi \tag{3.33c}$$

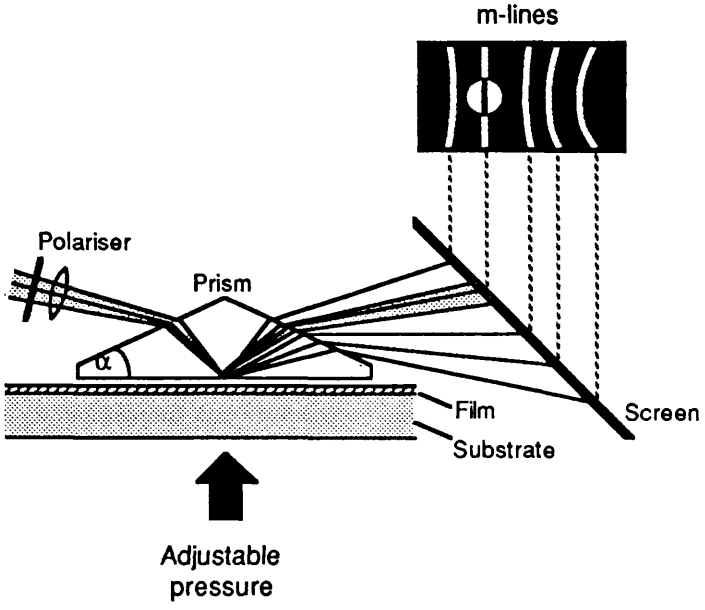

FIGURE 3.8

Experimental arrangement for observation of the mode spectrum of a thin− film waveguide.
Each m− line is set for one mode, the main beam being on the m− line of the corresponding excited mode.

are real, then ψ in (3.33) is an homogeneous plane wave, which propagates at an angle φ, with respect to the x− axis.

Now, let us consider k_x and k_z as complex numbers defined by:

$$k_x n = b - ia \qquad (3.34)$$

$$k_z n = \beta - i\alpha \qquad (b)$$

so that the modulus of the wave vector: **k**, still satisfies the relation: $|\mathbf{k}| = k$.
Due to the complex value of the wave vector along the x− axis of both media of refractive indices: n_1 and n_2, the reflection of a TE and a TM wave are no longer total (see fig 3.9b), so that in general, the magnitude of the reflection coefficient cannot be unity. Therefore, some energy is refracted into the less dense medium, even if the incident angle, θ_1, is larger than the critical angle, θ_c. However, for $\theta_1 > \theta_c$ and for $\beta \gg \alpha > 0$, the refracted energy is small and the magnitude of the reflection coefficient is close to unity. This implies that, some energy leaks into the outer region, as for example at the interface between the guiding layer and the superstrate in fig. 3.9.b. This leakage rate is expressed by rewriting the plane wave equation as in (3.33), but this time with the complex propagation coefficient, such that:

$$\psi = \psi_0 \exp(ax + \alpha z) \exp i(bx + \beta z) \qquad (3.35)$$

where the imaginary part of the propagation coefficient is responsible for the radiation loss, which is consistent with a field decay of the form $\exp(-\alpha z)$ along the longitudinal axis.

Consequently, (3.34) is still a plane wave because the equi− phase and equi− amplitude of the fields are plane. This wave is known as an inhomogeneous plane wave because the variation of the field intensity along any equi− phase line is plane.

b. Leaky wave in beam coupler

First of all, we consider a planar guide formed by a film on a substrate, in which a surface wave of propagation constant β_{sw} is guided. Next, we introduce a prism on top of the film, leaving an air− gap between the two.

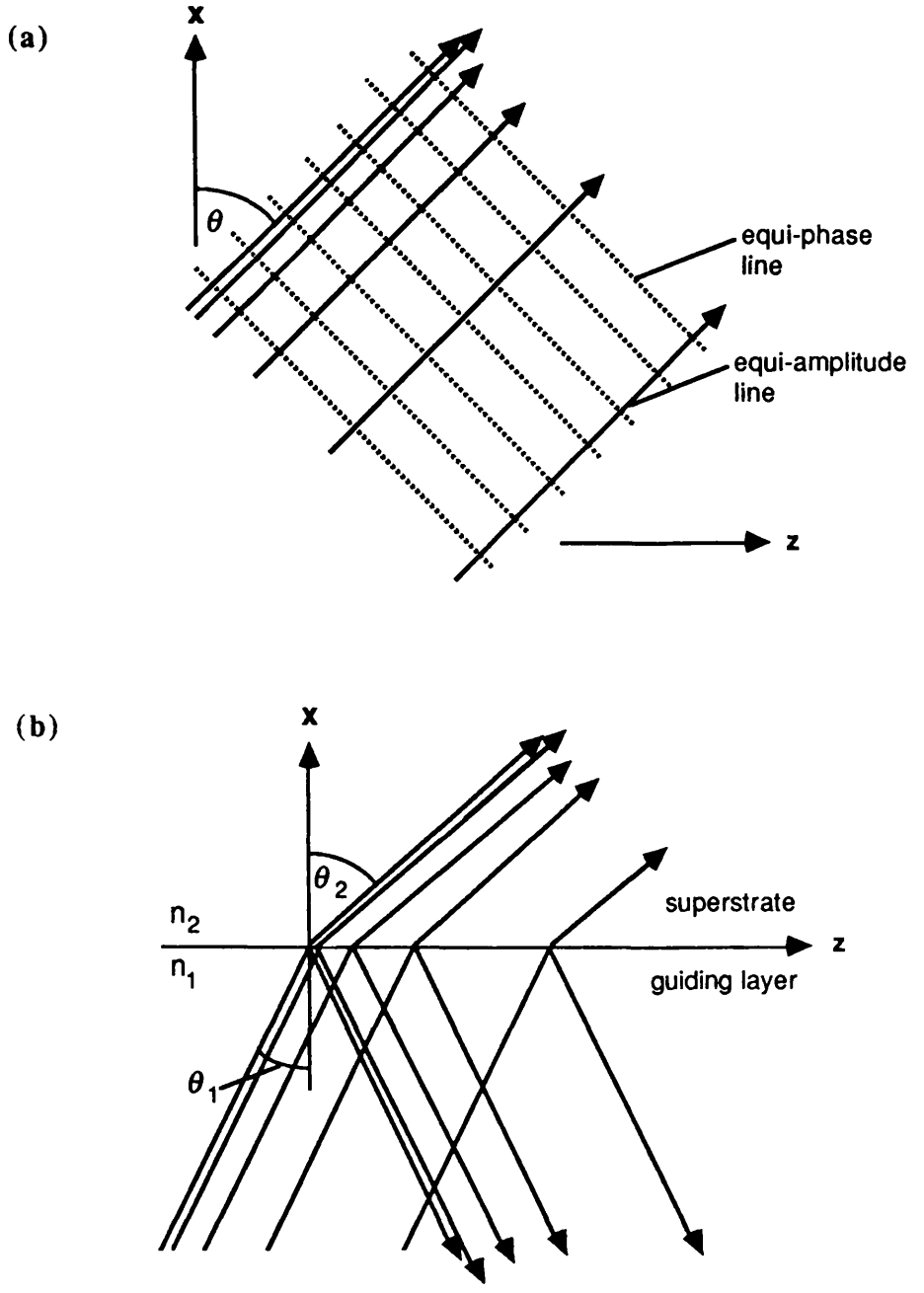

FIGURE 3.9

Fields of inhomogeneous plane wave:

a. Propagation of an inhomogeneous plane wave in free space.

b. Reflection and refraction (leakage) of an inhomogeneous plane wave at the interface between two dielectric media. The density of the amplitude (flux) lines suggests the magnitude of the field intensity, which decays in a direction parallel to the equi– phase lines.

Therefore, the reflection of the wave at the film/air−gap interface is frustrated by the presence of the higher refractive index prism. It follows, that the wave in the film below the prism is a leaky wave, having a propagation constant: $k_z = \beta - i\alpha$. If β is now very close to β_{sw}, and if the leakage is weak, i.e., $\alpha \ll \beta$, a surface wave varying as $\exp(-i\beta_{sw}z)$ and incident from the left as in fig. 3.10a, will be smoothly transmitted as a leaky wave varying as $\exp(-ik_z z)$, past the $z=0$ plane. Due to the leakage of energy in the region where $z>0$, power is radiated away from the thin film as in fig. 3.10b, in the form of a beam that progresses in the film at an angle, θ_1, given by the relation:

$$\theta_1 = \tan^{-1}(\beta/b) \qquad (3.36)$$

Then the angle of radiation of the fields in the prism, θ_2, is deduced from the refraction law, so that:

$$\theta_2 = \sin^{-1}((n_1/n_2)\ \sin\theta_1) \qquad (3.37)$$

Finally, note that an eigenvalue equation or transverse resonance equation can still be used to identify a leaky mode. The phase shifts are then complex rather than real, but the picture of the wave inside the guide is still a zig−zag wave, as shown in fig. 3.10.

3.3 PRISM COUPLING TO A FIBRE

The prism to fibre coupler is a development of the prism to thin film coupler previously described. The ray approach is however valid only for multimode fibres. Starting from Maxwell's equations in the core region, it can be shown that for large values of core radius, the waves in the guide can be described in plane wave terms, with three orthogonal wave vector components: k_z, k_φ, and k_r. These are illustrated in fig. 3.11. Also shown in the same figure, are the angles α_s and α_e, which respectively indicate the angle of skew and the angle of elevation of the local plane wave in the fibre. These relations are simply expressed as in:

$$\alpha_s = \tan^{-1}(k\varphi/\beta) \qquad (3.38)$$

$$\alpha_e = \tan^{-1}(kr/\beta) \qquad (b)$$

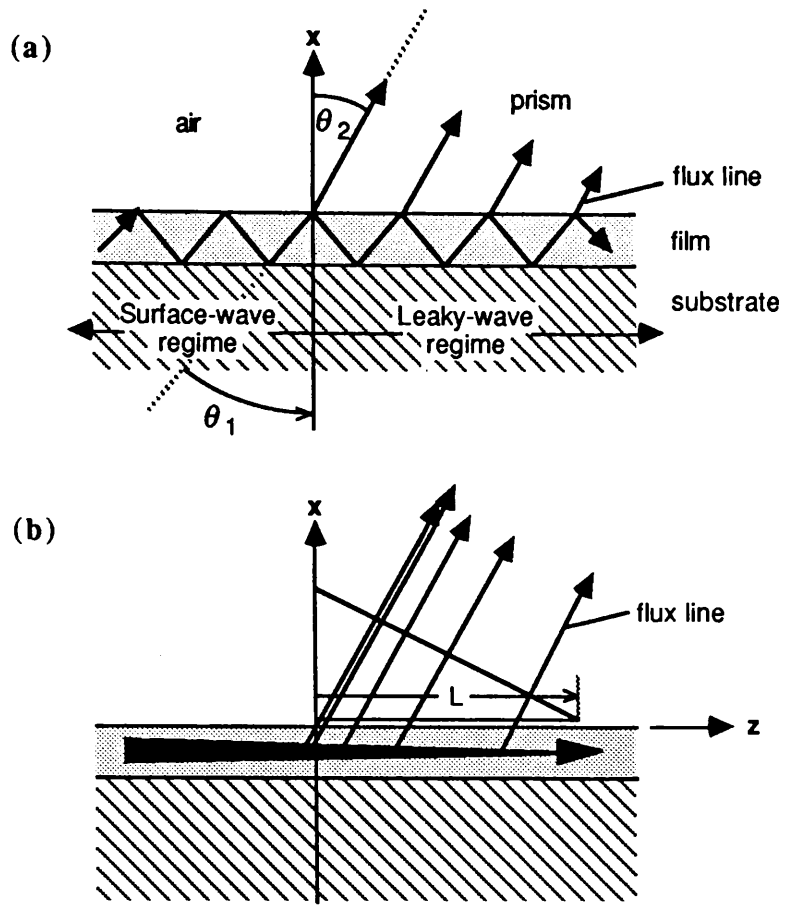

θ_1 : incidence angle inside the film

θ_2 : radiation angle due to leakage of energy inside the film

FIGURE 3.10

Leaky wave description of prism coupler:

a. basic film– on– substrate configuration;

b. leakage due to prism coupling. The density and thickness of flux lines suggests intensity variation.

where $\mathbf{k}(\varphi,r,z)$ is the wave vector in a homogeneous medium of refractive index n_c, so that:

$$|k| = k^2 n_c^2 = k_r^2 + k_\varphi^2 + \beta^2 \qquad (3.39)$$

3.3.1. Modification of the cladding

Optical fibres have thick cladding layers, specially chosen so that the evanescent field at the outer cladding surface is negligibly small for all well guided modes. Therefore, to reach the evanescent field of the fibre, and thus allow optical tunnelling of some energy from the fibre to the prism, or vice versa, the cladding thickness has to be reduced.

If enough cladding is removed so that the core is nearly reached, it is possible to create a leaky mode situation for all guided modes of the fibres.

There are several ways of doing this:

1. One method was illustrated by Midwinter [Md], who tapered down a fibre on its full circumference. The result is that the light of an output coupler radiates all around the modified cladding in the shape of a cone. Consequently, only low efficiency coupling is possible, as the field distribution of the equivalent output coupler is impossible to reproduce. This tapered fibre cannot be used to couple to other guides, and is thus of little interest.

2. Secondly, the cladding can be modified locally at one side of the fibre contour. This is effectuated by polishing, as for the directional coupler (see sect. 1.2.1), or by etching a D–fibre locally. By the etching process, some cladding is removed all around the core, including the flat surface, which remains flat. Thus, we obtain a smaller core–flat distance, which enables evanescent field coupling.

3. Finally, a D–fibre with a very small core/flat distance can be used (see sect.1.2.2), although with this method the fibre becomes very sensitive to bending. Nevertheless, a small sample of D–fibre can be spliced to a normal fibre to reduce radiation losses outside the coupling region.

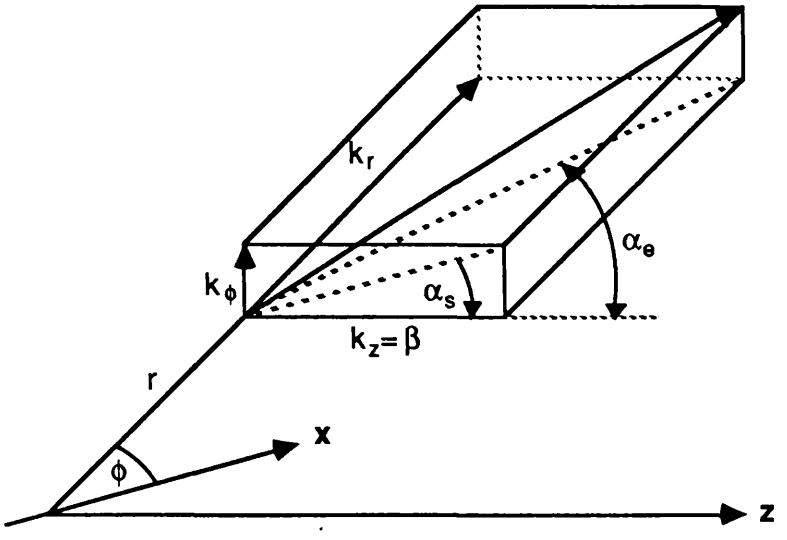

$\alpha_e = \tan^{-1}(k_{r/\beta})$: elevation angle

$\alpha_s = \tan^{-1}(k_{\phi/\beta})$: skew angle

β : propagation constant of a guided mode

FIGURE 3.11

Definition of the vector wave components in a cylindrical coordinate system with: $\mathbf{k} = k_\varphi\ \varphi + k_r\ r + k_z\ z$, where $\beta = k_z n$ is the propagation constant of a guided mode inside the fibre, n being the refractive index of the fibre core.

3.3.2 Phase matching conditions

From the study of the prism to thin film coupler, it is evident that efficient coupling is achieved when the best possible phase matching occurs between an incoming quasi− plane wave from a laser beam, and the local plane wave of the fibre at the point of conjunction. Note that, the condition of a sufficient overlap between the evanescent wave at the base of the prism, and the evanescent radial wave of the fibre, is implicit.

Thus, for the optimum excitation of a particular mode, the synchronous and tilt angles: θ_m and φ_e, at the entrance of the prism, must be selected to phase match the characteristic skew and elevation angles: α_s and α_e, of the ray inside the fibre corresponding to the chosen mode.

From simple geometrical considerations as seen in fig. 3.12, we obtain:

$$\theta_m = \sin^{-1}[n_p \sin(\sin^{-1}(\sin\alpha_e\, n_{core}/n_p) - \alpha_p)] \qquad (3.40)$$

$$\varphi_e = \sin^{-1}(n_p \sin\alpha_s) = \sin^{-1}(n_p k_\varphi) \qquad (b)$$

where the subscript m denotes the angle at the entrance of the prism,

n_p and α_p are the prism refractive index and angle, respectively,

and k_φ is the angular component of the vector wave, expressed in a cylindrical coordinate system as defined previously in fig. 3.11.

Observe that, as in the prism to thin film coupler, each mode of the fibre has its corresponding m− line, which allows the characterization of its different propagation constants. Finally, note that as the fundamental mode (HE_{11} or LP_{01}) and the higher order HE_{1m} modes of a fibre satisfy the scalar wave equation, they have no azimuthal variation, i.e., $\alpha_s = 0$. Therefore, they are formed by meridional rays only.

3.3.3 Launching efficiency of a prism to fibre coupler

As a first approximation, the coupling region can be divided into the xy and xz− planes, and the efficiency in each plane is discussed separately.

In the xz− plane, we can apply the results for the efficiency of a plane wave such as in the prism/film coupler (see sect. 3.2.3), which can be noted as η_{xz}, and

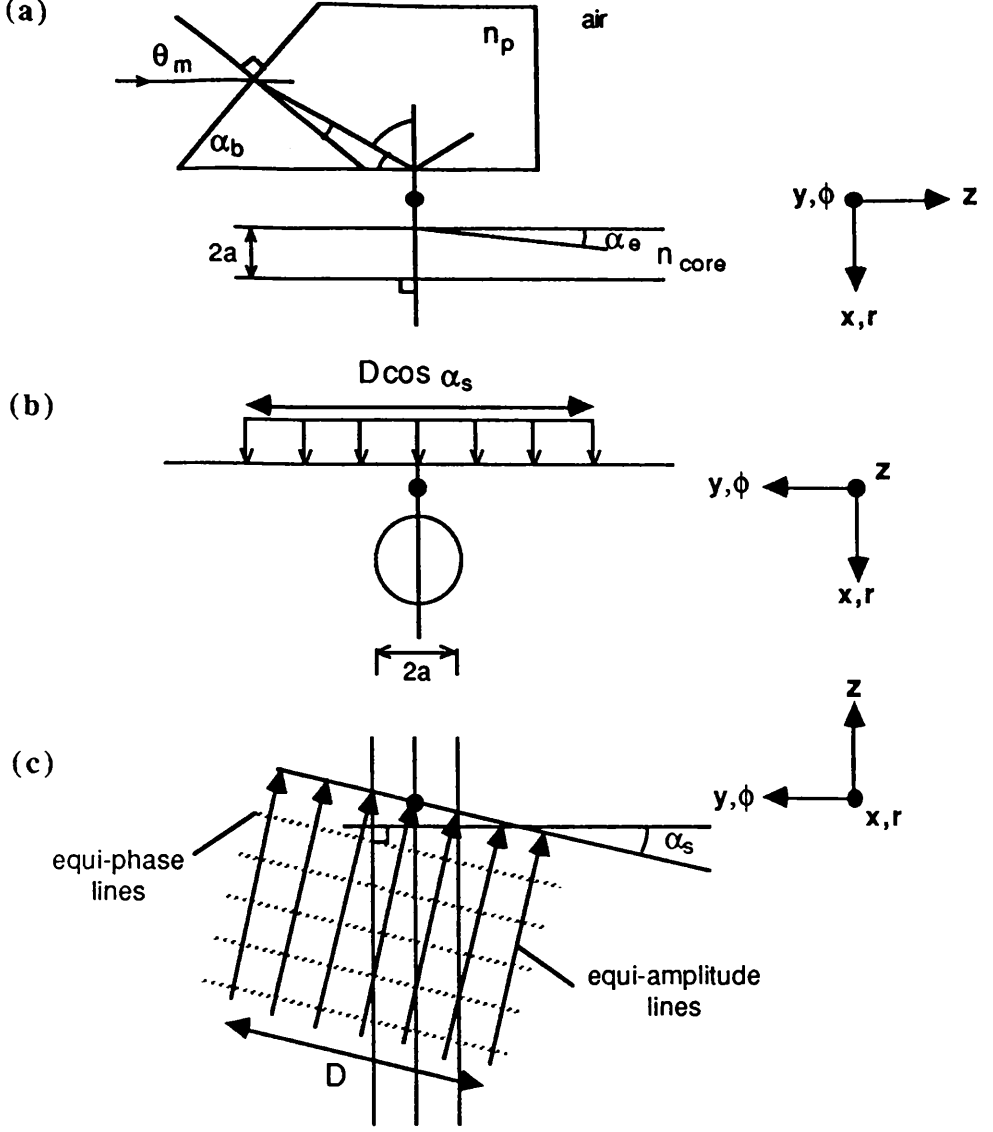

θ_m : synchronous angle

α_b : base angle of the prism

2a : diameter of the fibre core

α_e : elevation angle

α_s : skew angle

D : diameter of the incoming beam

FIGURE 3.12

Geometry of prism/circular fibre coupler.

a. The synchronous angle, θ_m, at the entrance of the prism, allows the phase matching of the elevation angle, α_e, inside the fibre core.

b, c. The appropriate skew angle, α_s, defined in fig. b and c is obtained by variation of a tilt angle, $\varphi_e = \sin^{-1}(n_p \sin\alpha_s)$, of the prism.

is equal to the value in equation (3.31).

However, in the xy– plane the situation is more complex. Not only does the strength of the coupling vary in the y– direction, but due to the geometry of the cross– section, the radial wave vector component, k_r, becomes mismatched with the incoming evanescent wave vector in the air– gap medium along the y– axis. Therefore, coupling occurs only over a small region, which is defined by Millar [M] as:

$$y(0) \pm \delta_y \sec\alpha_s/2 \qquad (3.41)$$

so that the efficiency, η_{xy}, in the xy– plane will be:

$$\eta_{xy} = \delta_{xy} \sec\alpha_s/D \qquad (3.42)$$

where D is the width of the incoming beam.

Note, that δ_y has been estimated as an order lower than the fibre diameter.

Finally, we deduce the total efficiency as the product of the two efficiencies, the first one in the xz– plane and the other in the xy– plane, so that:

$$\eta_{total} = \eta_{xy}\,\eta_{xz} \qquad (3.43)$$

CHAPTER FOUR DEFINITION OF THE PROBLEM AND USE OF THE GREEN FUNCTION METHOD

4.1 DEFINITION OF THE PROBLEM AND ASSUMPTIONS

The aim of this project is to try to formulate and solve the perturbation theory for a fibre core in a half−space cladding, by means of the Green functions (GF). We then want to calculate the propagation constants of the perturbed fibre, knowing the refractive indices of the step index fibre. Note, that the core/flat distance as defined in fig. 4.1 can take any value between zero and the distance corresponding to a circular fibre. Thus, we include all the range of D− fibres which can be drawn from a preform (see sect. 1.2.2), or any half− directional coupler formed by a polished fibre (see sect. 1.1.2).

Now let us define the assumptions of our problem.

a. At first, we consider that the whole structure formed by the core, the modified cladding, and the surrounding medium, is translationally invariant in the z− direction, i.e., in the direction of propagation. The problem is therefore reduced from a three dimensional to a two dimensional one.

b. Secondly, the fibre used in our study is weakly guiding, i.e., the profile height is small (see sect. 2.2.3). The previous assumption allows us to substitute the vector wave equation by the scalar wave equation. Hence, we ignore the polarization dependence of the mode fields in the fibre.

c. Finally, we assume that the modes are far from their cutoff frequency (see sect. 2.2.4). This implies a strong guidance of the modes inside the core, and a small evanescent field outside the core. Consequently, as the modes are well confined inside the core, the boundary at the cladding/surrounding medium is supposed to be at infinity, on all but one side. This means that the core is considered to be in a half− space cladding.

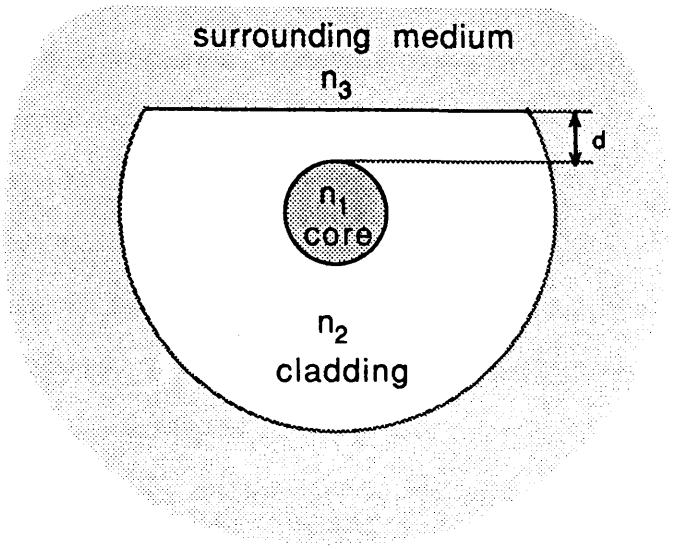

d : variable core/flat distance

n_1 : refractive index of the core

n_2 : refractive index of the cladding

n_3 : refractive index of the surrounding medium

FIGURE 4.1

Fibre core with variable core/flat distance, d, in a half−space cladding.
If $n_1 > n_2 > n_3$, we have the situation of a D−fibre surrounded by a low refractive index medium, for example the air in the case of a D−fibre in isolation.
If $n_3 > n_1 > n_2$, we have a prism coupling situation, provided that the core/flat distance is sufficiently small.

4.2 GENERAL THEORY ON GREEN FUNCTIONS (GF)

We want to study the guiding structure formed by a fibre core in a half-space cladding, as defined in the previous section, by means of the GF. Therefore, let us first introduce the GF and their properties.

4.2.1 Definition and properties of the GF

First of all, let us recall that the electric and magnetic field vectors, E(r,t) and H(r,t), respectively, in a homogeneous medium of refractive index $n=(\epsilon/\epsilon_0)^{1/2}$, satisfy the following Maxwell or field equations:

$$\nabla\times E + \mu_0 \partial H/\partial t = - M \qquad (4.1)$$

$$\nabla\times H - \epsilon \partial E/\partial t = J \qquad (b)$$

where the source excitation: J(r,t) and M(r,t) are, respectively, the vector electric and magnetic current densities, and where ϵ_0 and μ_0 represent, respectively, the dielectric constant and the permeability in the vacuum.

At any time, the field equations are supplemented by the auxiliary equations:

$$\nabla\ \epsilon E = \rho \qquad (4.2)$$

$$\nabla\ \mu_0 H = \rho_m \qquad (b)$$

where ρ and ρ_m are respectively, the electric and magnetic charge densities.

Then, due to the linearity of the field equations, the field can be expressed in terms of the excitation charge densities in the following integral representation:

$$E(r) = -\int G_{11}(r,r')\ \rho(r')\ dr' - \int G_{12}(r,r')\ \rho_m(r')\ dr' \qquad (4.3)$$

$$H(r) = -\int G_{21}(r,r')\ \rho(r')\ dr' - \int G_{22}(r,r')\ \rho_m(r')\ dr' \qquad (b)$$

where the integrals are extended over a volume, within which the currents M and J are non-vanishing, and where the implicit time dependence has been omitted.

From the above equations, we identify the dyadic components $G_{11}.e'$ and $G_{21}.e'$ as being the negative of the vector electric and magnetic field, respectively, at r produced by a unit electric current density at r', in the direction e'. Correspondingly, $G_{12}.e'$ and $G_{22}.e'$ are the negative components of the vector electric and magnetic field, respectively, at r produced by a unit magnetic current

density at r', in the direction e'. The four dyadics are called Green's functions of the electromagnetic fields.

We deduce from the above integral equation that if $G_{11}(r,r')$ is the electric field at the observation point r, caused by a unit source point r'. Thus, the field at the observation point r, caused by a source distribution $\rho(r')$, is proportional to an integral of the GF over the whole range of unit source points constituting the total source. In other words, the field caused by any source distribution can be calculated by adding the effects of each elementary portion of source.

4.2.2 Wave equation for the GF

As the current application involves no magnetic charge densities, ρ_m, we consider a uniform medium with none. It follows that, by substitution of (4.3a,b) into the field equations, we obtain the following defining equations:

$$\nabla \times G_{21} + \epsilon \, \partial G_{11}/\partial t = -1 \, \delta(r - r') \qquad (4.4)$$

$$\nabla \times G_{11} + \mu_0 \, \partial G_{21}/\partial t = 0 \qquad (b)$$

where $\delta(r - r')$ is the delta function,

and 1 is the unit dyadic which is defined by: $1.A = A.1$, with A being a vector.

Next, on elimination of the GF: G_{21}, in the defining equation, we obtain the second order differential equation for the electric type of GF: G_{11}, for an homogeneous medium. Hence:

$$\nabla\times\nabla\times G_{11} + \frac{n^2}{c^2} \frac{\partial^2 G_{11}}{\partial t^2} = - \mu_0 \frac{\partial}{\partial t} 1.\delta(r-r') \qquad (4.5)$$

Therefore, G_{11} satisfies the inhomogeneous vector wave equation.

From the above equation, Felsen [Fm] in sect.1, showed that the electromagnetic fields in an unbounded region are derivable from a scalar Green's function: $g(r,r')$, which satisfies the following scalar wave equation:

$$\left[\nabla^2 - \frac{n2}{c^2} \frac{\partial^2}{\partial t^2} \right] g(r,r') = - \delta(r-r') \qquad (4.6)$$

subject to the boundary conditions $g=0$ if $|r - r'| \to \infty$

4.2.3 Boundary conditions and surface charges

At first, we want to show how the solution of an inhomogeneous equation, with homogeneous boundary conditions (BC), will help us to solve a homogeneous equation with inhomogeneous BC. We consider, for example, a homogeneous differential equation in terms of a scalar field potential: $\varphi(x,y)$, which must satisfy an arbitrary set of Dirichlet BC on a surface S (i.e., $\varphi \equiv \varphi_S$ on the surface). This is done by replacing the inhomogeneous BC on S by homogeneous BC: $\varphi = 0$, together with a surface layer of charge density: ρ_S / ϵ, just inside the surface, S, as shown in fig. 4.2, with ρ_S being the surface charge density. The distance to the boundary surface, ϵ, is taken to be much smaller than the radius of curvature of the surface, and also smaller than the distance over which ρ_S varies appreciably. Therefore, for a distance of order ϵ, the surface is plane, and the charge density may be considered uniform. Furthermore, from electrostatics, we can consider that, the normal gradient of potential changes by an amount: $4\pi\rho_S / \epsilon$, when going through such a charge layer. Because ϵ is assumed small, the gradient between the charge layer and the boundary must be very much larger than that outside the charge layer, and can therefore be neglected. Thus, in this region between $x = -\epsilon$ and $x = 0$, the potential must be:

$$\varphi = -(4\pi \rho_S / \epsilon) x \quad , \quad \text{with } -\epsilon < x < 0 \qquad (4.7)$$

Consequently, if we make the surface density: ρ_S, which is infinitesimally close to the boundary, equal to $\varphi_S / 4\pi$, the potential just outside the charge layer at $x = -\epsilon$, is φ_S, and the potential at $x = 0$ is $\varphi = 0$, i.e., the new boundary value we wish to satisfy. Of course, we have not proved the equivalence between a homogeneous equation with inhomogeneous BC, and an inhomogeneous equation with homogeneous BC, but we have made it plausible.

Thus, we deduce that the above property is applicable to either the homogeneous or inhomogeneous scalar wave equation, with inhomogeneous or homogeneous BC, respectively. This implies that the same GF can be used to build up a solution for an arbitrary charge distribution inside the definition domain, as shown by fig. 4.3a, and also for an arbitrary set of Dirichlet BC on the surface enclosing the same definition domain, as described in fig. 4.3b.

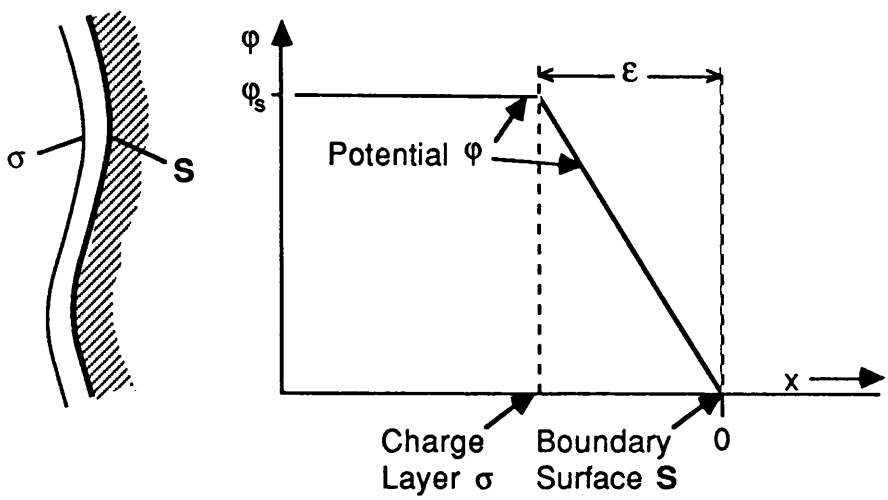

FIGURE 4.2

Potential of a source layer, σ, over a small distance, ϵ, outside a grounded surface S.

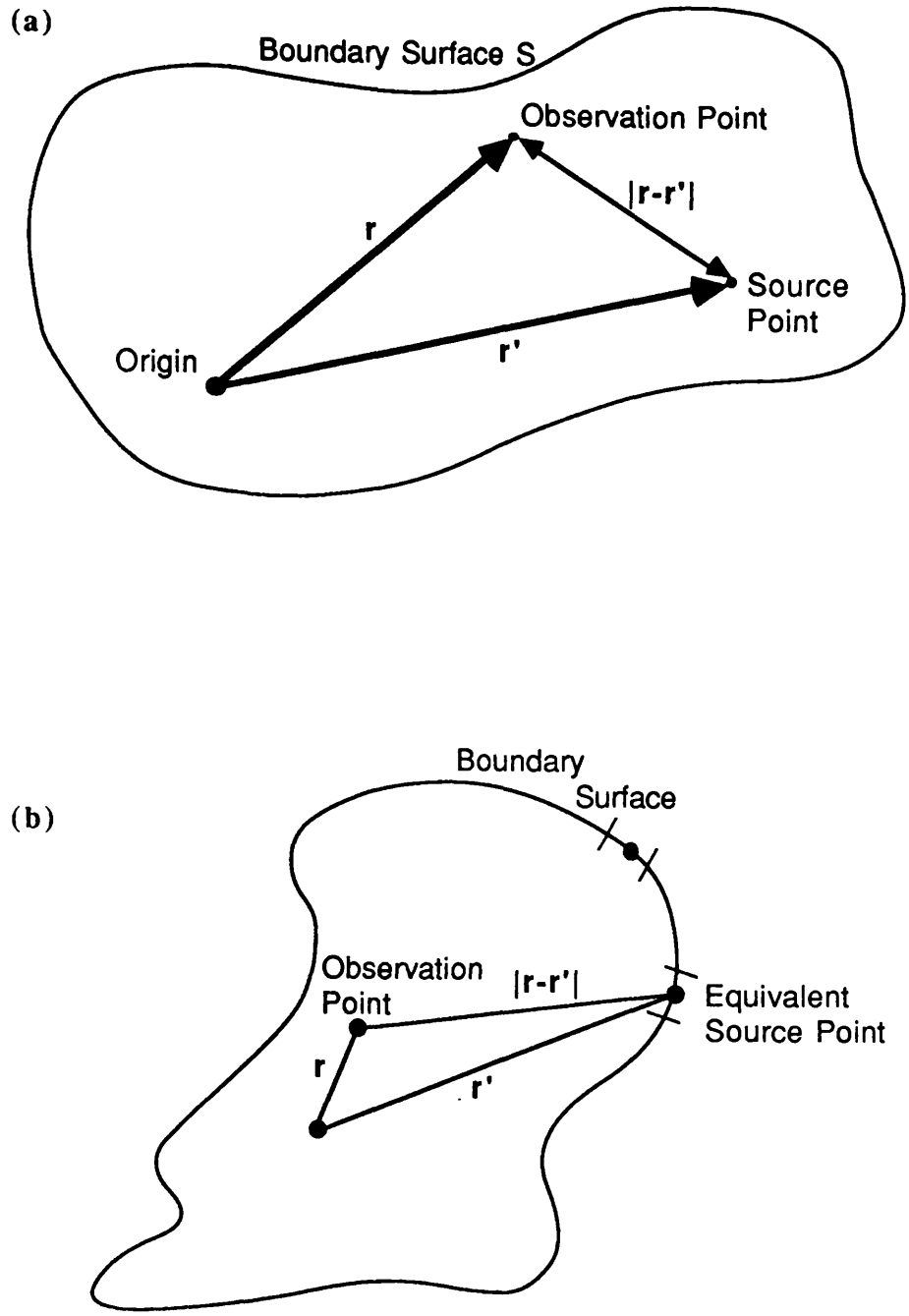

FIGURE 4.3

a. Definition domain of the GF used to build up the solution of an inhomogeneous scalar wave equation with homogeneous boundary conditions (BC). The source and observation points are inside or on the boundary defined by the surface S.

b. Definition domain of the GF leading to the solution of a homogeneous scalar wave equation with inhomogeneous BC. The value of the field at that boundary is replaced by an equivalent unit source distribution, so that the GF is that of an equivalent source point at that boundary.

Therefore, we suppose at first that we know the scalar field: $\psi(\mathbf{r}_s')$ (and/or its gradient), on a surface S. The value of $\psi(\mathbf{r}_s')$, which represents the BC, can be thought of as being equivalent to a unit source distribution on this surface. Thereafter, we want to calculate the field at the observation point: $\mathbf{r}$, with the BC equal to zero, at every point on the surface, except at the point: $\mathbf{r}_s'$. The boundary value behaves as a delta function at this equivalent source point, meaning that the integral over a small surface around $\mathbf{r}_s'$ is unity. Hence, this field at the observation point: $\mathbf{r}$, caused by an equivalent source point at: $\mathbf{r}_s'$, is also a GF noted $g(\mathbf{r},\mathbf{r}_s')$, which will enable us to calculate the inhomogeneous wave equation (4.6).

Finally, as a result of the above equivalence, and the linearity of the scalar wave equation, we can also solve the inhomogeneous equation with inhomogeneous BC, by superposition of the two individual solutions.

4.2.4 Reciprocity relations

We want to show that the GF is a symmetric function of the source and observation point at $\mathbf{r}'$ and $\mathbf{r}$, respectively. We start from (4.6) with the scalar GF: $g(\mathbf{r},\mathbf{r}')$, rewritten below with the implicit time dependence, so that:

$$\nabla^2 g(\mathbf{r},\mathbf{r}') + k^2\, g(\mathbf{r},\mathbf{r}') = -\,\delta(\mathbf{r}-\mathbf{r}') \qquad (4.7)$$

Let us now consider a source point at $\mathbf{r}_1'$, and then write its corresponding differential equation as in:

$$\nabla^2 g(\mathbf{r},\mathbf{r}_1') + k^2\, g(\mathbf{r},\mathbf{r}_1') = -\,\delta(\mathbf{r}-\mathbf{r}_1') \qquad (b)$$

Next, we multiply (4.7a) by $g(\mathbf{r},\mathbf{r}')$, and (4.7b) by $g(\mathbf{r},\mathbf{r}_1')$, and subtract the two resulting equations. Thereby, we obtain after integrating over a volume:

$$0 = \iiint g(\mathbf{r},\mathbf{r}_1')\nabla^2 g(\mathbf{r},\mathbf{r}') - g(\mathbf{r},\mathbf{r}')\nabla^2 g(\mathbf{r},\mathbf{r}_1')\; dV$$

$$+ \iiint g(\mathbf{r},\mathbf{r}_1')\delta(\mathbf{r}-\mathbf{r}') - g(\mathbf{r},\mathbf{r}')\delta(\mathbf{r}-\mathbf{r}_1')\; dV \qquad (4.8)$$

We now recall the second Green's formula, which gives the following relation between a surface and a volume integral, such that:

$$\iint [u\,\nabla v - v\,\nabla u]\, \mathbf{n}_s\; dS = \iiint [u\,\nabla^2 v - v\,\nabla^2 u]\; dV \qquad (4.9)$$

where S is a closed surface bounding the volume V, and $\mathbf{n}_s$ denotes the normal unit

vector, n_S, directed outward from the volume enclosed by the surface S (see fig. 4.4a). The continuity conditions on u and v are defined by Kreizig [Kr] in sect. 9.7, for example. As a result of the above relation, (4.8) becomes:

$$\iint g(r,r')\nabla(g(r,r_1') - g(r,r_1')\nabla(g(r,r')\, n_s\, dS = g(r_1',r') - g(r',r_1')$$

Since both $g(r,r')$ and $g(r,r_1')$ satisfy the same homogeneous BC, the surface integral vanishes, and therefore we have demonstrated the following reciprocity relation:

$$g(r,r') = g(r',r) \qquad (4.10)$$

as long as both r and r' are inside or on the surface of integration.

4.3 DEFINITION OF THE ANALYTICAL PROBLEM: KIRCHHOFF– HUYGENS INTEGRAL

4.3.1. Data

First of all, let us define the problem of a guiding structure formed by a fibre core in a half–space cladding. This guide can be either a D–fibre or a half–fibre coupler based on a conventional fibre, and both fibres are assumed to be monomode with step index profiles. The geometry of the guide implies a longitudinal translational invariance. Each region of the guide is also supposed to be homogeneous. Finally, the fibre is assumed to be weakly guiding, so that the transverse electromagnetic fields satisfy the scalar wave equation (see sect. 2.1.3) in each region, so that:

$$\nabla_t{}^2\psi + K\,\psi = 0 \qquad (4.11)$$

with

$$\nabla^2\psi = \nabla_t{}^2\psi - \beta^2\psi \quad \text{and} \quad K^2 = k^2n^2 - \beta^2 \qquad (b,c)$$

where ψ is the scalar field.

Note that, we have assumed a time harmonic and z–dependence of the form $\exp\{i(\beta z - \omega t)\}$. This assumption also applies to the the next equations.

Then, the fields must also satisfy the boundary conditions (BC) at the core/cladding and cladding/surrounding medium interfaces, as described in fig. 4.1. However, due to the boundary at the flat surface of the cladding, it is impossible to

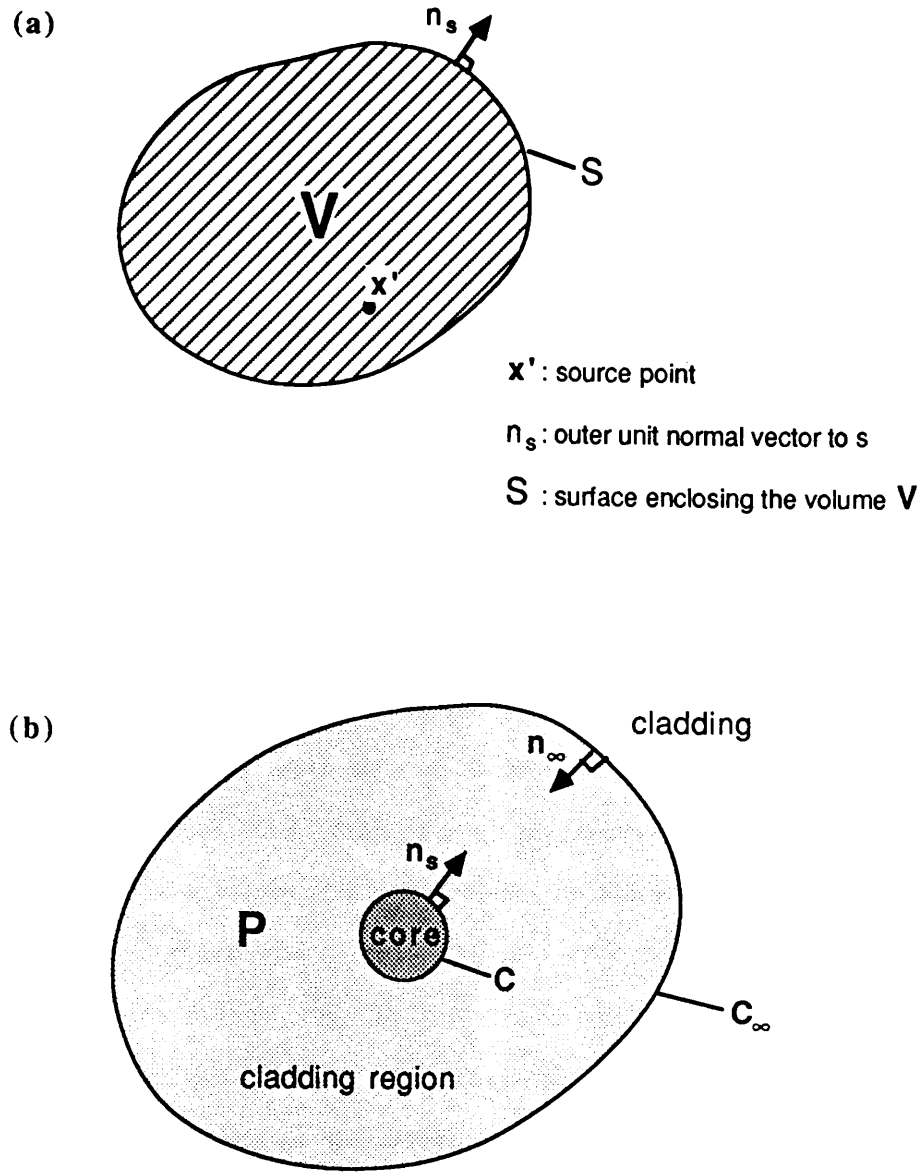

FIGURE 4.4

a. Definition domain for Green's second formula with the source points inside or on the surface, S, enclosing the definition domain, P, and applied to a three dimensional problem.

b. Definition domain for Green's second formula with the source points on or outside the contour, C. Note, that the definition domain defined between the contours C and C_∞, is closed at infinity by the contour, C_∞.

find an appropriate coordinate system which would enable the separation of the partial differential equation (4.11) in terms of coordinates: ξ_n, so that each boundary would correspond to one (or more) coordinate equal to a constant, i.e., ξ_n= constant.

This explains the reason for the use of a numerical method, in our case the GF method as opposed to the eigenfunction method or modal expansion Mf.

4.3.2 Development leading to the Kirchhoff– Huygens integral

Now we consider the GF of our study. In sect. 4.2, we have shown that a GF expressed the field at one observation point (r), caused by one source point when the BC are homogeneous and the equation to satisfy is inhomogeneous. The same GF applies if the GF is caused by one equivalent source point, when the BC are inhomogeneous and the scalar wave equation homogeneous, as in our problem. In both cases the GF, which must satisfy the inhomogeneous scalar wave equation (4.7a), written below, with a time and $z-$dependence as defined in (4.11b,c), as in:

$$\nabla_t^2 g(\mathbf{r},\mathbf{r}') + K\, g(\mathbf{r},\mathbf{r}') = -\,\delta(\mathbf{r}-\mathbf{r}') \qquad (4.12)$$

Let us assume that we know the GF for an equivalent source point at the core/cladding interface, which will be calculated in chapter 5, and which will also satisfy the boundary conditions at the cladding/surrounding medium interface. With the previous considerations, we can thus show that the homogeneous scalar wave equation having inhomogeneous BC at the core/cladding interface, may be expressed in terms of $g(\mathbf{r},\mathbf{r}')$.

To do this, we first multiply (4.12) by ψ and (4.11) by $g(\mathbf{r},\mathbf{r}')$, and subtract the product, exchanging $\mathbf{r}$ for $\mathbf{r}'$ at the same time, so that:

$$\psi(\mathbf{r}')\,\nabla_t^2 g(\mathbf{r},\mathbf{r}') - g(\mathbf{r},\mathbf{r}')\,\nabla_t^2\psi(\mathbf{r}') + \psi(\mathbf{r}')\,\delta(\mathbf{r}-\mathbf{r}') = 0 \qquad (4.13)$$

As the $z-$invariance implies a two dimensional problem, we want to integrate equation (4.13) over the xy– plane, and then by using the second Green's formula (see 4.9), to reduce it to a line integral. Therefore, let the definition domain: P, as shown in fig. 4.4b, be limited between the contour of the core: C, which is included, and a contour closed at infinity: C_∞.

Their corresponding normal unit vectors: $\mathbf{n}_s$ and $\mathbf{n}_\infty$, are directed outwards for C and inwards for C_∞, to the centre of the core.

Note that the definition domain is the same for both the source and observation point, so that $C'=C$, $C_\infty'=C'$, and $\mathbf{n}_s'$, $\mathbf{n}_s$ have the same direction.

Thus, the integral of (4.13) over the definition domain, P, with the source points (or equivalent source points) on or outside the contour of the core, becomes:

$$\iint_{S_\infty'} \psi(r')\,\nabla_t^2 g(r,r') - g(r,r')\,\nabla_t^2\psi(r') + \psi(r')\,\delta(r-r')\,ds_\infty' + \iint_{S'} \psi(r')\,\nabla_t^2 g(r,r') - g(r,r')\,\nabla_t^2\psi(r')\,ds' \qquad (4.14)$$

where S_∞' and S' represent, respectively, the surfaces enclosed by the contours C_∞' and C'.

Sommerfeld's radiation conditions at infinity make the integral over S_∞' tend to zero, as defined for example by Jones [Jo] in sect. 1.31 and 1.34.

As a consequence of the previous conditions, and the property of the delta function, the integral around S_∞' is equal to $\psi(r')$, which is the scalar field at the source point (4.14) is reformulated as in:

$$\iint_{S'} \psi(r')\,\nabla_t^2 g(r,r') - g(r,r')\,\nabla_t^2\psi(r')\,dS' + \psi(r') = 0 \qquad (4.15)$$

Thereafter, using Green's formula in the plane, we obtain the following line integral:

$$\oint_{C'} \psi(r')\,\frac{\partial g(r,r')}{\partial n_s'} - \frac{\partial \psi(r')}{\partial n_s'}\,g(r,r')\,dl' = -\psi(r) \qquad (4.16)$$

where l' is the integration path along the contour C'.

Consequently, the above equation is the Kirchhoff–Huygens integral for a two dimensional problem with the following variables:

1. The Green function: $g(r,r')$ is the value chosen for an equivalent source point on the core, which takes into account the boundary conditions at the core/cladding interface due to the equivalence between a boundary condition and a unit source distribution on the contour of that boundary (see sect. 4.2.3).

2. $\psi(\mathbf{r}')$ is the general solution of the homogeneous scalar wave equation at the coordinate of the selected source point.

3. $\psi(\mathbf{r})$ is the expression of scalar field at any observation point inside the definition domain.

Finally, note that the choice of this Kirchhoff– Huygens integral will be justified by further analytical development in chapter 5, leading to one unknown: the propagation constant, β.

4.4 JUSTIFICATION OF THE CHOICE OF THE NUMERICAL GF METHOD

4.4.1 Diverse aspects of numerical methods

A D– fibre with its surrounding medium, constitutes a multi– layer longitudinal uniform waveguide. In order to characterize the guide, Maxwell's equations are the basic relations. These equations are valid over each layer or region, and are subject to the boundary conditions, such that the tangential field components must be continuous at the interface between two regions.

The various numerical methods satisfying Maxwell's equations differ mainly according to three different criteria.

1. Some methods are directly applied to the Maxwell equations, their integral form, or any other reduced forms. However, the majority of the methods are semi– numerical, in the sense that the original equations are transformed through various mathematical modelling schemes, into a system of linear equations solvable by standard matrix techniques.

2. Secondly, one method may approximate the fields over each dielectric layer, or over a subregion of a dielectric layer, as in the finite elements method. Note, that for our GF method, the field is explicitly expressed only for the cladding region (which is sufficient to find β), although the GF has been formulated for all the regions.

3. Thirdly, methods differ from the way they deal with the boundary at infinity.

4.4.2 Different methods to solve a homogeneous problem

Saad [Sm] gives a review of the main methods used in the analysis of the arbitrarily shaped dielectric waveguides. In the case of an isotropic homogeneous guide, our D– fibre for example, for simplicity he considers three main approaches, although a combination between several methods sometimes offers the best solution for one particular case.

1. The first and one of the oldest approaches is the point matching method [Jm], which uses an expansion in series of the fields in each region, and a matching of the tangential field at optimal selected points around the boundaries. However this method would be cumbersome if applied to our problem, and is therefore excluded.
2. The second group of methods is formed by the variational and integral approaches, for example our GF method.
3. Thirdly, the finite elements method [R,Sv] is considered. This method offers probably the most powerful and efficient numerical solution of the most general problem (i.e., for an arbitrarily shaped, inhomogeneous, and anisotropic guide).

Consequently, for the selection of the most appropriate method for our problem, the finite elements method and the GF method were taken into consideration. As the latter method was previously described, we will now give a brief explanation of the finite elements method. For this approach, the waveguide cross– section is divided into a large number of triangles (or elements), and the fields in each element are represented by a polynomial. The continuity conditions of the fields are then imposed on all the interfaces between the different elements. By employing a variational expression for Maxwell's equations, or its equivalent wave equation, an eigenvalue matrix equation is obtained, and solved using standard methods.

4.4.3 Choice of the appropriate numerical method

First of all, we consider the main criterion for selection of the appropriate numerical method for our study, which is the formulation of the boundary conditions, in particular, those at infinity.

For example, the conventional finite elements method is based on the fact that the fields of a mode above cutoff decay in the cladding, so that the infinite cladding can be approximately modelled by a closed region bounded by an artificial Dirichlet boundary, or others [Yh,Mb]. However, in the case of our D− fibre used in coupling situations, the distance core/flat surface of the cladding cannot be considered as infinite. Therefore, in a guided mode situation, the evanescent field also extends into the surrounding medium. Then, if the refractive index of the surrounding medium is higher than that of the cladding as in prism coupling, for example, and if the core/flat distance is small, the evanescent field decay of a guided mode of the D− fibre is slower than that of a guided mode propagating in a similar circular fibre with a cladding supposed to be infinite. Consequently, a larger number of elements outside the fibre in the surrounding medium, would be necessary, as the evanescent field decays very slowly.

On the contrary, for the GF method, the boundary conditions at infinity are formulated in the same way for any refractive index of the surrounding medium. What is more, they are easily included in the GF formulation (see (5.23) and (5.28)), which constitutes one element of our integral equation (5.30), and thus simplifies the calculation leading to the final eigenvalue matrix (5.42).

Furthermore, if we consider the case where the core/flat distance is small enough to allow a non− negligible penetration of the evanescent field inside the surrounding medium, which has a refractive index higher than that of the core, the D− fibre can become leaky. In that situation, the boundary at infinity has no significance, since a leaky mode represents a free radiation in the surrounding medium, and therefore, the field does not decay towards zero at infinity (see sect. 3.2.6). Nevertheless, with the GF method, it would still be possible to calculate the complex propagation constants of the leaky modes, by analytical continuation of the

theory elaborated for the real propagation constants of the guided modes. However, as the finite elements method is purely numerical, no analytical continuation is possible, and thus a leaky mode guiding structure cannot be considered.

Consequently, for a D– fibre supporting guided modes, the GF formulation of the boundary conditions at infinity is exact, and simpler than that of the finite elements method, which requires an approximation of the boundary at infinity and does not enable the direct extension of the study to include leaky modes.

Next, we consider the convenience of the two methods with respect to the particular geometry of the D– fibre. The GF method is ideally suited to planar stratified environments, where the GF can be calculated by an elementary Fourier method. The finite elements method is better suited to application to linear boundaries. The curved boundaries present in our problem would increase the number of numerical operations.

Another important criterion of selection is based on the computational efficiency. As the GF method is not a direct method, it requires more programming tasks to obtain the final matrix, than the finite elements method. At first, in order to solve the Helmholtz equation for the GF, the inverse Fast Fourier transform must be computed, and an iteration of the GF in the x– direction is necessary for each sampling point around the core.

Therefore, the program must be optimized to minimize the computing storage requirement. However, the matrix of the finite elements method is sparser than that of the GF method, but its order is higher.

In conclusion, despite the additional computing requirements, the GF has been chosen to calculate the propagation constant of a D–fibre, with different core/flat distances and surrounded by different refractive index media, because of the intrinsic formulation of the boundary conditions, and the possible extension to leaky mode situations.

5.1 ANALYTICAL PART OF THE CALCULATION OF THE GF

In the previous section we have seen that the GF must satisfy the boundary conditions at the core/cladding and cladding/surrounding medium interfaces. Furthermore, as the definition domain of the GF was chosen on and outside the contour of the core, the scalar field must tend towards zero at infinity.

We have also assumed that the GF would be the that of an equivalent source point at the core/cladding boundary.

Finally, the complete GF must also include the effect of the flat/surrounding medium boundary, the cladding being supposed infinite on all but one side (see fig. 5.4).

Therefore, let us first calculate the GF of a source point in a half-space cladding as defined in fig. 5.1, before solving the Kirchhoff-Huygens integral, from which the different propagation constants of the guided modes of a D-fibre (i.e., for β real) with a variable core/flat distance, will be determined.

5.1.1 Fourier transform of the Helmholz equation

a. Helmholtz equation and choice of the coordinate system

As defined in sect. 4.3, a GF is the solution of the Helmholtz equation, except at the source point. Hence, this equation can be rewritten as below:

$$\frac{\partial^2 g}{\partial x^2} + \frac{\partial^2 g}{\partial y^2} K^2 = - \delta(x-x') \, \delta(y-y') \qquad (5.1)$$

where $K^2 = n^2k^2 - \beta^2$,

$g(\mathbf{r},\mathbf{r}')$ is the scalar GF,

$\mathbf{r}(x,y)$ is the vector position of the observation point,

$\mathbf{r}'(x',y')$ is the vector position of the source point,

n is the refractive index of the medium,

k is the free space wave number,

and β is the propagation constant of one guided mode, and is thus real.

Now, let us choose the appropriate coordinate system for the calculation of the GF of a unit source point in the cladding region, as defined in fig. 5.1.

As the cladding and surrounding medium are infinite along the x− axis, the wave equation possesses a translational invariance along this axis. It follows that, in the x− direction, the solution, which is our GF, depends only on the difference in abscissa between the observation and source points, i.e., on $(x - x')$. Consequently, we can set the abscissa of the source point equal to zero (i.e., $x' = 0$), so that the origin of the x− axis is moving with the source point. Secondly, let the origin of the y− axis be at the interface between the flat surface of the cladding and the surrounding medium. The refractive indices: n_2 and n_3, are those of the cladding and the surrounding medium, respectively.

b. Fourier transform of the differential equation

As the partial differential equation (5.1) is translationally invariant in the x− direction, a Fourier transformation in terms of x, reduces the partial differential equation (5.1) into an ordinary differential equation, with y as the variable, as in:

$$\frac{\partial^2 G}{\partial y^2} + (K^2 - \gamma^2)G = -\delta(y - y') \qquad (5.2)$$

where $K^2 = n_j^2 k^2 - \beta^2$, and n_j is the refractive index of either the cladding $(n_j = n_2)$ or the surrounding medium $(n_j = n_3)$.

Note that we use the time convention $\exp(-i\omega t)$. The Fourier transform is thus defined as:

$$G(\gamma) = \int_{-\infty}^{+\infty} g(x)\, e^{-i\gamma x}\, dx \qquad (5.3)$$

where γ is the spatial angular frequency,

and where the inverse Fourier transform is defined as:

$$g(x) = \frac{1}{2\pi} \int_{-\infty}^{+\infty} G(\gamma)\, e^{i\gamma x}\, d\gamma \qquad (b)$$

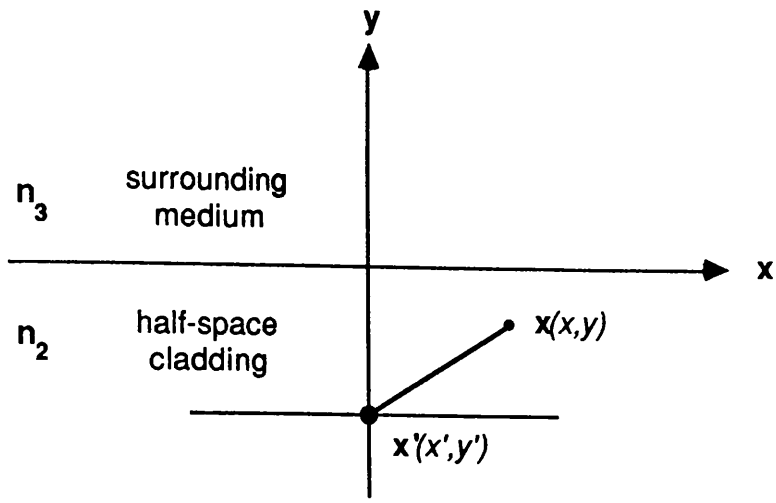

x' : coordinates of the source point

x : coordinates of the observation point

n_3 : refractive index of the surrounding medium

n_2 : refractive index of the cladding

FIGURE 5.1

Definition of the parameters of our GF.
The source and observation points are inside a half-space cladding (interface included). The origin of the x-axis is based on the source point, and that of the y-axis at the interface between the two media.

Now, by rewriting (5.2) for the cladding and surrounding medium regions, we obtain:

$$\frac{\partial^2 G}{\partial y^2} + (K_2^2 - \gamma^2)G = -\delta(y - y') \quad , \qquad \text{for } y < 0 \qquad (5.4)$$

$$\frac{\partial^2 G}{\partial y^2} + (K_3^2 - \gamma^2)G = 0 \quad , \qquad \text{for } y \neq y' \text{ and } y > 0 \qquad (b)$$

with $K_2^2 = n_2^2k^2 - \beta^2$, n_2 being the refractive index of the cladding, and with $K_3^2 = n_3^2k^2 - \beta^2$, n_3 being the refractive index of the surrounding medium.

Then, let us define the sign of the constants: K_2^2 and K_3^2.
If we consider the structure for a D− fibre surrounded by a semi− infinite medium, several refractive index profiles are possible. The value of the propagation constant, β, or its effective refractive index, n_e, determines the possible guidance of a mode as shown in fig. 5.2 and described below.

a. The first case allowing the guidance of a mode is that of a D− fibre/surrounding medium structure with refractive indices satisfying the following inequality as in fig. 5.2a: $n_3 < n_2 < n_e < n_1$. The refractive index of the surrounding medium is lower than that of the cladding, as in the case of a D− fibre surrounded by an air medium.

b. The second case still allows guidance inside the fibre, and is formed by a fibre surrounded by a medium with a higher refractive index than that of the cladding, but lower than the effective refractive index of the mode, as in: $n_2 < n_3 < n_e < n_1$.

c. However, if the effective refractive index is lower than at least one of the refractive indices of the cladding or surrounding medium, this corresponding mode is not guided into the D− fibre, but is leaky.
This is the case of a prism to fibre coupler where the leakage is due to the high refractive index of the surrounding medium. The values of the refractive indices satisfy the following inequation: $n_2 < n_e < n_3$, and their values in comparison with the effective refractive index of the mode are

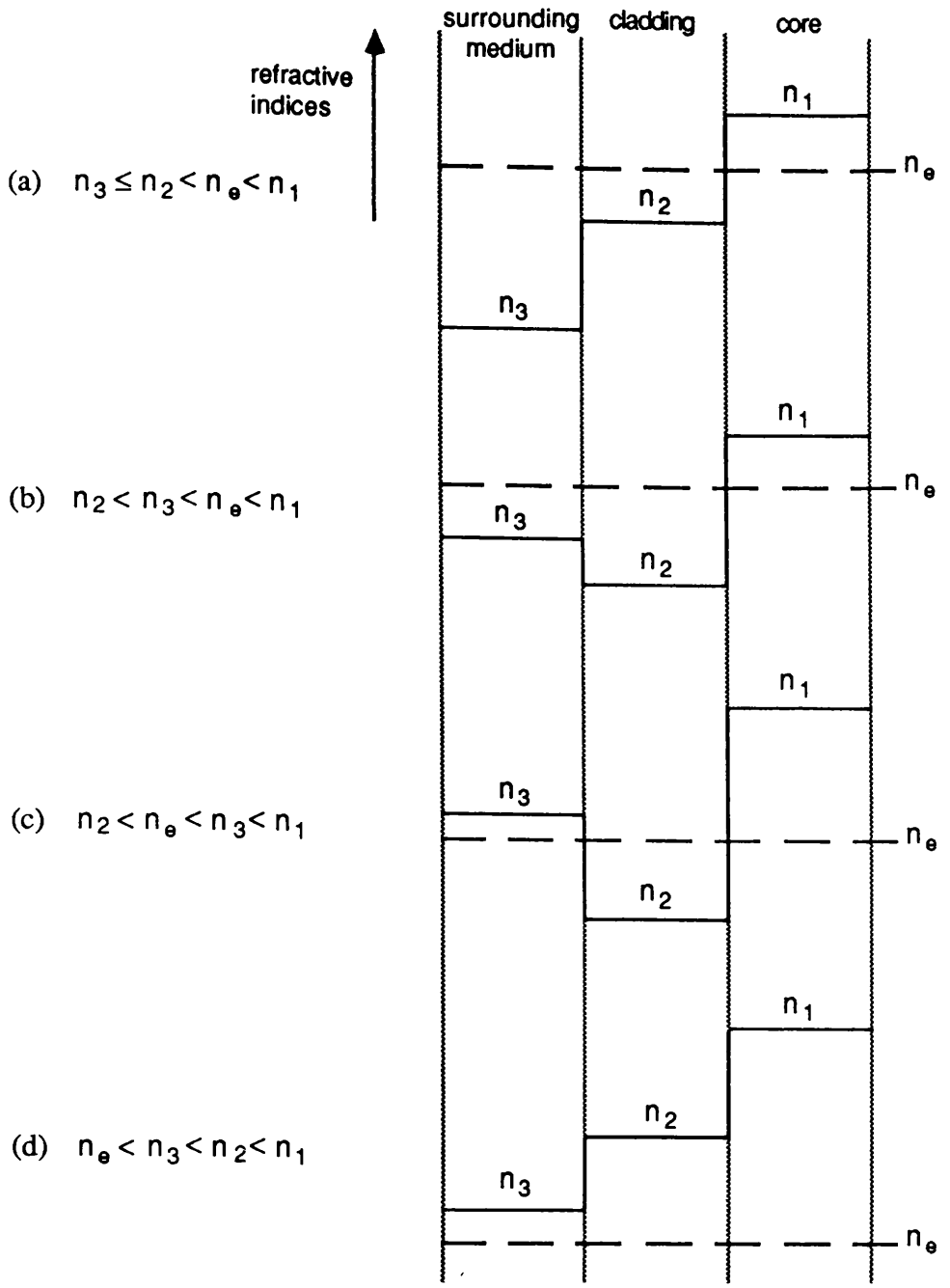

FIGURE 5.2

Definition of the different refractive index profiles.
a. Refractive index profile of a D− fibre surrounded by a low refractive index medium, for example the air. Thus the guided mode has an effective refractive index profile superior to the refractive indices of the cladding and surrounding medium.
b. Refractive index profile for a surrounding medium of a higher refractive index than that of the cladding, but lower than the effective refractive index of the guided mode.
c. Refractive index profile of a fibre to prism coupler. A refractive index of the surrounding medium higher than the effective refractive index of the mode creates a leaky mode situation.
d. If the effective refractive index of a mode is lower than the refractive index of the cladding and/or the surrounding medium, the mode is leaky.

represented in fig. 5.2c.

Even if the D– fibre is surrounded by air, the guide can support leaky modes, for example after coupling from a laser to a fibre, until all the energy injected into that mode has leaked out and radiated inside the air medium.

In conclusion, as in our problem we want to consider only the guided modes with a real propagation constant, the first two cases are considered. It follows that for a given value of the core and refractive indices, the range of propagation constants, β, is defined by the following inequality (see sect. 2.1.2):

$$k^2 n_3^2 < k^2 n_2^2 < \beta^2 < k^2 n_1^2 \qquad (5.5)$$

or

$$k^2 n_2^2 < k^2 n_3^2 < \beta^2 < k^2 n_1^2 \qquad (b)$$

Consequently, we can write the following inequations:

$$K_2^2 < 0 \qquad (5.6)$$

and

$$K_3^2 < 0 \qquad (5.7)$$

5.1.2 General solution of the ordinary differential equation

First of all, let us make the following change of variables:

$$\eta_2^2 = \gamma^2 - K_2^2 > 0 \qquad (5.8)$$

$$\eta_3^2 = \gamma^2 - K_3^2 > 0 \qquad (b)$$

Hence, with the above change of variables we can rewrite the ordinary differential equation for the three regions, as defined in fig 5.3, which will lead to the different particular solutions. The first region is formed by the surrounding medium, and its corresponding differential equation is:

$$\frac{\partial^2 G}{\partial y^2} - \eta_3^2 G = 0 \quad , \qquad \text{with } y > 0 \qquad (5.9)$$

The second region is formed by the cladding region from the source point (included) to the cladding/surrounding medium interface, and its corresponding equation is:

$$\frac{\partial^2 G}{\partial y^2} - \eta_2^2 \, G = - \delta(y - y') \, , \qquad \text{with } y_0 < y < 0 \qquad (5.9b)$$

The third and last region is formed by the cladding region below the source point, and its corresponding equation is:

$$\frac{\partial^2 G}{\partial y^2} - \eta_2^2 \, G = 0 \, , \qquad \text{with } y < y_0 \qquad (5.9c)$$

Note that the distance from the source point to the boundary between the cladding and the surrounding medium, is implicitly given by the ordinate of the source point.

Next, we want to include the boundary conditions, which will define the particular solution of the differential equation in each region.

First of all, due to conservation of the energy, the GF that represents the field produced by a source point (at y'), must tend towards zero at infinity, i.e., for $y = \pm\infty$. Hence, the GF along the y– axis must have an evanescent decay for an observation point in the surrounding medium, i.e., for $y > 0$ in region 1, and also for the values of the ordinate of the observation point inferior to those of the source point, i.e, for $y < y'$ in region 3.

However, due to the reflection at the interface between the two media of refractive indices n_2 and n_3, the solution in region 2 (for $y' < y < 0$) is the sum of a progressive and retrograde wave.

Therefore, from the following general solutions for each region:

$$G = A \, e^{-\eta_3 \, y} \qquad \text{with } y > 0 \qquad (5.10)$$

$$G = C \, e^{-\eta_2 \, y} + D \, e^{\eta_2} \qquad \text{with } y' < y < 0 \qquad (b)$$

$$G = B \, e^{\eta_2 \, y} \qquad \text{with } y < y' \qquad (c)$$

the particular solutions are determined by the calculation of the constants: A, B, C, D, which depend on the boundary conditions at the interface between the two media, and at the source point: i.e., at $y = 0$ and $y = y'$, respectively.

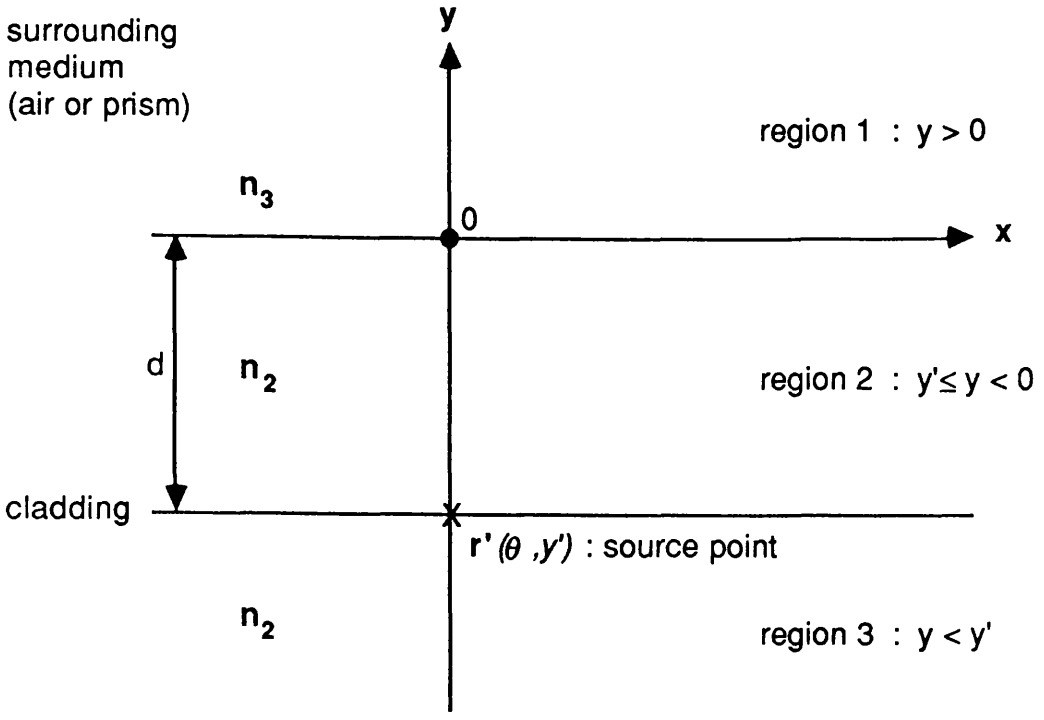

d : distance from the source point to the surrounding medium

n_2, n_3 : refractive indices of the cladding and surrounding medium, respectively

FIGURE 5.3

Definition of the region for the resolution of the system of differential equations (5.7).
Region 1 is formed by the surrounding medium.
Region 2 is formed by the cladding from the source point to the cladding/surrounding medium interface.
Region 3 is formed by the cladding below the source point.

5.1.3 Boundary conditions and particular solution of the ordinary differential equation

First of all, we want to calculate the boundary at the interface between the cladding and the surrounding medium. At $y=0$, the tangential component of the GF must be continuous. This can be achieved by making the Fourier transform of the GF and its derivative continuous. It follows that, at $y=0$:

$$G\Big|_{0^-} = G\Big|_{0^+} \qquad \text{then } A = C + D \qquad (5.11)$$

$$\frac{\partial G}{\partial y}\Big|_{0^-} = \frac{\partial G}{\partial y}\Big|_{0^+} \qquad \text{then } -\eta_3 A = \eta_2(-C + D) \qquad (b)$$

Secondly, at the source point, the boundary condition also implies that the Fourier transform of the GF must be continuous, to satisfy the law of conservation of energy. However, the l.h.s term in (5.9b) is equal to a delta function, and therefore the 1st derivative must decrease by unity at this source point as in:

$$\frac{\partial G}{\partial y}\Big|_{y'+} - \frac{\partial G}{\partial y}\Big|_{y'-} = -1$$

as described in fig. 5.4, such that:

$$\frac{\partial^2 G}{\partial y^2} = -\delta(y - y')$$

Hence, from the above equations the boundary condition at $y=y'$ becomes:

$$B\, e^{\eta_2 y'} = C\, e^{-\eta_2 y'} + D\, e^{\eta_2 y'} \qquad (5.12)$$

$$\text{and } (D - B)\, e^{\eta_2 y'} - C\, e^{-\eta_2 y'} = -\frac{1}{\eta_2} \qquad (b)$$

After some calculations, the insertion of the constants in the general solution gives the particular solution of the ordinary differential equation in the three regions, such as,

for region 1, where $y > 0$:

$$G = \frac{e^{\eta_2 y'}\, e^{-\eta_3 y}}{\eta_2 + \eta_3} \qquad (5.13)$$

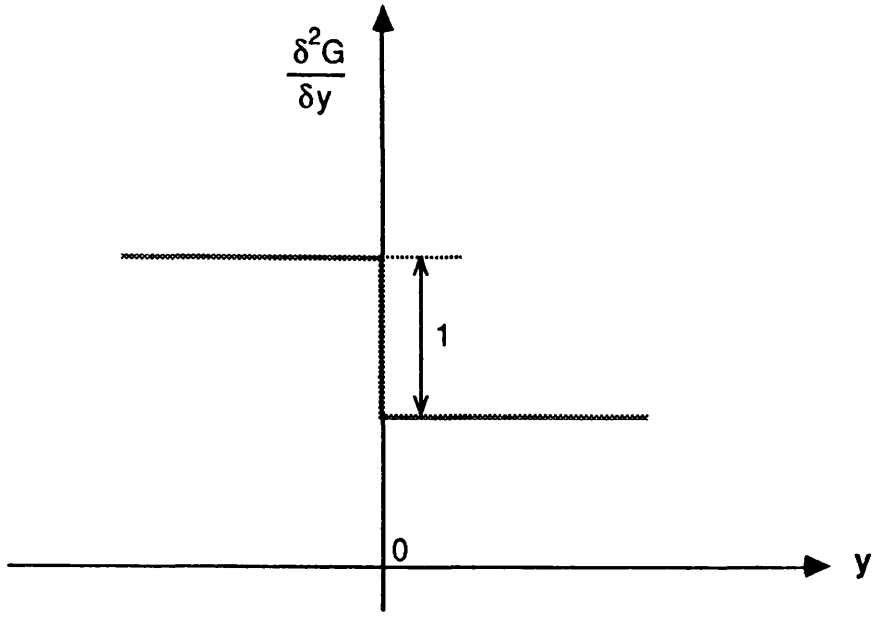

FIGURE 5.4

Representation of the unit step of the first derivative of the Fourier transform of the GF, leading to a delta function of the differential equation (5.7).

for region 2, where $y' < y < 0$:

$$G = \frac{e^{\eta_2 y'} e^{-\eta_2 y}}{2\eta_2} + \left[\frac{\eta_2 - \eta_3}{\eta_2 + \eta_3}\right] \frac{e^{\eta_2 y'} e^{\eta_2 y}}{2\eta_2} \qquad (b)$$

for region 3, where $y < y'$:

$$G = -\frac{e^{\eta_2 y'} e^{-\eta_2 y}}{2\eta_2} + \left[\frac{-\eta_2 + \eta_3}{\eta_2 + \eta_3}\right] \frac{e^{\eta_2 y'} e^{\eta_2 y}}{2\eta_2} \qquad (c)$$

Observe that all the boundary conditions have been included, i.e., the one at infinity and the one at the interface flat/surrounding medium, by solving the above ordinary differential equation. The resolution of the BC by the FT of the original partial differential equation, is the appropriate calculation method because of the translational invariance of the field along the x− axis. Remember also, that the boundary at the core/cladding interface is implicitly satisfied by the definition of the GF for an equivalent source point at that boundary.

In conclusion, from the above equation if we want to solve the Helmholtz equation, which was the original partial differential equation, and thus find our GF, the solution of the ordinary differential equation must be inverse Fourier transformed.

5.1.4 Integral form of the GF

a. Integral form of the total GF

As we choose the equivalent source points of the GF to be on the contour of the core, we are concerned by region 2 in fig. 5.3, formed by the cladding from the source point, which is included in the region, to the flat/surrounding medium interface. Therefore, its corresponding particular solution is the one where $y' < y < 0$, and will lead to the whole range of the GF. The solution of the corresponding partial differential equation is then calculated by means of an inverse Fast Fourier transform (FFT^{-1}), in order to reintroduce the $x-$dependence of our GF. From the definition of the FFT^{-1} in (5.3b), the integral form of our GF is written as:

$$g(r,r') = \frac{1}{2\pi} \int_{-\infty}^{+\infty} \left\{ \frac{e^{\eta_2 y'} e^{-\eta_2 y}}{2\eta_2} + \left[\frac{\eta_2 - \eta_3}{\eta_2 + \eta_3} \right] \frac{e^{\eta_2 y'} e^{\eta_2 y}}{2\eta_2} \right\} e^{i\gamma x} d\gamma \qquad (5.14)$$

At first note, as our problem is translationally invariant along the x− axis (see sect.5.1.1), the system of coordinates was centred on the source point for the x− axis. The value of the source point was thus assumed to be equal to zero, i.e., $x'=0$. Hence, in the above equation the variable x can be replaced by the difference in abscissa between the source and observation points, i.e., $(x-x')$. Secondly, we replace the variables η_2 and η_3, by their equivalents in (5.8). It follows that the above integral form of the GF becomes:

$$g(r,r') = \frac{1}{2\pi} \int_{-\infty}^{+\infty} \frac{e^{-(\gamma^2-K_2^2)^{1/2}(y-y')}}{2(\gamma^2-K_2^2)^{1/2}} e^{i\gamma(x-x')} d\gamma$$

$$+ \frac{1}{2\pi} \int_{-\infty}^{+\infty} \frac{(\gamma^2-K_2^2)^{1/2}-(\gamma^2-K_3^2)^{1/2}}{(\gamma^2-K_2^2)^{1/2}+(\gamma^2-K_3^2)^{1/2}} \frac{e^{(\gamma^2-K_2^2)^{1/2}(y+y')}}{2(\gamma^2-K_2^2)^{1/2}} e^{i\gamma(x-x')} d\gamma \qquad (5.14.b)$$

From sect. 5.1.1b, we have defined that the propagation constant of a free wave in the surrounding medium is inferior to that of a guided mode in the fibre, i.e., $K^2 n_3^2 < \beta^2$. This integral form of the GF is valid only for a surrounding medium with a refractive index lower than the effective refractive index of the guided mode. Remember that:

$$K_2^2 = n_2^2 k^2 - \beta^2 < 0, \quad \text{so that } (K_2^2)^{1/2} = i|K_2|$$

$$K_3^2 = n_3^2 k^2 - \beta^2 < 0, \quad \text{so that } (K_3^2)^{1/2} = i|K_3|$$

Consequently, the above integral equations are the same for a surrounding medium of high or low refractive index, if guidance exists. Furthermore, this solution, and the boundary conditions (5.11 and 12) do not vary in form with different values of the refractive indices.

b. Separation of the GF into two parts

From (5.14) we can separate the integral equation into two terms, so that:

$$g(r,r') = g_1(r,r') + g_2(r,r') \tag{5.17}$$

The first term does not involve the refractive index of the surrounding medium, and therefore is independent of the surrounding medium. Hence, this term is valid for any value of K_3^2, and is defined from (5.14) as in:

$$g_1(r,r') = \frac{1}{2\pi} \int_{-\infty}^{+\infty} \frac{e^{-(\gamma^2-K_2^2)^{1/2}\,(y-y')}}{2\,(\gamma^2-K_2^2)^{1/2}}\, e^{i\gamma(x-x')}\, d\gamma \tag{5.18}$$

The second term of the GF depends on the refractive index of the surrounding medium and is defined by the following integral:

$$g_2(r,r') = \frac{1}{2\pi} \int_{-\infty}^{+\infty} \frac{(\gamma^2-K_2^2)^{1/2} - (\gamma^2-K_3^2)^{1/2}}{(\gamma^2-K_2^2)^{1/2} + (\gamma^2-K_3^2)^{1/2}}\, \frac{e^{(\gamma^2-K_2^2)^{1/2}\,(y+y')}}{2\,(\gamma^2-K_2^2)^{1/2}}\, e^{i\gamma(x-x')}\, d\gamma \tag{5.18b}$$

Note that $\gamma^2 - K_2^2 < 0$ and $\gamma^2 - K_3^2 < 0$.

A physical explanation of this separation of the GF into two terms will be given in the following subsection.

5.1.5 1st term of the GF

The first term of the GF can be solved analytically. First of all, let us make the following change of variables:

$$\gamma = (K_2^2)^{1/2} \mathrm{ch}(\theta - i\varphi) = i\,|K_2|\,\mathrm{ch}(\theta - i\varphi) \tag{5.19}$$

$$d\gamma = (K_2^2)^{1/2} \mathrm{sh}(\theta - i\varphi)\, d\theta$$

$$x - x' = R\cos\varphi = R\,\mathrm{ch}(i\varphi) \tag{b}$$

$$y - y' = R\sin\varphi = -i\,R\,\mathrm{sh}(i\varphi)$$

Hence, $\left((x-x')^2 + (y-y')^2 \right)^{1/2} = R$, and $\varphi = \mathrm{tg}[(y-y')/(x-x')]$

Thereby, we find:

$$g_1 = \frac{1}{2\pi}\int_{-\infty}^{+\infty} \frac{e^{-\{K_2^2[\,ch^2(\theta-i\varphi)-1\,]\}^{1/2}[\,-iRsh(i\varphi)\,]+i(K_2^2)^{1/2}ch(\theta-i\varphi)Rch(i\varphi)}}{2\,\{K_2^2[\,ch^2(\theta-i\varphi)-1\,]\}^{1/2}} (K_2^2)^{1/2}sh(\theta-i\varphi)\,d\theta$$

Then, as $ch^2u - sh^2u = 1$, this integral is transformed and becomes:

$$g_1(r,r') = \frac{1}{4\pi}\int_{-\infty}^{+\infty} e^{-i(K_2^2)^{1/2}R\,[\,sh(\theta-i\varphi)\;sh(i\varphi)\;+\;ch(\theta-i\varphi)\;ch(i\varphi)\,]}\,d\theta \qquad (5.20)$$

Now, thanks to the properties of the hyperbolic functions, the argument of the exponential is simplified, and the above integral expression of the first part of the GF is explained such that:

$$g_1(r,r') = \frac{1}{4\pi}\int_{-\infty}^{+\infty} e^{i(K_2^2)^{1/2}R\;ch\theta}\,d\theta$$

Then, as $[K_2^2]^{1/2} = i|K_2|$, and as the function to be integrated is even, the limits of the integral are changed as written below:

$$g_1(r,r') = \frac{1}{2\pi}\int_{0}^{+\infty} e^{-|K_2|\;R\;ch\theta}\,d\theta \qquad (5.21)$$

Finally, we use an integral expression of a modified Bessel function (see equ. 9.6.24 in Abramowitz and Stegun [A]), which is rewritten for the zero order of the Bessel function as in:

$$K_0(z) = \frac{1}{2}\int_{0}^{+\infty} e^{-\,z\,cht}\,dt \quad , \text{ with } |\arg z| < \pi/2 \qquad (5.22)$$

This implies that we can write the solution of the first part of the GF in terms of a modified Bessel function as in:

$$g(r,r') = 1/\pi\; K_0\{|K_2|\;R\} \quad , \text{ where } |K_2|R > 0 \text{ and real} \qquad (5.23)$$

This solution can be transformed into a Bessel function of the third kind, of order zero, also called a Hankel function: H_ν. The relation between the two Bessel functions is given below for the zeroth order (see Abramowitz and Stegun [A] equ. 9.6.4):

$$K_0(z) = i\pi/2\ H_0^{(1)}[z\ \exp(i\pi/2)] = i\pi/2\ H_0^{(1)}(iz) \qquad (5.24)$$

where $-\pi < \arg z \leq \pi/2$, and z is a complex number.

Hence, we find the following expression of the first part of the GF as in:

$$g_1(r,r') = i/2\ H_0^{(1)}[(K_2^2)^{1/2}] = i/2\ H_0^{(1)}[i|K_2|R] \qquad (5.25)$$

where the argument of the Bessel function is purely imaginary.

Note that, the expansion of $H_0^{(1)}(u)$ for a large argument (see [SL] equ. 37.87), i.e., for $u \longrightarrow \infty$, is:

$$H_0^{(1)}(u) \cong \left[\frac{2}{\pi u}\right]^{1/2} \exp[i\ (u - \pi/4)] \qquad (5.26)$$

If we apply the above relation, the solution of the first part of the GF would be proportional to:

$$g(r,r') \simeq \exp(-|K_2|R)/\ [\pi|K_2|R]^{1/2}, \quad \text{with } R \longrightarrow \infty \qquad (5.27)$$

This shows that, if the distance between the source and observation point (R) tends towards infinity, the first GF tends towards zero according to the conservation of energy law.

Note that the first part of the GF is independent of the refractive index of the surrounding medium (n_3), and thus is independent of the boundary at the cladding/surrounding medium interface. Therefore, this part of the GF is equivalent to that of a source point in an unbounded medium. It follows that, if the observation point is far from the source point, the field produced by that source point becomes negligible. Furthermore, this term is completely symmetrical, and depends only on the magnitude of the distance R, between the source and observation point. Finally, this first GF is also regular and continuous everywhere, except when the source point has the same coordinates as the observation point, i.e., for $r = r'$.

5.1.6 2nd term of the GF

The second term of the GF (5.18.b) is not simply a function of the distance between the source and observation point. The distance between the cladding/surrounding medium interface and the source point, appears implicitly in the expression $(y+y')$, as $y=0$ at that interface (see fig. 5.3). This second part of the GF also depends on the refractive index of the surrounding medium (n_3). Therefore, this term takes account of the boundary conditions, and is regular and continuous everywhere inside the contour formed by the boundary of the cladding.

However, this second term of our GF can only be solved by means of a numerical Fourier transform. With the following change of variable: $x-x'=x$, this term becomes:

$$g_2(r,r') = FT^{-1}\left[(C \text{ or } C')\, e^{(\gamma^2-K_2^2)^{1/2}(y+y')}\right] \qquad (5.28)$$

where the constant C is for the case where $\gamma^2 > K_3^2$, and equal to:

$$C = \left[\frac{(\gamma^2-K_2^2)^{1/2}-(\gamma^2-K_3^2)^{1/2}}{(\gamma^2-K_2^2)^{1/2}+(\gamma^2-K_3^2)^{1/2}} \quad \frac{1}{2\,(\gamma^2-K_2^2)^{1/2}}\right] \qquad (5.29)$$

Observe from (5.28), that the function to be inverse Fourier transformed is an even and real function, so that the second part of the GF will also be an even and real function, with $x=x-x'$ as abscissa, and with y and y' being constant and selected for each pair of source and observation points as shown in fig. 6.2.

5.1.7 Discussion

The GF has been separated into two terms: its first term is equivalent to the GF of a source point in an unbounded medium, has an analytical solution, and is regular and continuous everywhere, except at the source point. The second term takes the boundary conditions into account. It is regular and continuous everywhere inside the definition domain of the Kirchhoff–Huygens integral, and leads to the integral form of the GF in the cladding region, i.e. from the source point to the cladding/surrounding medium interface. However, this second GF must be solved

numerically. Remember that the source points have been chosen on the contour of the core in sect. 5.2, and are included in the definition domain.
Note finally, that these properties of the GF are explained in sect. 7.2 by Morse and Fesbach [MF].

In conclusion, defining the refractive indices of the cladding and the surrounding medium (prism or air), and the distance from the source point to the flat surface of the cladding, implies that the Green function of the problem is totally defined (see (5.25) and (5.28)), leaving the propagation constants of the different guided modes as the only unknowns.

5.2 ANALYTICAL APPROACH TO THE EIGENVALUE PROBLEM

5.2.1 Introduction: elements of the Kirchhoff–Huygens integral

The chosen Kirchhoff–Huygens integral (4.16) expresses the scalar field: $U(r_c)$ with $r_c(x_c,y_c)$, on the contour of the core and in the cladding, in terms of a line integral around the contour (C') of the core, and is written below with the origin of the Cartesian coordinates centred on the core (see fig. 5.5).

$$U(r_c) = \int_{C'} U(r_c') \frac{\partial g(r_c,r_c')}{\partial n'} - \frac{\partial U(r_c')}{\partial n'} g(r_c,r_c') \, dl' \qquad (5.30)$$

where r_c and r_c' defined the position of the observation and source point, respectively.

The first element of this integral is the GF previously expressed in sect. 5.1. The GF is chosen for an equivalent source point at the core/cladding boundary, with the observation point defined on the contour and in the cladding region. Note, that the boundary conditions at the cladding/surrounding medium interface and at infinity have also been included (see sect. 5.2.4c).

The second element of this integral is the particular value of the field on the contour C': $U(r_c')$, satisfying the homogeneous scalar wave equation at the coordinates of the equivalent source point.

As we want to determine the propagation constants (β) of the guided modes

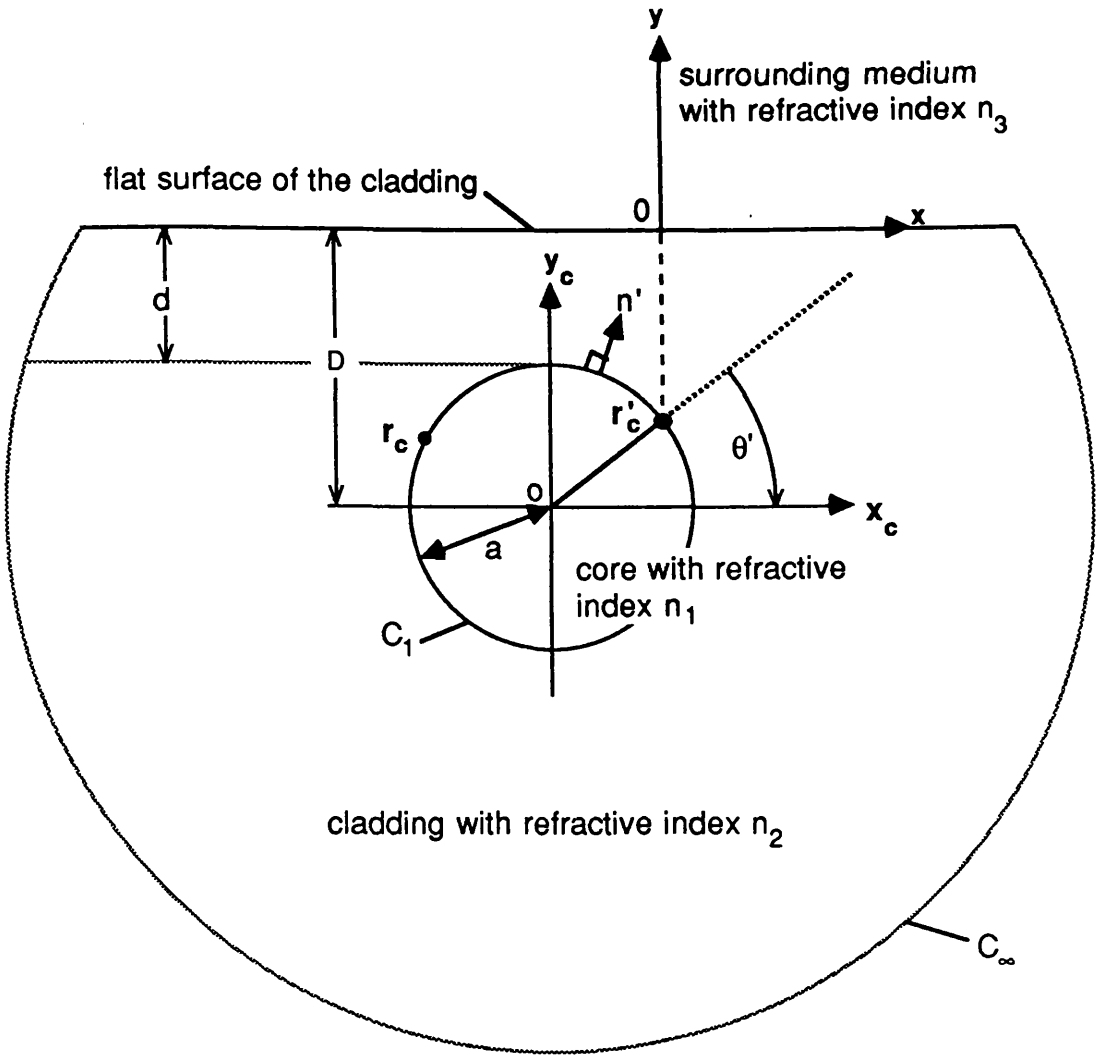

a : is the core radius

d : core/flat distance

D : difference in ordinate between the two Cartesian coordinate systems Oxy, $Ox_c y_c$

n' : normal outer vector to the contour of the core, C_1

C_1 : core/cladding boundary

C_∞ : boundary of the cladding at infinity

FIGURE 5.5

Definition of the different coordinate systems, where:
Oxy is the Cartesian coordinate system with the origin of the y− axis on the flat surface of the cladding, and the origin of the x− axis based on the source point,
$Ox_c y_c$ is the Cartesian coordinate system centred on the core,
and $Or'\theta'$ is the polar coordinate system also centred on the core.

of a D− fibre, implicitly expressed in the GF, the unknowns $U(r_c)$, $U(r_c')$ and $\partial U(r_c')/\partial n'$ have to be eliminated. Therefore, the Kirchhoff− Huygens integral is only an intermediate equation, which is worked out below to obtain an eigenvalue problem with β as the only unknown.

5.2.2 Formulation of the eigenvalue problem

a. Expansion of $U(r_c')$ and $\partial U(r_c')/\partial n'$

First of all, note that the transverse component of the field and its derivative are continuous at the core/cladding boundary. Thus, its formulation inside the core is also valid at the boundary. Furthermore, the spatial transverse dependence of a field, which has a circular cylindrical symmetry in a homogeneous medium, can be expanded in a Fourier series, as for example in our problem, for a point inside or on the contour of the core. Consequently, the field at the core boundary is expanded in polar coordinates, with the origin of the coordinate system also taken at the centre of the core (see fig. 5.5). This gives:

$$U(r_c')\Big|_{r'=a} = \sum_{m=-\infty}^{+\infty} u_m \, J_m(\gamma_1 r') \, e^{im\theta'} \tag{5.31}$$

where the Fourier coefficient: u_m, is given by:

$$u_m = \frac{1}{2\pi} \int_{-\infty}^{+\infty} U(r_c') \, e^{-im\theta'} \, d\theta' \tag{b}$$

where $\gamma_1 = (n_1^2 k^2 - \beta^2)^{1/2}$ (5.32)

and where n_1 is the refractive index of the core.

r', θ' are the radius and the angle of a source point in polar coordinates, which is chosen at the core/cladding boundary.

Next, starting from the above expansion, we derive $U(r_c')$ with respect to the normal vector: $\mathbf{n}'$, defined outward from the contour of the core. Thus, we obtain the corresponding expansion of the derivative of the first part of the GF:

$$\left.\frac{\partial U(r_c')}{\partial n'}\right|_{r'=a} = \left.\frac{\partial U}{\partial r}\right|_{r'=a} = \sum_{m=-\infty}^{+\infty} u_m J_m'(\gamma_1 r)\, e^{im\theta'} \qquad (5.33)$$

where $\partial U(r_c')/\partial\theta' = 0$.

b. Introduction of the expansion of U

Now, starting from the Kirchhoff–Huygens integral this time expressed in coordinates centred on the core, we substitute U and $\partial U/\partial n'$ by their above corresponding expansions. Hence,

$$U(r_c) = \sum_{m=-\infty}^{+\infty} a\, u_m\, J_m(\gamma_1 a) \int_0^{2\pi} e^{im\theta'} \frac{\partial g(r_c, r_c')}{\partial r'}\, d\theta'$$

$$- \sum_{m=-\infty}^{+\infty} a\, u_m\, J_m'(\gamma_1 a) \int_0^{2\pi} e^{im\theta'} g(r_c, r_c')\, d\theta' \qquad (5.34)$$

Note, that C' is defined by $r'=a$ and by $0<\theta'<2\pi$, and $dl'=r'd\theta'$.

Next, if we multiply the above equation by $\exp(-in\theta)$, and integrate over θ along the contour C (i.e. for $r=a$ and $0<\theta<2\pi$), the above equation becomes:

$$\frac{1}{2\pi}\int_{\theta=0}^{2\pi} e^{-in\theta} U(r_c)\, d\theta = \frac{1}{2\pi}\sum_{m=-\infty}^{+\infty} a\, u_m\, J_m(\gamma_1 a) \iint_{\theta',\theta=0}^{2\pi} e^{im\theta'-in\theta} \frac{\partial g(r_c, r_c')}{\partial r'}\, d\theta' d\theta$$

$$- \frac{1}{2\pi}\sum_{m=-\infty}^{+\infty} a\, u_m\, J_m'(\gamma_1 a) \iint_{\theta',\theta=0}^{2\pi} e^{im\theta'-in\theta} g(r_c, r_c')\, d\theta' d\theta \qquad (5.35)$$

where r, θ are the radius and the angle, respectively, of one observation point. All the observation points are also chosen to be on the contour of the core, and therefore inside the limits of the definition domain (see fig. 5.4) of the Kirchhoff–Huygens integral. Thus, the r.h.s of (5.35) has the form of a Fourier coefficient of $U(r_c)$, as in:

$$u_n = \frac{1}{2\pi} \int_0^{2\pi} U(r_c)\, e^{-in\theta}\, d\theta \qquad (5.36)$$

As both the observation and the source point are selected on the contour of the core, both contours C and C' are equal. The expansion (5.31) is thus applicable to $U(r_c)$, provided the exchange of variables θ', r', m for θ, r, n. Therefore, both $U(r_c)$ and $U(r_c')$ have the same Fourier coefficient (i.e., (5.36) equal (5.31.b)).

It follows that (5.35) can be reformulated by the following linear equation:

$$u_n = \sum_{m=-\infty}^{+\infty} a\, u_m\, J_m(\gamma_1 a)\, G_{mn}' - \sum_{m=-\infty}^{+\infty} a\, u_m\, J_m'(\gamma_1 a)\, G_{mn} \qquad (5.37)$$

with:

$$G_{mn}' = \frac{1}{2\pi} \iint_{\theta', \theta=0}^{2\pi} e^{im\theta' - in\theta}\, \frac{\partial g(r_c, r_c')}{\partial r'}\, d\theta' d\theta \qquad (b)$$

$$G_{mn} = \frac{1}{2\pi} \iint_{\theta', \theta=0}^{2\pi} e^{im\theta' - in\theta}\, g(r_c, r_c')\, d\theta' d\theta \qquad (c)$$

Finally, we apply a last change of variable:

$$\Lambda_{mn} = a\, J_{mn}(\gamma_1 a)\, G_{mn}' - a\, J_{mn}'(\gamma_1 a)\, G_{mn} \qquad (5.38)$$

so that (5.37) is reduced to a simple infinite series:

$$u_n = \sum_{m=-\infty}^{+\infty} \Lambda_{mn}\, u_m\,, \qquad \text{with } -\infty < n < +\infty \qquad (5.39)$$

Consequently, the Kirchhoff–Huygens integral (5.30) has been transformed into an eigenvalue problem, which can be rewritten by the following set of linear equations:

$$\begin{aligned}
\lambda_{-\infty}\, u_{-\infty} &= \sum_{m=-\infty}^{+\infty} \Lambda_{m,+\infty}\, u_m \\
&\vdots \\
\lambda_n\, u_n &= \sum_{m=-\infty}^{+\infty} \Lambda_{m,n}\, u_m \\
&\vdots \\
\lambda_{+\infty}\, u_{+\infty} &= \sum_{m=-\infty}^{+\infty} \Lambda_{m,-\infty}\, u_m
\end{aligned}$$

where the eigenvalues $\lambda_{-\infty},\ldots,\lambda_n,\ldots,\lambda_{+\infty}$ are equal to 1.

Thus, in the matrix notation, the system of equations becomes:

$$\lambda\, U = M\, U \tag{5.41}$$

$$\text{with } \lambda = 1\ ,\ U = \begin{vmatrix} u_{-\infty} \\ \vdots \\ u_n \\ \vdots \\ u_{+\infty} \end{vmatrix}\ ,\qquad M = \begin{vmatrix} \Lambda_{-\infty-\infty} & \cdots & \Lambda_{+\infty-\infty} \\ \vdots & & \vdots \\ \cdots & \Lambda_{mn} & \cdots \\ \vdots & & \vdots \\ \Lambda_{-\infty+\infty} & \cdots & \Lambda_{+\infty+\infty} \end{vmatrix}$$

As we want a non-trivial solution of our eigenvalue problem, the determinant of the resulting matrix must be equal to zero, as in:

$$\det\{\, M - \lambda I \,\} = 0 \tag{5.42}$$

where λ is a real number equal to one. First of all, observe that the scalar field at the source and observation points: $U(r_c)$ and $U(r_c')$, respectively, and $\partial U(r_c')/\partial n'$ have been suppressed from (5.42). Consequently, the only unknown of our problem is now the propagation constant: β, which appears explicitly in the formulation of the GF and its derivative in (5.23) and (5.28). This implies that, the above equation totally defines the values of the propagation constants of the guided modes of a D-fibre. One value of the above determinant equal to zero, yields one propagation constant of one guided mode of our D-fibre.

5.2.3 Conclusions

Starting from the scalar wave equation, we have calculated the Kirchhoff-Huygens integral, which includes a GF as one of its elements. This integral is an intermediate equation, which has been transformed through some formal analytical procedures, into an eigenvalue problem, leaving the propagation constant of a guided mode as the only variable. Thus, we have obtained a system of equations, which can only be satisfied for the values of the different propagation constants of the guided mode in the D-fibre. These discrete values will be calculated by an iterative method, and some classical matrix calculation.

Furthermore, after the calculation of the different propagation constants (β), it is possible to return to the Kirchhoff-Huygens integral, and therefore, to calculate the transverse electromagnetic field at any observation point, either inside the cladding region or on the surface of the core.

CHAPTER SIX

REFORMULATION OF THE EQUATIONS FOR COMPUTER APPLICATIONS

6.1 INTRODUCTION

The programming language in use for numerical calculation is Turbo– Pascal. Its disadvantage is that the complex numbers are not defined as in Fortran. Therefore, the calculation of the real and imaginary parts has to be considered separately. The main calculus routines come from the book: 'Numerical Recipes: The Art of Scientific Computation' [P].

Starting from the eigenvalue problem defined in the previous chapter in sect. 5.2.2b, we want to calculate numerically the different propagation constants of the guided modes of the D– fibre. However, the analytical equations defining our problem need some further development before their insertion into the calculus routines and the programme itself.

Before initiating further calculations, we recall the equations leading to the eigenvalue matrix.

At first let us recall the separation of the GF into two parts, as in:

$$g(r,r') = g_1(r,r') + g_2(r,r') \tag{6.1}$$

given in (5.23) and (5.28). Then the derivative of the 2nd GF has to be calculated, with the derivative of the total GF expressed as in:

$$\frac{\partial g(r,r')}{\partial r'} = \frac{\partial g_1(r,r')}{\partial r'} + \frac{\partial g_2(r,r')}{\partial r'} \tag{6.2}$$

Next, we rewrite the two main constants of the elements of the eigenvalue matrix:

$$G_{mn} = \frac{1}{2\pi} \int_0^{2\pi}\int e^{im\theta' - in\theta}\, g(r_c,r_c')\, d\theta' d\theta \tag{6.3}$$

$$\text{with } G_{mn} = G_{mn1} + G_{mn2} \tag{b}$$

$$G_{mn}' = \frac{1}{2\pi} \int_0^{2\pi}\int e^{im\theta' - in\theta}\, \frac{\partial g(r_c,r_c')}{\partial r'}\, d\theta' d\theta \tag{6.4}$$

$$\text{with } G_{mn} = G_{mn1}' + G_{mn2}' \ . \tag{b}$$

Note, that the GF is expressed in Cartesian coordinates with the origin of the y− axis on the flat, and that of the x− axis based on the source point (see fig. 5.5). Therefore, a reformulation of the above equation into a polar coordinate system is necessary to solve the double integral leading to the above constants, otherwise the result of the GF would have to be interpolated for each angular sampling point of the integrals in terms of θ and θ'. Moreover, we recall the expression of the elements of the eigenvalue matrix, as in:

$$\Lambda_{mn} = r' \, J_m(\gamma_1 \, r') \, G_{mn}' - r' \, J_m'(\gamma_1 \, r') \, G_{mn} \qquad (6.5)$$

with r' being equal to the core radius, a, i.e., r' = a,

so that the matrix M is rewritten such that:

$$M = \begin{vmatrix} \Lambda_{-\infty-\infty} & \cdots & \Lambda_{+\infty-\infty} \\ \vdots & & \vdots \\ \cdots & \Lambda_{mn} & \cdots \\ \vdots & & \vdots \\ \Lambda_{+\infty-\infty} & \cdots & \Lambda_{+\infty+\infty} \end{vmatrix} \qquad (6.6)$$

where $-\infty < n < +\infty$.

Finally, β are found by satisfying the following determinant equation:

$$\det\{ M - \lambda I \} = 0, \qquad (b)$$

with $\lambda = 1$ as defined in sect. 5.2.2b, and I is the identity matrix.

6.2 REFORMULATION OF THE 1ST PART OF THE GF

6.2.1 Expression in polar coordinates

The first part of the GF in (5.23) is expressed in Cartesian coordinates centred on a source point along the x− axis, with the origin of the y− axis on the flat surface of the cladding. However, the variables G_{mn}' and G_{mn} are in polar coordinates centred on the fibre core. Therefore, reformulation of this equation is necessary. The first part of the GF depends only on the distance from the source to the observation point,

$$R = [\, (x - x')^2 + (y - y')^2 \,]^{1/2}$$

where r'(x',y') is the source point,

and r(x,y) is the observation point.

Consequently, this term is valid for any Cartesian coordinate system, and in particular for the one centred on the core as in fig. 5.5. Finally, we rewrite the relationship between the Cartesian and polar coordinate system, as in:

$$x_c = r\cos\theta \qquad y_c = r\sin\theta \qquad (6.8)$$

$$x_c' = r'\cos\theta' \qquad y_c' = r'\sin\theta'$$

where x_c', y_c' and x_c, y_c express the position of the source and observation points, respectively, in a Cartesian coordinate system centred on the core;

and where r', θ' and r, θ are the radius and the angle of the source and observation points, respectively, in polar coordinates.

Then R is transformed by this change of coordinate system to:

$$R = (r^2 + r'^2 - 2r\,r'\cos(\theta - \theta'))^{1/2} \qquad (6.9)$$

As both source and observation point are on the contour of the core (i.e., r= r'= a), the above equation is simplified such that:

$$R = a\,[2(\,1 - \cos(\theta - \theta')\,)]^{1/2} \qquad (b)$$

with a being the core radius.

It follows, that the solution of the 1st GF in terms of a modified Bessel function as in (5.23), leads to the corresponding expression in polar coordinates to give:

$$g_1(r_c, r_c') = i/2\; H_0^{(1)}\{ i|K_2|[\, r^2 + r'^2 - 2rr'\cos(\theta - \theta')\,]^{1/2}\}$$

$$\text{with } i|K_2| = n_2^2k^2 - \beta^2. \qquad (6.10)$$

This implies that, for a source and observation point at the core/cladding boundary, the 1st GF becomes:

$$g_1(r_c, r_c') = i/2\; H_0^{(1)}\{ i|K_2|\, a\,[2(\,1 - \cos(\theta - \theta')\,)]^{1/2}\}_{(b)}$$

6.2.2 Reformulation with Graf's expansion: G_{mn1}

If the source and observation points have the same angular coordinate, i.e., $\theta'= \theta$, the corresponding Bessel function in (6.10) tends towards infinity, as both points were selected to be on the contour of the core so that: r= r'. Thus, the

numerical calculation of the double integral leading to the variable G_{mn} would be impossible.

Nevertheless, the use of Graf's expansion will allow the calculation of G_{mn}. Therefore, let us rewrite Graf's expansion given in equ. 7.1.79 in Abramowitz and Stegun [AS] as follows:

$$C_\nu(w)\ \cos(\nu\gamma) = \sum_{p=-\infty}^{+\infty} C_{\nu+p}(u)\ J_p(v)\ \cos(p\alpha) \qquad (6.11)$$

where C_ν is a Bessel function and where u, v, w, γ, and α are defined in fig. 6.1, so that w satisfies the cosine theorem:

$$w = (u^2 + v^2 - 2uv\ \cos\alpha)^{1/2} \qquad (b)$$

Additionally, the following inequality:

$$\left| v\ e^{\pm i\alpha} \right| < u \qquad (c)$$

must be satisfied.

The corresponding parameters for our expansion are defined in fig. 6.1. It follows that the first part of the GF in (6.10a) becomes:

$$g_1 = i/2 \sum_{p=-\infty}^{+\infty} H_p^{(1)}\{i|K_2|r\}\ J_p\{i|K_2|r'\}\ e^{ip(\theta-\theta')} \qquad (6.12)$$

Note, that the condition on u and v expressed in (6.11c), is satisfied by supposing that the observation point is just outside the core–cladding boundary, as defined in fig. 6.1b. In fact that supposition can be neglected once the expansion (6.12) is introduced into the double Fourier integral (6.3a), which becomes:

$$G_{mn1} = \frac{1}{4\pi} \sum_{p=-\infty}^{+\infty} H_p^{(1)}\{i|K_2|r\}\ J_p\{i|K_2|r'\} \iint_0^{2\pi} e^{i(m-p)\theta'}\ e^{i(p-n)\theta}\ d\theta\ d\theta' \qquad (6.13)$$

This double integral is not equal to zero only if p= m= n. It follows, that the variable G_{mn} is defined for any value of θ and θ', and is simplified such that:

$$G_{mn1} = \frac{1}{4\pi}\ H_m^{(i)}\{i|K_2|r\}\ J_m\{i|K_2|r'\}\ \delta(m-n) \qquad (6.14)$$

where $-\infty < m,n < +\infty$.

(a)

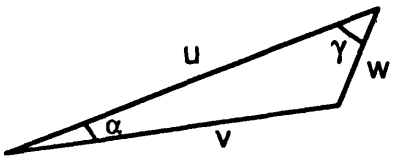

(b)

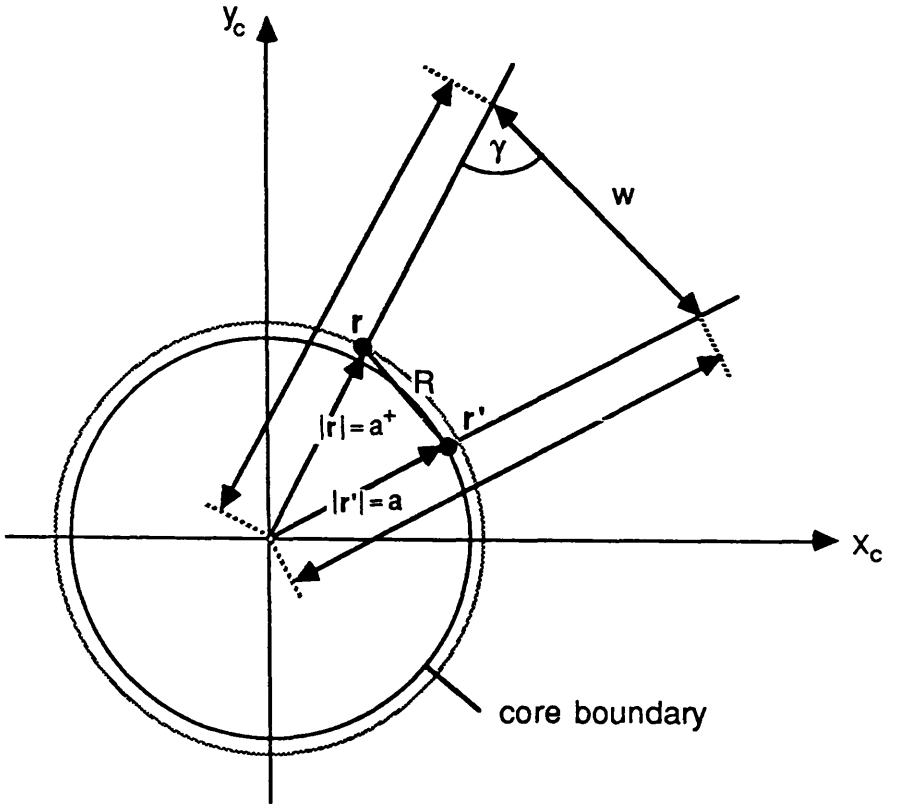

r' : coordinate of the source point

r : coordinate of the observation point

$O\,x_c y_c$: Cartesian coordinate system centred on the core

R : distance between the source and observation point

FIGURE 6.1

a. Relation between the different variables of the cosine theorem:
$w = (u^2 + v^2 - 2uv \cos\alpha)^{1/2}$

b. Variables for the application of Graf's expansion to the Bessel function: $K_0\{ |k_2| R \}$, with:
$|k_2| r = u$
$|k_2| r' = v$
$|k_2| R = w$
The source point is supposed to be just outside the core–boundary, so that: $r = a^+$, where a is the core radius.

Thereafter, the infinite number of integer components m and n, have to be reduced to a finite number, to allow numerical calculation. It follows that, the different variables: G_{mn1}, associated with the chosen range of discrete integer values m and n, lead to a matrix with only the diagonal elements non zero, as in:

$$G_1 \simeq \begin{vmatrix} H_{-m}^{(1)} J_{-m} & \cdots & 0 & \cdots & 0 \\ \vdots & & \vdots & & \vdots \\ 0 & \cdots & H0^{(1)} J_0 & \cdots & 0 \\ \vdots & & \vdots & & \vdots \\ 0 & \cdots & 0 & \cdots & H_0^{(1)} J_0 \end{vmatrix} \qquad (6.15)$$

where $m_{max} = n_{max} < +\infty$ (b)

6.3 DERIVATIVE OF THE 1st GF AND ITS INTEGRATION: G_{mn_1}'

The derivative of the 1st GF could be calculated from its expression in terms of the Bessel function K_0 in (5.23). However, we encounter the same problem as for the function itself, i.e., the infinite value when the source and observation points are superposed. Therefore, we calculate this derivative with respect to the normal to the contour of the core from Graf's expansion of the Bessel function (6.12), as in:

$$\frac{\partial g_1}{\partial r'} = \frac{-i|K_2|}{2} \sum_{p=-\infty}^{+\infty} H_p^{(1)}\{i|K_2|r\} \left[-J_{p+1}\{i|K_2|r'\} + \frac{p}{i|K_2|r'} J_p\{i|K_2|r'\}\right] e^{ip(\theta-\theta')} \qquad (6.16)$$

where $J_\nu'(z) = -J_{\nu+1}(z) + \nu/z\, J_\nu(z)$ and $z = i|K_2|r'$.

Further, as developped in the previous section, the term G_{mn1}' including the derivative of the 1st GF is expanded as in:

$$G_{mn1}' = \frac{-i|K_2|}{4\pi} H_m^{(1)}\{i|K_2|r\} \left[-J_{m+1}\{i|K_2|r'\} + \frac{p}{i|K_2|r'} J_m\{i|K_2|r'\}\right]\delta(m-n)$$

where $-\infty < m,n < +\infty$, (6.17)

and leads to the corresponding diagonal matrix:

$$G_1' \simeq \begin{vmatrix} H_{-m}^{(1)}\left[-J_{-(m+1)}+cJ_{-(m)}\right] & \cdots & 0 & \cdots & 0 \\ \vdots & & \vdots & & \vdots \\ 0 & \cdots & H_0^{(1)}\left[J_{-1}+cJ_0\right] & \cdots & 0 \\ \vdots & & \vdots & & \vdots \\ 0 & \cdots & 0 & \cdots & H_m^{(1)}\left[-J_{(m+1)}+cJ_m\right] \end{vmatrix}$$

where $m_{max} = n_{max} < +\infty$, and where $c = m/i|K_2|r'$. (6.18)

In conclusion, using Graf's expansion of the Bessel function in the first part of the GF and its derivative avoids the numerical integration leading to the variables G_{mn1}

and G_{mn1}'.

6.4 REFORMULATION OF THE DERIVATIVE OF THE 2nd GF

As seen in (5.28), the 2nd GF is still an integral, and the inverse Fourier transform must be achieved by a numerical method. In order to obtain the variable G_{mn2}' in (6.4), this 2nd GF has to be derived, which can be done prior to the FT^{-1}, as demonstrated in the following equation:

$$\frac{\partial g_2}{\partial r'} = \frac{1}{2\pi} \int_{-\infty}^{+\infty} \frac{\partial G_2}{\partial r'} e^{i\gamma(x-x')} \, d\gamma + \frac{1}{2\pi} \int_{-\infty}^{+\infty} G_2 \frac{\partial \left[e^{i\gamma(x-x')} \right]}{\partial r'} \, d\gamma \qquad (6.19)$$

As the derivative with respect to r', is calculated in polar coordinates centred on the core (see fig. 5.5), the FT of the 2nd GF: G_2, in (5.28), requires two successive changes of variables. The first one transforms the integral expression of G_2 from the Cartesian coordinate system with its y− axis origin at the flat surface of the cladding, into a Cartesian coordinate system centred on the core (see fig. 5.5). The relation between the two systems is as follows:

$$y = y_c - D \qquad \text{with } D = d + a \qquad (6.20)$$

$$y' = y_c - D$$

where the subscript c denotes the coordinate system with the core centre as origin, and no subscript denotes the one with the origin of the y− axis based on the flat surface of the cladding.

Remember, that d is the core/flat distance, a is the core radius, and y' and y are the ordinates of the source and observation points, respectively.

Note that, as the abscissa appears only as a difference between the source and observation point, its expression is the same for any Cartesian coordinate system, thus:

$$x - x' = x_c - x'_c \qquad (b)$$

This implies that the integral form of the 2nd GF becomes:

$$g_2(r_c,r_c') = -1/2\pi \int_{-\infty}^{+\infty} C\, e^{(\gamma^2 - K_2^2)^{1/2}(-2D+y_c+y_c')}\, e^{i\gamma(x_c-x_c')}\, d\gamma \quad (6.21)$$

with C = C or C', as defined in (5.28).

Secondly, we transform the expression under the above integral into polar coordinates by the following change of variables:

$$x_c' = r' \cos\theta' \qquad y_c' = r' \sin\theta' \quad (6.22)$$

$$x_c = r \cos\theta \qquad y_c = r \sin\theta$$

where r',r, and θ',θ are the radius and the angle in polar coordinates of the source and observation points, respectively.

Thus, we find:

$$\frac{\partial g_2}{\partial r'} = \frac{1}{2\pi} \int_{-\infty}^{+\infty} C \frac{\partial}{\partial r'} \left\{ e^{(\gamma^2-K_2^2)^{1/2}(r \sin\theta + r'\sin\theta' - 2D)}\, e^{i\gamma(r\cos\theta - r'\cos\theta')} \right\} d\gamma \quad (6.23)$$

Then, after calculating the derivative of the above product, we revert back using this result to the original Cartesian coordinates based on the flat surface of the cladding for the y− axis.

Hence,

$$\frac{\partial g_2(r,r')}{\partial r'} = \frac{1}{2\pi} \sin\theta' \int_{-\infty}^{+\infty} C\, (\gamma^2-K_2^2)^{1/2}\, e^{(\gamma^2-K_2^2)^{1/2}(y+y')}\, e^{i\gamma(x-x')}\, d\gamma$$

$$- \frac{i}{2\pi} \cos\theta' \int_{-\infty}^{+\infty} C\, \gamma\, e^{(\gamma^2-K_2^2)^{1/2}(y+y')}\, e^{i\gamma(x-x')}\, d\gamma \quad (6.25)$$

Next, by setting $x = x - x'$ as the spatial domain variable, and γ as the frequency domain variable, we can explain the above equation in terms of two FT^{-1}, such that:

$$\frac{\partial g_2(x,y,y')}{\partial r'} = \sin\theta' \; FT^{-1}\left\{ C\,(\gamma^2-K_2^2)^{1/2}\; e^{(\gamma^2-K_2^2)^{1/2}(y+y')} \right\}$$

$$- \cos\theta' \; FT^{-1}\left\{ i\,C\,\gamma\; e^{(\gamma^2-K_2^2)^{1/2}(y+y')} \right\} \qquad (6.26)$$

Observe that, the sine and cosine terms are independent of the integration variable of the FT^{-1}, and have not been transformed into Cartesian coordinates. Thus, (6.26) is one element of the double integral, with θ and θ' as integration variables, leading to the formulation of G_{mn}'.

Note that, from the properties of the FT^{-1}, a real and even function is transformed into a real and even function, and an imaginary and odd function, into a real and odd function. Thus, (6.26) will be transformed by the two internal FT^{-1}'s, into the sum of two real functions which can be reformulated as below:

$$\frac{\partial g_2}{\partial r'} = \frac{\partial g_{2r}}{\partial r'} + \frac{\partial g_{2i}}{\partial r'} \qquad (6.27)$$

where $\dfrac{\partial g_{2r}}{\partial r'} = \sin\theta' \; FTG_{2r}$, $FTG_{2r}(x,y,y') = FT^{-1}\{C\,(\gamma^2-K_2^2)^{1/2}$ ...see (6.26)$\}$ (6.28)

where $\dfrac{\partial g_{2i}}{\partial r'} = \cos\theta' \; FTG_{2i}$, $FTG_{2i}(x,y,y') = FT^{-1}\{C\,\gamma$ ...see (6.26)$\}$ (6.29)

6.5 INTEGRATION OF THE 2nd GF AND ITS DERIVATIVE: G_{mn2}, G_{mn2}'

6.5.1 Development

We want to formulate the complex integrals (6.3) and (6.4) into two integrals, one for the real part, and the other for the imaginary part, to enable numerical integration. At first, we transform the exponential complex term into a real and an imaginary part such as:

$$e^{im\theta' - in\theta} = \cos(m\theta'-n\theta) + i\,\sin(m\theta'-n\theta) \qquad (6.30)$$

Secondly, as $g_2(x,y,y')$ is only a real function as seen in (5.28), the double integral

can be separated into real and imaginary parts, so that:

$$G_{mn2} = G_{mn2real} + G_{mn2im} \tag{6.31}$$

where $G_{mn2real} = 1/2\pi \int_0^{2\pi}\int \cos(m\theta'-n\theta)\, g_2(x,y,y')\, d\theta' d\theta$ (b)

and $G_{mn2im} = 1/2\pi \int_0^{2\pi}\int \sin(m\theta'-n\theta)\, g_2(x,y,y')\, d\theta' d\theta$ (c)

with $x = x - x'$.

As mentioned in the previous section, $\partial g_2/\partial r'$ in (6.27) is a real function only. The term $G_{mn2'}$, involving the derivative of the 2nd GF, can be developed as above. Hence:

$$G_{mn2'} = G_{mn2'real} + G_{mn2'im} \tag{6.32}$$

where:

$$G_{mn2real} = \frac{1}{2\pi}\int_0^{2\pi}\int \cos(m\theta'-n\theta)[\sin\theta'\ FGT_{2r}(x,y,y') - \cos\theta'\ FTG_{2i}(x,y,y')]d\theta' d\theta \tag{b}$$

$$G_{mn2im} = \frac{1}{2\pi}\int_0^{2\pi}\int \sin(m\theta'-n\theta)[\sin\theta'\ FGT_{2r}(x,y,y') - \cos\theta'\ FTG_{2i}(x,y,y')]d\theta' d\theta \tag{c}$$

6.5.2 Discussion

Firstly we should recall that the FT are in Cartesian coordinates, based on the flat surface of the cladding for the y− axis, and on the source point for the x− axis. It follows that, after their numerical FT^{-1}, the terms involved in the 2nd GF: $g_2(r,r')$ in (5.28), FTG_{2r} in (6.28a), FTG_{2i} in (6.28b), are functions of $x = x - x'$, y, and y'. However, the integrals leading to G_{mn2} and $G_{mn2'}$ are expressed in polar coordinates centred on the core. Therefore, the results of the numerical FT^{-1} must be interpolated to correspond to the discrete angular values of the integration steps. As the variables: y, y' are independent of the FT^{-1}, for each incrementation of the source and observation points: $j\Delta\theta'$ and $k\Delta\theta$ (j,k being integer numbers, and $\Delta\theta'$,$\Delta\theta$ being the angular incrementation of θ', θ), their corresponding y' and y in

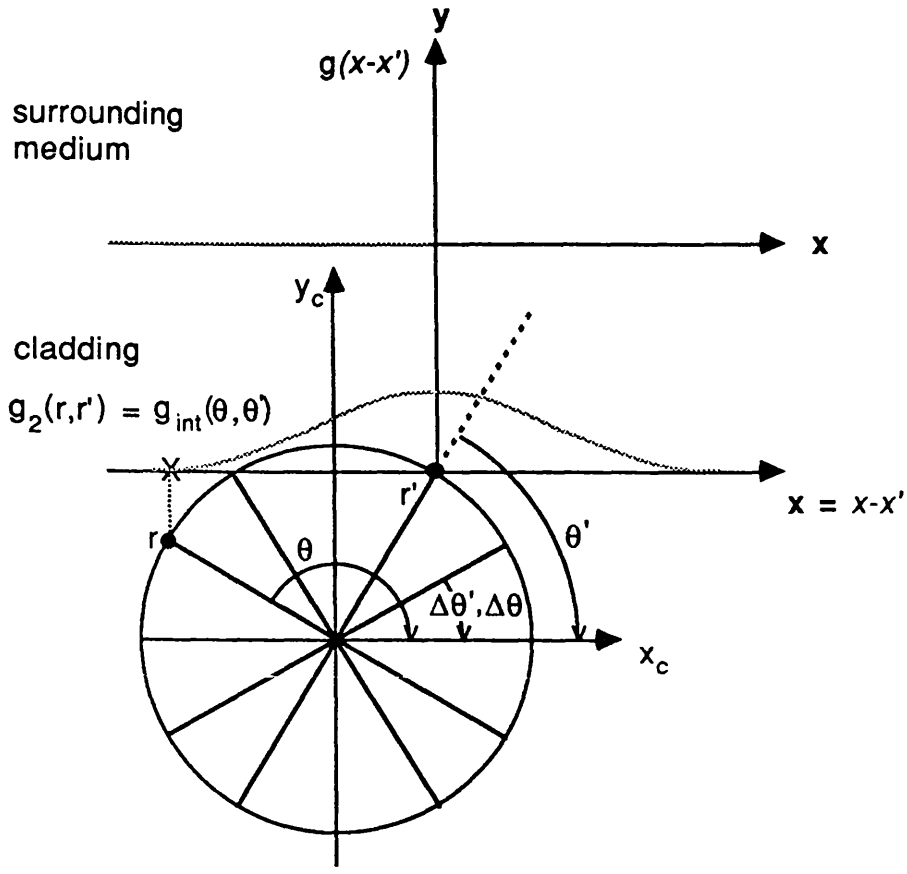

$\Delta\theta',\Delta\theta$: angular incrementation for numerical integration

r' : coordinates of the source point

r : coordinates of the observation point

Oxy : Cartesian coordinate system with the abscissa, x, based on the source point, and the ordinate, y, based on the flat surface of the cladding

Ox_cy_c : Cartesian coordinate system centred on the core

$g_{int}(\theta,\theta')$: result of the 2 nd GF after interpolation of the FFT $^{-1}g_2$ $(x-x')$

FIGURE 6.2

Definition of the angular incrementation for the numerical integration leading to Gmn2 and Gmn2' in (6.31) and (6.32).
Note that the 2nd GF: $g(r,r')$, is an element of the variable Gmn2. This term of the GF is calculated by means of a numerical Fast Fourier transform and then interpolated for the distance in abscissa corresponding to the difference in abscissa between the source and observation points: $x = x - x'$. This is also the case for the variables FTG_{2r} and FTG_{2i} leading to Gmn2'.

Cartesian coordinates, are directly calculated. Then, with these selected y, y' values, the FT^{-1} is worked out, and leads to a function with $x = x - x'$ as abscissa, as shown in fig. 6.2. Thereby, the 2^{nd} GF and its derivatives for a source and observation point corresponding to the angular incrementation of the integral in terms of θ' and θ, can be deduced by linear interpolation, knowing the difference in the x− direction from the source to the observation point.

Secondly, we want to reformulate the terms: G_{mn2} and G_{mn2}', in a matricial notation. In (6.31) and (6.32) only the sine and cosine depend on m and n. Let us consider G_{mn2} first, and in particular its real part: $G_{mn2real}$ (6.31b).

Using the following trigonometric relation:

$$\cos(m\theta'-n\theta) = \cos(n\theta-m\theta'),$$

we find:

$$G_{mnreal} = G_{nmreal} \tag{6.33}$$

Then for the imaginary part: G_{mn2im}, the following trigonometric relation:

$$\sin(m\theta'-n\theta) = -\sin(n\theta-m\theta')$$

leads to the equality:

$$G_{mn2im} = -G_{nm2im} \tag{6.34}$$

Thereby:

$$G_{mnreal} + i\,G_{mn2im} = G_{nmreal} - i\,G_{nm2im} \tag{6.35}$$

Next, in order to simplify the notation, we make the following change of variables:

$$G_{mn2real} = a_{mn}\,, \qquad G_{mn2im} = b_{mn}$$

Thus, the simplified notation of the complex matrix of G_{mn2} is reformulated as in:

$$G2 = \begin{vmatrix} a_{-\infty-\infty} + ib_{-\infty-\infty} & \cdots & a_{mn} + ib_{mn} & \cdots & \vdots \\ a_{mn} - ib_{mn} & \cdots & \cdots & \cdots & \vdots \\ \vdots & \cdots & \cdots & a_{+\infty+\infty} & +ib_{+\infty+\infty} \end{vmatrix} \tag{6.36}$$

Finally, a similar matricial formulation is applied to the elements: G_{mn2}', so that we can define the corresponding matrix: G2' as:

$$G2' = \begin{vmatrix} c_{-\infty-\infty} + id_{-\infty-\infty} & \cdots & c_{mn} + id_{mn} & \cdots & \vdots \\ c_{mn} - id_{mn} & \cdots & \cdots & \cdots & \vdots \\ \vdots & \cdots & \cdots & c_{+\infty+\infty} & +id_{+\infty+\infty} \end{vmatrix} \tag{6.37}$$

where:

$$G_{mn2real} = c_{mn}\,, \qquad G_{mn2im} = d_{mn}$$

Finally, observe that both matrices: $G2'$ and $G2$ are Hermitian, and thus:

$$G2' = G2'^{T*} \qquad G2 = G2^{T*} \tag{6.38}$$

with the superscripts T and * denoting a transposate and conjugate matrix, respectively.

6.6 REFORMULATION OF J_m'

The variable J_m' of the components: Λ_{mn}, of the eigenvalue matrix, is the last element to be reformulated. We can rewrite the property of the derivative of J_{mn} as follows:

$$\frac{dJ_m(z)}{dz} = \frac{1}{2}\{J_{m-1}(z) - J_{m+1}(z)\} \tag{6.39}$$

With the following change of variable:

$$z = \gamma_1 r' \qquad \text{and} \qquad dz = \gamma_1 dr'$$

the derivative of the Bessel function becomes:

$$\frac{dJ_m(\gamma_1 r')}{dr'} = \frac{1}{2}\{J_{m-1}(\gamma_1 r') - J_{m+1}(\gamma_1 r')\} \tag{b}$$

Note that: $J_{-m}(z) = (-1)^m J_m(z)$

Finally, note that the elements $r'J_m(\gamma_1 r')$ and $-r'J_m'(\gamma_1 r')$ constitute diagonal matrices written as in:

$$J = \begin{vmatrix} \ldots & 0 & 0 & 0 & \\ & r'J_{+m}(\gamma_1 r') & 0 & 0 & \\ & 0 & r'J_0(\gamma_1 r') & 0 & \\ & 0 & 0 & r'J_m(\gamma_1 r') & \\ & 0 & 0 & 0 & \ldots \end{vmatrix} \tag{6.40}$$

$$J' = \begin{vmatrix} \ldots & 0 & 0 & 0 & \\ & r'J_{+m}'(\gamma_1 r') & 0 & 0 & \\ & 0 & r'J_0'(\gamma_1 r') & 0 & \\ & 0 & 0 & r'J_m'(\gamma_1 r') & \\ & 0 & 0 & 0 & \ldots \end{vmatrix} \tag{6.41}$$

6.5 MATRICIAL REFORMULATION OF THE PROBLEM

With the previous matricial notation we can rewrite matrix M in (6.6) as in:

$$M = J\{G1' + G2'\} + J'\{G1 + G2\} \tag{6.42}$$

where:

- J and J' are the diagonal matrices given in (6.40) and (6.41),
- G1 and G1' are the diagonal matrices defined in (6.15) and (6.18) which include the effect of the 1st part of the GF and its derivative, respectively,
- G2 and G2' are the Hermitian matrices defined in (6.36) and (6.37) which include the effect of the 2nd part of the GF and its derivative, respectively.

For the computational operations, we separate the real and imaginary parts of the final matrix M as in:

$$M = A + i\,B \qquad (6.43)$$

The imaginary part is due to the 2nd GF and its derivative, and appears in the formulation of G2 and G2', as seen in (6.36) and (6.37).

7.1 INTRODUCTION

In order to optimize the numerical calculation of the propagation constants from the eigenvalue problem defined in sect. 6.5, it is necessary and interesting to know the behaviour of the GF for any pair of source and observation points on the contour of the core.

As the 1st part of the GF was analytically defined in equation (5.23) of section 5.1.5, we start by considering the values of the 2nd GF, which involves further numerical calculation from its integral form defined in equation (5.28).

7.2 FFT^{-1} AND LINEAR INTERPOLATION LEADING TO THE 2nd GF

As defined in sect. 5.1.7, the 2nd GF is regular and continuous everywhere, and is the part of the GF which takes the boundary conditions into account, and in particular those at the interface between the flat surface of the cladding and the surrounding medium. However, this term of the GF is calculated by a numerical inverse Fast Fourier transform (FFT^{-1}), followed by a linear interpolation for a pair of source and observation points.

7.2.1 Choice of the numerical parameters

From the results of the FFT^{-1}, for example in fig. 7.1, we first choose the sampling frequency: $\Delta\gamma \geq 1/(2\ dm)$, where dm is the core diameter, so as to include all the possible pairs of source and observation points on the contour of the core. Remember that the propagation constant, β, or its equivalent, the effective refractive index of its corresponding guided mode, n_e, is the only unknown of our eigenvalue problem defined in chapter 5. It follows that, we have to choose an arbitrary value of n_e to study the behaviour of the GF, for example, $n_e = 1.455$, which is included within the possible range of guided modes (i.e., $n_2 < n_e < n_1$). To define our problem, we set the core/flat distance equal to zero. Then, we define the refractive indices of the core, cladding and surrounding medium as: $n_1 = 1.4563$,

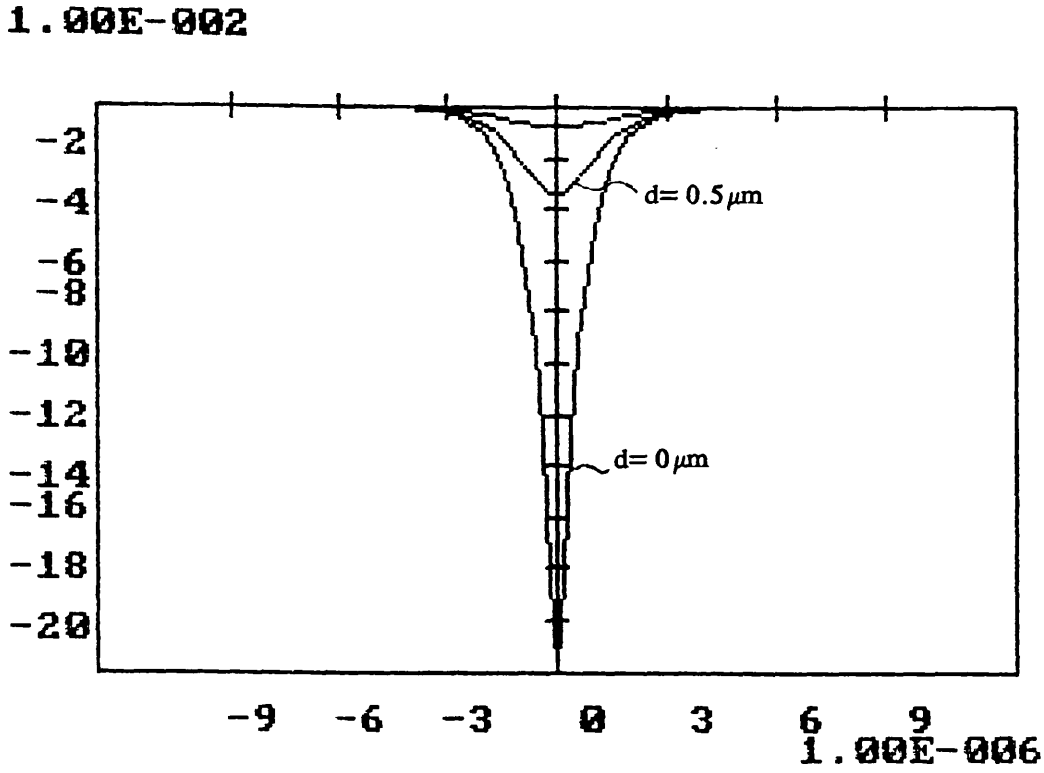

FIGURE 7.1

FFT^{-1} leading to the 2nd GF for an arbitrary value of the effective refractive index, n_e, of a guided mode, and several core/flat distances:
$d = 2, 1, 0.5, 0\ \mu m$.
The source and observation points have the following values:
$\theta = 80°$ and $\theta' = 90°$, or vice versa.
The refractive indices of the guiding structure are given by the following inequality:

$$n_3 < n_2 < n_e < n_1 ,$$

where
n_3 is the refractive index of the surrounding medium (air in this case),
n_2 is the refractive index of the cladding,
n_1 is the refractive index of the core.

$n_2 = 1.45$ and $n_3 = 1$, respectively, and a core radius of 4 μm. In this situation, to minimize the aliaising effects caused by the numerical Fourier transform, we choose that:

$$\Delta\gamma \geq 1/\{2\ (x-x')_{max} \quad \text{where } (x-x')_{max} = 3/2 \text{ dm}$$

where $x = (x - x')$ is the spatial domain variable of the FFT^{-1}.

The number of points is then optimized so that the linear interpolation of the FFT^{-1} is of sufficient accuracy, as shown in fig. 7.2. We could have chosen a higher order interpolation and a larger interval in the spatial domain, but the linear interpolation was preferred for the simplicity of the algorithm and because of its suitability to the discrete curve to be interpolated.

7.2.2 Results of the FFT^{-1}

Even with an arbitrary value of β, the result of the FFT^{-1} can already give an intuitive understanding of the behaviour of the 2nd GF by varying the core/flat distance and the angular position of the source and observation points.

a. We first analyse the effect of the core/flat distance on the result of the FFT^{-1}. From fig. 5.4, which defines the coordinate system, and from the formula (5.28) to be FFT^{-1}, we recall that the distance from the core to the flat surface of the cladding, is implicitly given by the choice of the y− coordinate at the cladding/surrounding medium interface. Having set the data of the FFT^{-1}, we can demonstrate the effect of the core/flat distance, d, by comparing the results for a pair of source and observation points with angular positions of 80° and 90°, respectively, where d= 0, 0.5 and 1 μm, as in fig. 7.1. We first observe that, the FFT^{-1} used to calculate the 2nd GF, induces a negative contribution which decreases with an increase in core/flat distance, for any difference in abscissa between the source and observation points, i.e., $x - x'$. This implies that, if the distance: d, is sufficiently large, the whole cladding is supposed infinite. We also confirm the reciprocity relation of the 2nd GF, i.e., $g_2(r,r') = g_2(r',r)$ by the symmetry of the FFT^{-1} in terms of its

a.

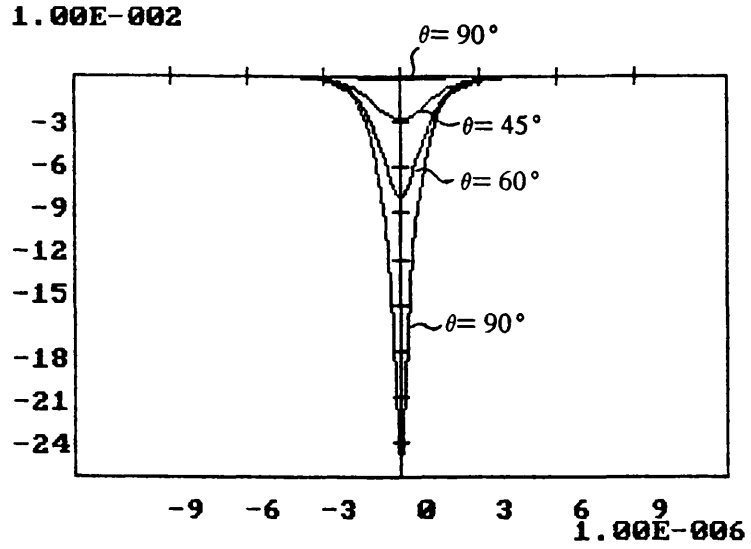

b.

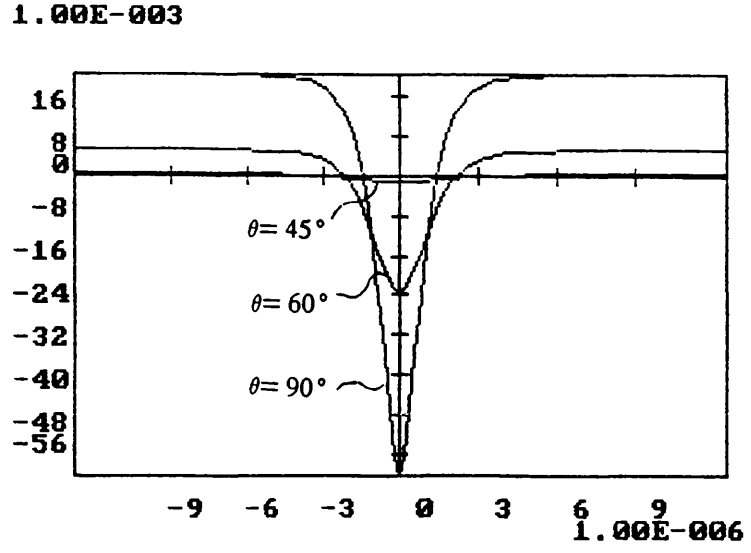

FIGURE 7.2

a. FFT^{-1} leading to the 2nd GF for a source point fixed with $\theta' = 90$, and the observation point variable with:
θ = 90°, 60°, 45° and 10°.
The other parameters are defined in fig. 7.1.

b. Value of the 2nd GF for the pair of source and observation points defined below, after the addition of the 1st GF and interpolation of the FFT^{-1} curves.
X represents the value of the total GF.

abscissa values: $x - x'$, and by the y and y' dependence of the function to be transformed, as in: $y + y' = y' + y$.

b. Secondly, we study the effect of the angular position of the source and observation points. From the previous subsection on the effect of the core/flat distance, we can deduce the additional effect caused by the angular position of both points decays exponentially with the distance to the flat of the cladding, or in other words for both source and observation point with an angular position of 90° (see fig. 7.3 for the definition of the angles). This property is confirmed by fig. 7.2a showing the FFT^{-1} with $x - x'$ as abscissa, with the ordinate of the source point at an angular position of 90°, and with several observation points (one per curve). We then observe that, for $\theta = 90°$ and $180° < \theta < 360°$, or vice versa according to the reciprocity relation, the maximal value of the GF becomes negligible. However, before the automatic suppression of the calculation of these FFT^{-1} producing negligible values, we want to take into account their interpolation which gives the value of the 2nd GF, and also the offset values caused by the addition of the 1st GF, as described in fig. 7.2b, and demonstrated in later subsections. We also recall that, the effective refractive index, n_e, is arbitrary. Consequently, it may affect the behaviour of the FFT^{-1}, and thus the whole GF, as explained below.

7.3 VARIATION OF THE GF AS A FUNCTION OF θ AND θ'

With the same parameters as the in the previous section, i.e., $d = 0$, $n_1 = 1.4563$, $n_2 = 1.45$, $n_3 = 1$, and $n_e = 1.455$, we want to analyse the effect of the angular position of all the range of source and observation points on the contour of the core. Therefore, we compute the GF for several source points, for example, $\theta' = 0°$, 30°, 60°, and 90° (one per curve), and for all the range of observation points, θ, which occur in the interval: $0 < \theta < 120°$, as abscissa.

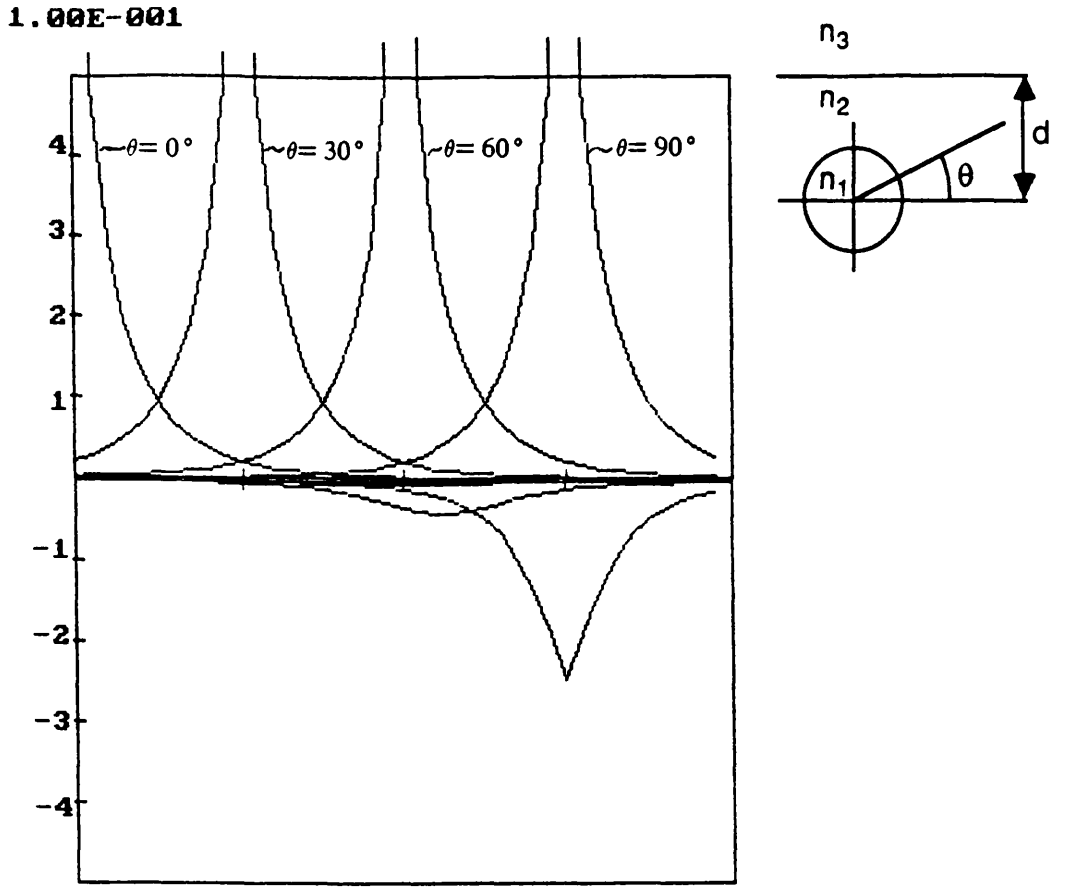

a.

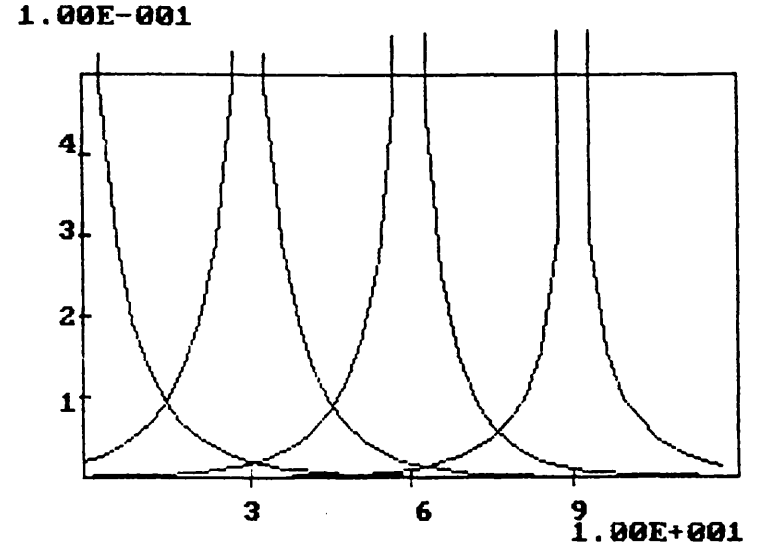

b.

FIGURE 7.3

a. Variation of the 1st GF and 2nd GF as a function of the angular position, θ', of the observation points, the source point having a fixed angular coordinate for each curve, i.e., for θ = 0°, 30°, 60° and 90°. The curves with positive values represent $g_1(\theta,\theta')$, and the negative ones $g_2(\theta,\theta')$.
The other parameters of the guide defined in fig. 7.1, are set as follows: d= 0, n_3= 1, n_2= 1.45, n_1= 1.4563, n_e= 1.455.

b. Variation of the total GF: $g_1(\theta,\theta')+g_2(\theta,\theta')$, with the same parameters as above.

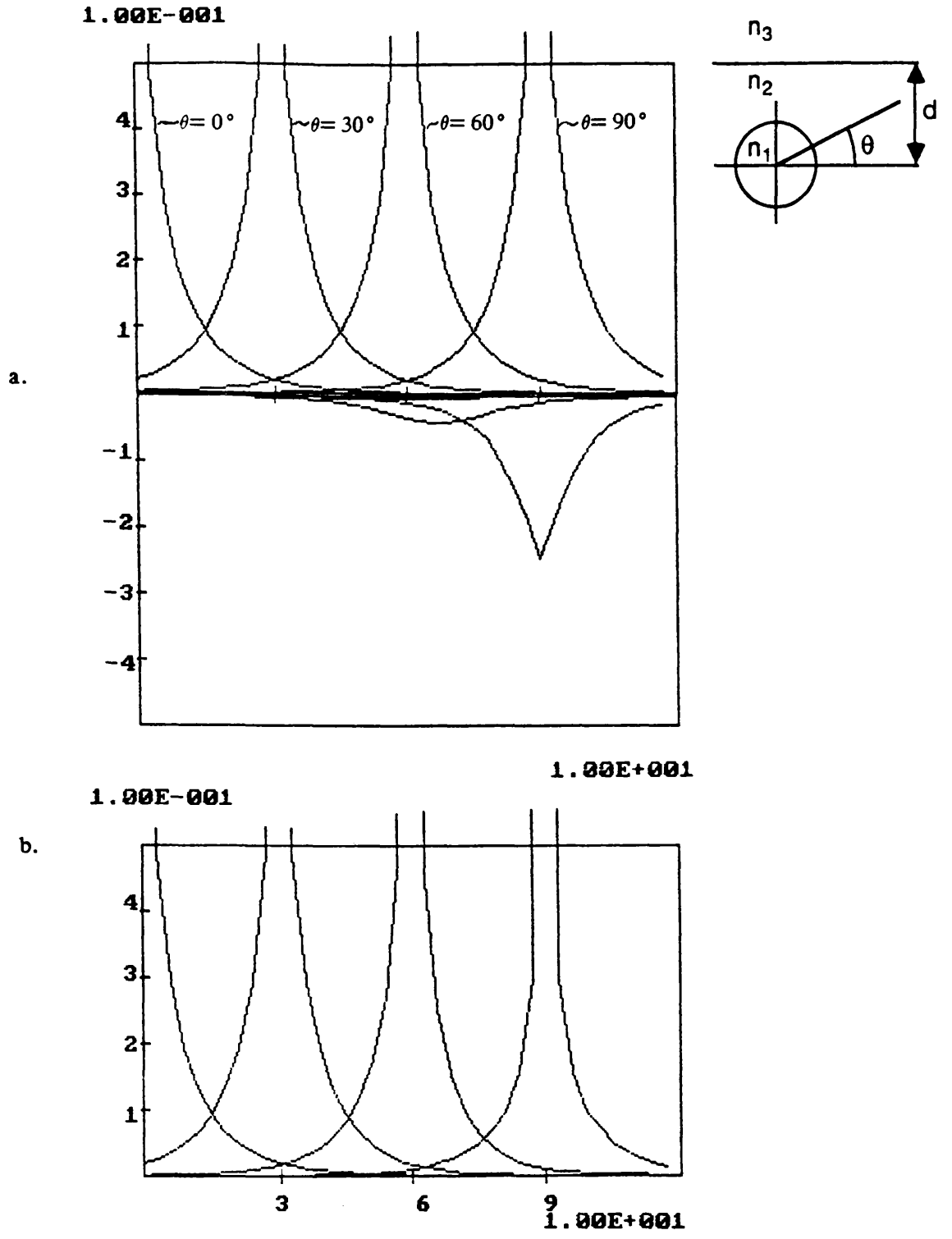

FIGURE 7.3

a. Variation of the 1st GF and 2nd GF as a function of the angular position, θ', of the observation points, the source point having a fixed angular coordinate for each curve, i.e., for θ = 0°, 30°, 60° and 90°. The curves with positive values represent $g_1(\theta,\theta')$, and the negative ones $g_2(\theta,\theta')$.
The other parameters of the guide defined in fig. 7.1, are set as follows: d= 0, n_3= 1, n_2= 1.45, n_1= 1.4563, n_e= 1.455.

b. Variation of the total GF: $g_1(\theta,\theta')+g_2(\theta,\theta')$, with the same parameters as above.

The upper values in fig.7.3 show the variation of the 1st GF as a function of the variation of the angular position of the observation point, with the source point fixed. Each curve is valid for one value of the observation point. We remember that the 1st GF represents the intensity of the field caused by a source point at an observation point also on the contour of the core (as set in chap. 5). This implies that the 1st GF is only dependent on the angular position of both source and observation points, i.e., $g_1(\theta,\theta')$. These field intensities have a positive value only. Their maximum value is infinity, when the coordinates of the selected source point are equal to that of the observation point, as seen in fig. 7.3. This confirms that the value of $g_1(\theta,\theta')$ for $\theta=\theta'$ in (5.23) is proportional to the Bessel function $K_0(0)=K_0(|K^2|R)$, with R being the distance between the source and observation points. Finally note, that each curve formed by the different values of the GF for all the range of observation points, has equal amplitude. This proves the independence of the 1st GF towards the boundaries, and its dependence of the distance between the source and observation points (R).

The lower values of fig. 7.3 represent the 2nd GF for an abitrary source point, as a function of the angular value of the observation point. As for the 1st GF, each curve is valid for one value of the source point. However, the 2nd GF is dependent on the boundary conditions. It follows that, its contribution to the total GF in fig. 7.3b will vary for different pairs of source and observation points around the core. The boundary conditions also imply a dependence of the 2nd GF as a function on the refractive index of the surrounding medium and the geometry of the guiding structure, i.e., on the core/flat distance, d. Any variation of these above parameters will also affect the value of the propagation constants of the modes and their corresponding effective refractive indices. Consequently, we will consider the effects of these different parameters in the following sections.

Now, let us explain the limitation of the range in abscissa (θ) of the curves in fig. 7.3a and 7.3b. The truncation of the figures along their abscissa was chosen to enable the full decay of the curve corresponding to the angular position of the source point at 90°. Then, the discrete values of the source points were chosen in

the first quadrant, i.e., for $0° < \theta' < 90°$, to induce a maximum effect on $g_2(\theta,\theta')$ from the boundary at the core/flat surface of the cladding. Due to the axial symmetry of the guide along the y− axis, i.e., $g(\theta,\theta') = g(\pi - \theta, \pi - \theta')$, the second quadrant could also have been chosen.

7.4 VARIATION OF THE GF AS A FUNCTION OF d AND n_3

7.4.1 GF(d)

First of all, we analyse the variation of the GF as a function of the distance from the surface of the core to the flat of the cladding (see fig. 4.1). We first consider the effect on the 1st GF and then on the 2nd GF.

a. As the 1st GF is independent of the boundaries, it is not directly dependent on the core/flat distance, but indirectly affected by the change of β. This change in propagation constant may be caused by the variation of the refractive index, n_3, of the surrounding medium at the side of the flat surface of the cladding, and of the core/flat distance, d, if it is small enough as defined in (5.14b). The other parameters, the refractive indices of the core, n_1, and the cladding, n_2, the core diameter of the fibre and the wavelength of the light source are fixed. Thus, the propagation constant of the coupler has a different value to that of a circular fibre built from the same preform and having a cladding supposed infinite. This effect has already been discussed in the CMT for a weak coupling situation in chapter 3.

b. The 2nd GF takes into account the boundary conditions and is directly dependent on the distance: d. In fig. 7.4a and 7.4b we show the values of the 2nd GF for different source points at 30°, 60° and 90°, with the observation points as abscissa. As mentioned in sect. 7.1.2 on the FFT^{-1} leading to the 2nd GF, its negative amplitude is at a maximum for both source and observation points at 90°, and its decay is proportional to an

a.

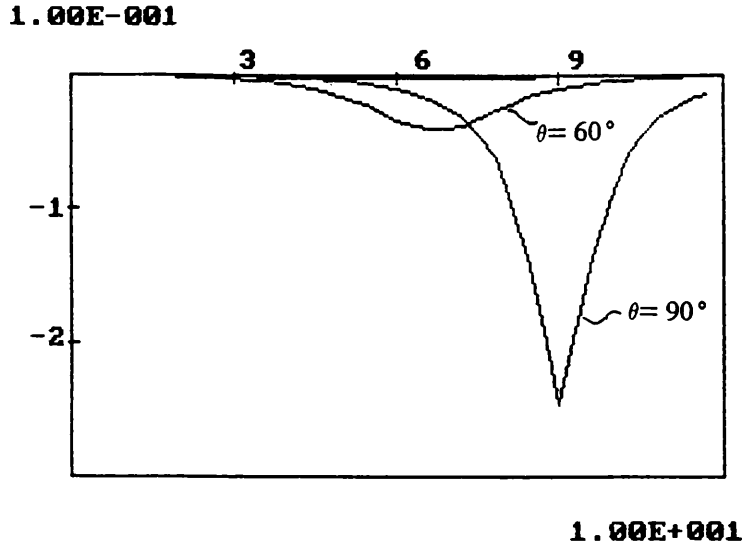

b.

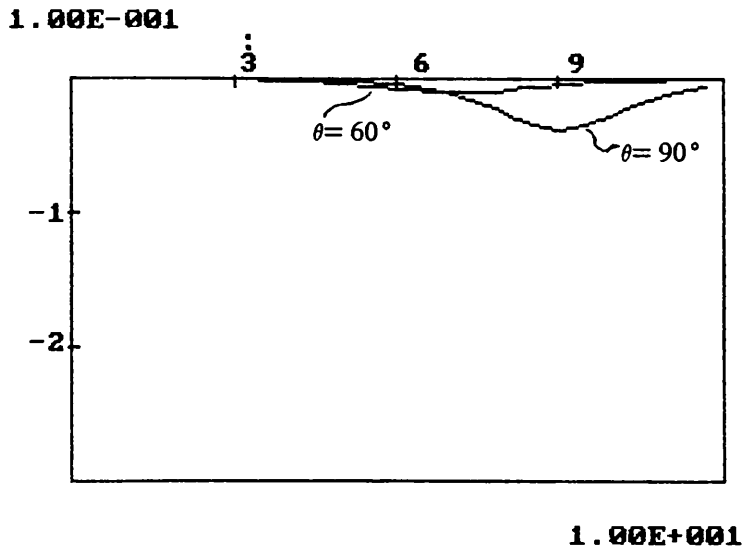

FIGURE 7.4

Variation of the 2nd GF as a function of the angular position, θ', of the observation points, the source point having a fixed angular coordinate for each curve, i.e., for θ = 0°, 30°, 60° and 90°.
The following parameters of the guide:
$n_3 = 1$, $n_2 = 1.45$, $n_1 = 1.4563$, $n_e = 1.455$
are defined in fig. 7.1.

a. The first figure represents $g_2(\theta, \theta')$ with a value of the core/flat distance equal to zero, i.e., d = 0μm.

b. The second figure represents $g_2(\theta, \theta')$ with d = 0.5μm.

increase in the core/flat distance. For $d \geq 1\,\mu m$ the maximum of the GF becomes negligible for the guiding structure defined in sect. 7.2.

7.4.2 GF(n3)

We now study the variation of the GF as a function of the refractive index of the surrounding medium. We set the core/flat distance equal to zero, to allow the maximum effect of the boundary between the cladding and the surrounding medium, and assume a constant value of β as above. We also recall that the calculation of β by the GF applies to all the values of n_3, allowing at least the propagation of one guided mode.

At first, we consider the effect of n_3 on the 1st GF. This function is independent of n_3, and thus the same comments as those previously used to analyse the effect of d, apply to the variation of β caused by the change of n_3.

We then consider the second part of the GF for different n_3, which can be either superior or inferior to the refractive index of the cladding. Note that, in both cases at least one guided mode must propagate inside the D– fibre (with $n_3 < n_e < n_1$) as explained below.

a. In the first case, the 2nd GF induces a negative contribution on the total GF as described by fig. 7.5a, and for example, as assumed in the previous sections where $n_3 = 1 < n_2 < n_e$. This can be seen as if one equivalent source point taken on the contour of the core, was reflected at the cladding– surrounding medium interface, and then observed at one observation point also on the contour of the core.

b. The second case, described in fig. 7.5b is valid for: $n_2 < n_3 < n_e$. It induces the positive contribution from the 2nd GF on the total GF, as if the equivalent source point was this time transmitted at the cladding– surrounding medium interface.

a.

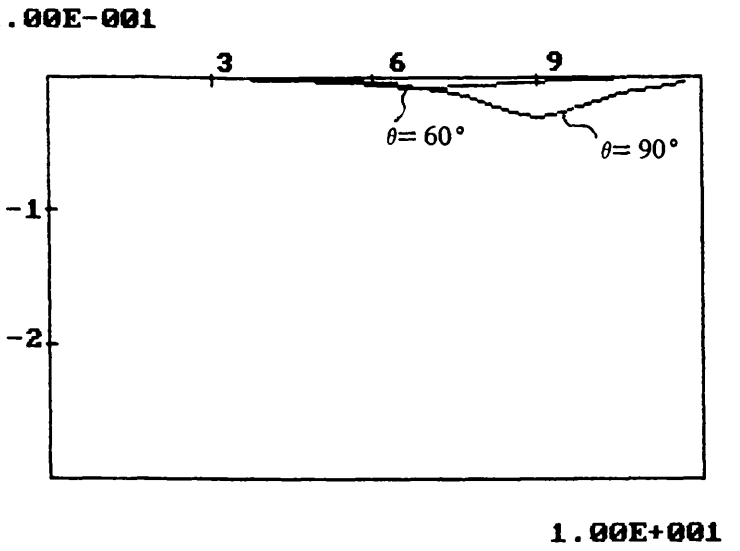

b.

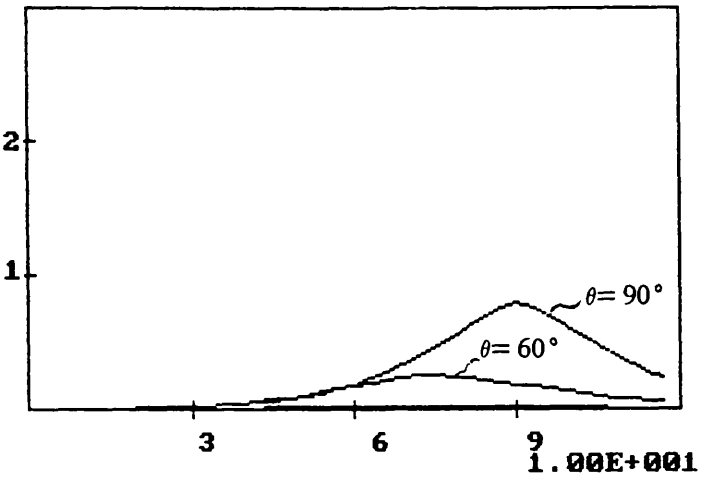

FIGURE 7.5

Variation of the 2nd GF as function of the angular position, θ', of the observation points, the source point having a fixed angular coordinate for each curve, i.e., for θ = 0°, 30°, 60° and 90°.
The following parameters of the guide:
d= 0, n_2= 1.45, n_1= 1.4563, n_e= 1.455
are defined in fig. 7.1.

a. The first figure represents $g_2(\theta,\theta')$ for a value of the refractive index of the surrounding medium satisfying the following inequality: $n_3 > n_2$, and in particular: $n_3 = n_e = 1.455$

b. The second figure represents $g_2(\theta,\theta')$ for $n_3 < n_2$ and in particular for: $n_3 = 1.445$.

7.5 VARIATION OF THE GF AS A FUNCTION OF n_e

Finally, let us see the influence of the effective refractive index of a guided mode on the 2nd GF. The maximal possible value of n_e, occurs when its value is equal to the refractive index of the core. In this situation, the mode is well confined inside the core, and its evanescent field decays rapidly inside the cladding region. This implies, that the perturbation caused by the reduced cladding at one side of the fibre is minimal. However, when the value of n_e is close to the refractive index of the cladding, the mode has a weak confinement, and its evanescent field extends further into the cladding than in the previous situation. It follows that, the influence of the boundaries increases for an effective refractive index closer to the value of n_2 than that of n_1. We demonstrate this effect by comparing the curves describing $g_2(90°,\theta)$: one with $n_e = n_1$ and the other with $n_e \approx n_2$, as in fig. 7.6a and 7.6b, respectively. This effect is also seen on the total GF as shown in fig. 7.7.

7.6 DISCUSSION

First of all, we recall that the parameters of the numerical calculation (FFT^{-1} and interpolation) of the 2nd GF, using the intermediate analytical result obtained in (5.28) as the basic formula, have been determined in the previous sections.

Then, from the analytical approach to the eigenvalue problem where the propagation constant of the guided mode, β, is the only variable, we remember that both source and observation points were chosen on the contour of the core (see sect. 5.2.2). Thus, the radial angular coordinate of both points satisfies the following equality: $r = r' = a$ (a being the core radius), and the GF is simply a function of the angular position, i.e., $g(\theta,\theta')$. We also recall from sect. 7.3, that the number of FFT^{-1} to be calculated, can be reduced due to the following properties of the GF:

$$g(\theta,\theta') = g(\theta',\theta)$$

and $$g(\pi-\theta,\pi-\theta') = g(\theta,\theta')$$

However, as β (or the corresponding effective refractive index, n_e) is the unknown of our problem, it is impossible to determine if the calculation of the FFT^{-1} is

a.

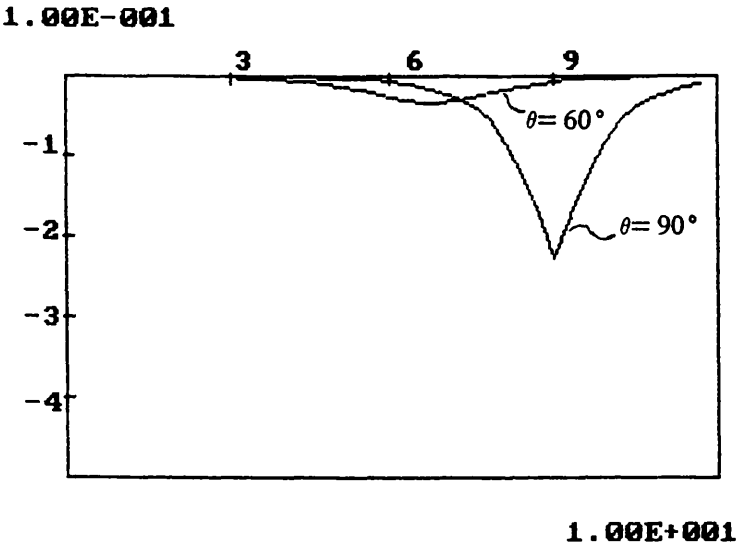

b.

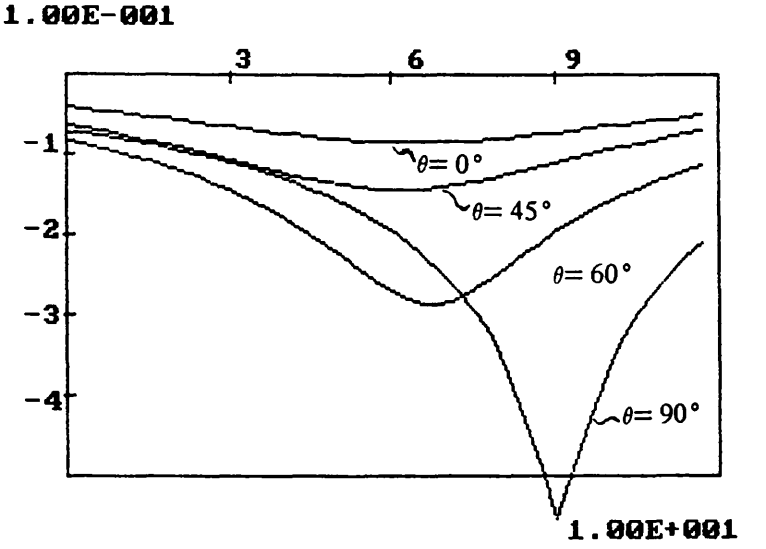

FIGURE 7.6

Variation of the 2nd GF as a function of the angular position, θ', of the observation points, the source point having a fixed angular coordinate for each curve, i.e., for θ = 0°, 30°, 60° and 90°.
The following parameters of the guide:
d= 0, n_1= 1.4563, n_2= 1.45, n_3= 1,
are defined in fig. 7.1.

a. The first figure represents $g_2(\theta,\theta')$ for a value of the effective refractive index of a guided mode equal to the refractive index of the core, i.e., for $n_e = n_1$.

b. The second figure represents $g_2(\theta,\theta')$ for a value of the effective refractive index of a guided mode equal to the refractive index of the cladding, i.e., for $n_e = n_2$.

a.

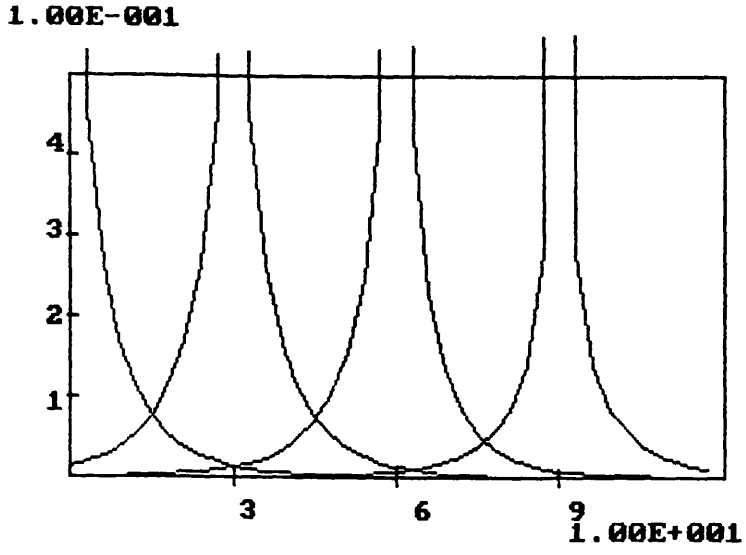

b.

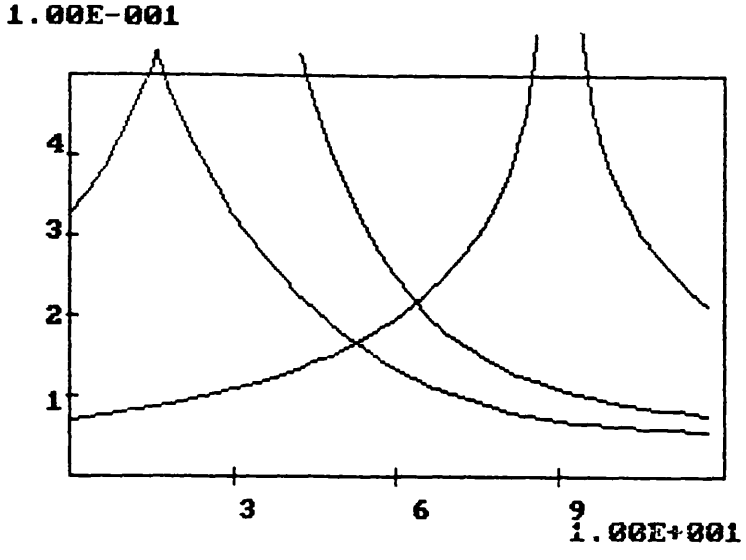

FIGURE 7.7

Variation of the total GF as a function of the angular position, θ', of the observation points, the source point having a fixed angular coordinate for each curve, i.e., for θ = 0°, 30°, 60° and 90°.
The following parameters of the guide:

$d = 0$, $n_1 = 1.4563$, $n_2 = 1.45$, $n_3 = 1$,

are defined in fig. 7.1.

a. The first figure represents $g(\theta,\theta')$ for a value of the effective refractive index of a guided mode equal to the refractive index of the core, i.e., for $n_e = n_1$.

b. The second figure represents $g(\theta,\theta')$ for a value of the effective refractive index of a guided mode equal to the refractive index of the cladding, i.e., for $n_e = n_2$.

necessary for the full range of source and observation point, with angular positions between: $180° < \theta', \theta < 360°$. For these values of θ' and θ, it would be possible to suppress the calculation of the 2nd GF, and therefore its FFT^{-1}, for a value of n_e close to the refractive index of the core. In this situation only, the corresponding guided mode is well confined inside the core, and the disturbance of the evanescent field by the surrounding medium is weak, and thus the 2nd GF is small and negligible in comparison with the value of the 1st GF.

Consequently, the program developed to calculate the GF (see appendix 1) will help us to reduce the operational time of the main program, which calculates the propagation constant of a D– fibre with different values of the refractive index of the surrounding medium. What is more, several procedures used and tested in this first program calculating the GF, will be introduced in the main program, for example: the FFT–1, INTERPOLATION, and BESSEL procedures.

Note finally, that the numerical calculation and the introduction of the 1st GF into the total GF, will not be used in the main program. As seen in chapter 6, the 1st GF is reformulated with Graf's expansion, and introduced inside a double integral (6.13) to suppress the singularity caused by $g_1(\theta, \theta') = K(0)$ in (6.14), when the angular coordinate of the source point equals that of the observation point.

7.7 FURTHER DEVELOPMENTS AND CONCLUSIONS

Using the results and some of the procedures from the program calculating the GF, we can now develop the main program which calculates the propagation constant of a guided mode, β, of a D– fibre. Its proposed flow chart is given in appendix 2. Its procedures have been tested separately, although the full program is not in operation. This program stores several important matrices simultaneously. We give the dimensions of the main matrices below:

2 x cpnt–M, created in the G1–G2–CALC. procedure

4 x nb–angle x nb–angle, created in the g2–FTG2r–FTG2i–CALC. procedure

2 x cpnt–M x cpnt–M, created in the M–CALCULATION procedure.

Each of these procedures has one internal important matrix of the following

dimensions: cpnt–serie, 2 x point, and 2 x nb–angle, respectively.

The integer variables: cpnt–M, nb–angle, cpnt–serie, and point are defined in appendix 2 in the INPUT–CONST procedure. The only matrix in which the optimum number of elements (cpnt– M) has to be determined by running the whole program is the complex matrix M= A+ iB as seen in sect. 6. We recall that the real and imaginary part of a complex matrix are calculated separately because of the choice of programming language. In chapter 6, the number of components of the matrices A and B is still defined as infinite, i.e., $-\infty < m,n < +\infty$, with m being the number of column elements, and n being the number of row elements. The real and imaginary part of the elements of matrix M, i.e., Amn and Bmn as defined in sect. 6.5, are negligible for a high order value of their row or column elements. Therefore, we can truncate matrices A and B, so that:

– cpnt–M div 2 < m,n < cpnt–M div2,

with cpnt–M being the number of elements of these square matrices. Now, if we suppose a value of cpnt–M equal to 20, the total storage capacity used to memorized the above matrices simultaneously, is approximately 37 Kbytes. However, we cannot double the number of angular integration points without exceeding the maximum memory capacity assigned to data by the operational system DOS (i.e, 64 Kbytes. Another inconvenience of using Turbo Pascal– 3 on a personal computer, in our case the IBM– AT, is the operational time. The transfer of the program to a main frame computer, would overcome these disdvantages.

Having thus defined the program calculating the propagation constant, we will be able to compute by successive iterations, the β eigenvalues which are the solutions of our problem as defined in (5.42). The different β are real, as we have defined our problem for guiding situations only. Their variation is a combination of the core/flat distance, d, and the refractive index of the surrounding medium, n_3. The other parameters are fixed by the characteristics of the fibre and the wavelength of the laser. The two main observations which can be made on the variation of β are described below.

a. At first, we determined the full range of core/flat distances, d, and refractive indices of the surrounding medium, n_3, which still allows the propagation of at least one guided mode inside our D− fibre. The limiting case of the existence of β, will give the condition on d and n_3 for the loss of a guided mode in favour of a leaky mode.

The loss of one guided mode propagating in a D− fibre surrounded by an air medium, in comparison with the propagation constant of the same fibre surrounded by a higher refractive index medium, implies that this mode leaks out into the surrounding medium. Therefore, if this high refractive index surrounding medium is locally introduced on top of a D− fibre, for example as in a fibre to prism coupler, the energy of the initial guided mode, leaks and couples out into the radiation mode with the same propagation constant as the initial guided mode of the D− fibre.

Observe that, if we increase the value of n_3 for a small value of d, the real propagation constant of the high order guided mode will disappear before that of low order. This is due to a value of the effective index of a higher order mode closer to n_2 than that of a low order mode. The effect of n_e has been discussed in sect. 7.5.

b. Secondly, we will also be able to calculate the difference in propagation constants induced by the reduced cladding of a D− fibre and/or a refractive index of the cladding superior to that of the air. For example, the difference in propagation constants between a D− fibre and its corresponding circular fibre pulled from a similar preform, is found by calculating the β for a value of the refractive index of the surrounding medium different to that of the cladding, i.e., for $n_3 \neq n_2$, and then for a value of its refractive index equal to that of the cladding, i.e., $n_3 = n_2$.

Next, we observe that the definition of one β− value can enable the calculation of the scalar field in the caldding region, by the use of the Kirchhoff− Huygens

integral in (4.16) which was the basic function of our analytical development.

In conclusion, in this thesis we have considered several approaches to the evanescent field coupling of a D− fibre.

The simplest is the ray approach applied to a multimode fibre. By plane wave analysis, the input skew and elevation angle of a fibre to prism coupler, were defined (see sect. 3.3.1). The leaky rays provide a first understanding of an evanescent coupler formed by a fibre and a semi− infinite dielectric substrate (3.26).

We then studied the CMT (see sect. 3.1) which is defined for a weak coupling situation, and usually applied to a guiding structure formed by two similar guides, and which was extended by Arnaud [Ar2] to demonstrate the coupling from a planar guide to a semi− infinite medium acting as a mode sink. However, this method is not accurate.

Next, with the chosen GF method, we analysed the loss of confinement of a coupling structure formed by a D− fibre and a semi− infinite dielectric medium, for example a prism. This loss of one guided mode in favour of a leaky mode, characterizes the limiting values of the core/flat distance and refractive index of the surrounding medium, over which one guided mode of the fibre couples into the radiation mode of the prism.

Note that, this semi− numerical method is ideally suited to a planar stratified environment, and in particular our D− fibre, where the GF can be calculated by an elementary Fourier method. The use of the scalar field is appropriate for our weakly guiding fibre, and implies a scalar GF. The formulation of the boundary conditions is exact and intrinsic. The main disadvantage of the chosen GF comes from the important computational operations.

Finally, it would be of great interest to extend the GF method to leaky mode situations, by an analytical continuation of the theory elaborated for the guided modes. Therefore, it would be possible to calculate the complex propagation constants of the leaky modes, thus to totally define the evanescent field coupling of a D− fibre to a prism.

APPENDIX 1

PROGRAM FOR CALCULATION OF GF(θ,θ')

INPUT-CONST

dist: core/flat distance
n_3: refractive index of the surrounding medium interface
n_e: effective refractive index of the guided mode
delta: interval in the spatial domain of the FFT
nb–angle: number of pairs of source and observation points selected on the contour of the core

CALCULATION

- choice of the angular position of the source point:
  $\theta' = ?$
  $b = 0$ with $b\{0,\ldots,nb\text{-}angle\}$
- incrementation of the observation point:
  $\theta = b\,\Delta\theta$

GREEN-FUNCTION : calculation of $g(\theta,\theta')$
- calculation of x,x',y,y' of the source and observation point in coordinates of the flat surface of the cladding

- FUNCT
  calculation of the function to be FFT^{-1}
  separation in a real and imaginary part

- FFT^{-1}
  use of the FFT routine: FOUR, and
  correction of the phase and the amplitude

- calculation of the 1^{st} GF by the use of the Bessel function routine: BESSEL

- INTERPOLATION
  interpolation routine of the 2^{nd} GF

Y
if $\theta < 360°$

GRAPHIC
graphic of the GF for the selected source point and the observation point variable as abscissa.

Y
choice of another source point?

SUMMARY

summary of the input data

APPENDIX 2

PROGRAM FOR CALCULATION OF β FOR A D-FIBRE

INPUT-CONST

dist: core/flat distance
n_3: refractive index of the surrounding medium interface
n_e: effective refractive index of the guided mode
delta: interval in the spatial domain of the FFT
nb-angle: number of pairs of source and observation points selected on the contour of the core
cpnt-serie: number of elements of the Graf expansion for the calculation of the 1st GF
cpnt-M: order of the matrix M
nb-iteration: number of iterationsfor the calculation of β

it =0 , integer for the incrementation of the number of iteration, with its maximum: nb-iterations

G1-G2-CALCULATION

- calculation of the diagonal elements, Gmn1 (6.13) and Gmn1' of the matrices G1 (6.15) and G2 (6.18), respectively

- use of the procedures BESSEL-J and BESSEL-K for the calculation of K_m, J_{m+1} and J_m

g2-FTG2r-FTG2i-CALCULATION

- calculation of the variables:
  $g_2(\theta,\theta')$, $FTG_{2r}(\theta,\theta')$, $FTG_{2i}(\theta,\theta')$
  for all the range of $\theta' = a.\ \Delta\theta'$, a{0,...nb-angle}
  $\theta' = b.\ \Delta\theta'$, b{0,...nb-angle}

- use of the procedures FFT-1 and INTERPOLATION

M-CALCULATION

```
m=1
m=m +1 -(cpnt-M div 2)          : incrementation of the rows
    n=-1
    n=n +1 -(cpnt-M div 2)      : incrementation of the columns

    Gmn2-Gmn2'-calculation
      double numerical integral expressing:
         Gmn2real   in (6.31b)
         Gmn2im     in (6.31c)
         Gmn2'real  in (6.32b)
         Gmn2'im    in (6.32b)
    - calculation of Jmn (6.40) and Jmn' (6.41)
    - calculation of the real components of M:
      Amn = Jmn(Gmn2'real +Gmn2'im) +Jmn(Gmn2'real +Gmn2'im)
    - calculation of the imaginary components of M:
      Bmn = Jmn(Gmn2'im) +Jmn(Gmn2'im)

    if n<cpnt-M div 2

if m<cpnt-M div 2
```

DETERMINANT

calculation of the complex determinant of the matrix:
det(M - I), (I being the identity matrix)
using an algorithm with Gaussian elimination and
partial pivoting

ITERATION

if it>0 then iteration by the secant method algorithm:

$$\beta_{it+1} = \beta_{it} - \left| \frac{(\beta_{it-1} - \beta_{it}) \, | (det_{it} / det_{it-1})}{1 - (det_{it} / det_{it-1})} \right|$$

it = it + 1

Y

if (det>0 and it<nb-iterations)

N

SUMMARY

summary of the input data

LIST OF REFERENCES

Ab Abramowitz, M., Stegun, I.A.,
Handbook of mathematical functions
Dover, New York, 1965

Ad Adams
An introduction to optical waveguides
John Wiley & Sons

Al Alferness, R.C., Ramaswamy, V.R., et al.
Efficient single mode fibre to titanium diffused
lithium niobate coupling for λ=1.32 μm
J. Quant. Electron. 18, 10, 1982, p.1807

Ar Arnaud, J.A.
Transverse coupling in fiber optics.
Part I: coupling to trapped modes.
Bell Syst. Techn. J., 53, 2, 1974, p.217

Ar2 Arnaud, J.A.
Transverse coupling in fiber optics.
Part II: coupling to mode sinks
Bell Syst. Techn. J., 53, 1974, p.675

Bg Bergh R.A., Kottler, G., Shaw H.J.
Single mode fibre optical directional coupler
Electron. Lett. 16, 7, 1980, p.260

Bl Black, R.J., Pask, C.
Developments in the theory of equivalent step index fibres
J. Opt. Soc. Am., 1, 11, 1984, p.1129

Br Bradley, L., Millar, C.A.
A new method of fibre film coupling
Conf. on Lasers and Electr. Opt., San Francisco (U.S.A.), 1986
paper MF5

Br2 Bradley, L.P.
Evanescent field coupling between a single mode
optical fibre and a thin film waveguide
University of Glasgow, thesis 7502

Dg Digonnet, M.J.F., Shaw, H.J.
Analysis of a tunable single mode optical fibre coupler
IEEE, J. Quant. Electr., QE-6, 4, 1982, p.746

Dy Dyott, R.B., Schrank, P.F.
Self-locating elliptically core fibre with
an accessible guiding region
Electr. Lett. 18, 22, 1982, p.981

Fm Felsen, B.L., Marcuvitz,N.
Radiation and scattering of waves
Prentice Hall Inc., Englewood Cliffs, New Jersey

Ft Feit, M.D., Fleck, J.A.
Mode properties and dispersion for two optical fibre index
profiles by the propagating beam method
Appl. Optics, 19, 18, 1980, p.3140

Gl Gloge, D.,
Weakly guiding fibers
Appl. Opt. 10, 1971, p.2252

Hd Hardy, A., Streifer, W.
Coupled mode theory of parallel waveguides
J. Lightwave Techn., LT-3, 5, 1985, p.1135

Hm Hammer, J.M., Channin, D.J., Duffy, M.T.
Fast electro-optic waveguide deflector modulator
Appl. Phys. Lett., 23, 1973, p.176

Hn Handerek,V.A., Dyott, R.B.
Fused D-fibre couplers
SPIE, 574, 1985, p.115

Hr Harrey, A.F.
Microwave engineering
Academic Press London, 1963

Hs Hsu, H.S., Milton A.F.
Single mode optical fibre pick-off coupler
Appl. Opt., 15, 10, 1976, p.2310

Jh Johnson, C.C.,
Fields and wave electrodynamics
McGraw Hill, New York, 1965

Jm James, J.R., Gallet, I.N.L.
Point-matched solutions for propagation modes on
arbitrarily-shaped dielectric rods
Radio Electr. Eng., 42, 3, 1972

Jo Jones, D.S.
Acoustic and electromagnetic waves
Clarendon Press Oxford, 1980

K Kao, C.K.
Fiber Optics. Optical fiber communication technology
Electr. Comm. (GB), 54, 3, 1979, p.245

Km Komatsu, K., Kondo, M., Ohta, Y.,
Titanium/Magnesium double diffusion method for
efficient fibre lithium niobate waveguide coupling
IGWO, PDP-2, Atlanta, 1986, p.11

Kr Kreizig sect. 9.7 Mf or Fm
Advanced engineering mathematics
John Wiley & Sons, New York

Ln Linke, R.A., Kasper, B.L., et al.
Coherent lightwave transmission over 150 km fibre lengths at
400 Mb/s and 1 Gb/s data rates using DPSK modulation
IOOC-ECOC, Venice, 1985, p.35

Ls Louisell, W.H.
Coupled mode and parametric electronics
Wiley, New-York, 1960

Mb Mabaya, N., Lagasse, P.E., Vandenbulke, P.
Finite elements analysis of optical waveguides
IEEE Trans. Microwave Theory Techn., MTT-29, 1981, p.600

Md Midwinter, J.E.
Evanescent field coupling into a thin-film vaweguide
IEEE J. Quant. Electr., QE-6, 1970, p.583

Mf Morse, P.M., Fesbach, H.
Methods of theoretical physics
McGraw Hill book company, Inc. 1953

Mi Miller, S.E.

Bell Syst. Techn. J. 48, 1969, p. 2059

Ml Millar, C.A., Ainslie, B.J., et al.
Fabrication and characterisation of D-fibres with a range
of accurate controlled core/flat distances
Electr. Lett. 22, 6, p.322

Ml2 Millar, C.A.
Direct method of determining equivalent
step index profiles for monomodes fibres
Electr. Lett. 17, 13, 1981, p.458

Ml3 Millar, C.A.
Evanescent field coupling of thin film
and fibre optical waveguides
University of Glasgow, thesis 4512

Mp Murphy, E.J., Rice, T.C.
Low loss coupling of multiple fibre of multiple fibre arrays
to single mode waveguides
J. Lightwave Techn. LT-1, 3, 1983, p.479

Mr Marcuse, D.
The coupling of degenate modes in two dielectrical waveguides
Bell Syst. Techn. J., 50, 6, 1971, p.1791

Mw Mathews, J., Walker, R.L.
Mathematical methods of physics
W.A. Benjamin, Inc., New York 1970

My Miya, T., Terunama, Y., et al.
Ultimate low loss single mode fibre at 1.55μm
Electr. Lett. 15, 1979, p.106

Nk Nakamura, M., et al.
Laser oscillation in epitaxial GaAs waveguides
with corregation feedback
Appl. Phys. Lett., 23, 1973, p.224

Nt Nutt, A.C.G., Bristow, J.P.G., et al.
Fibre to waveguide coupling using Ion Milled grooves in lithium
niobate at 1.3 μm wavelength
Opt. Lett., 9, 10, 1984, p.463

Ny Nayar B.K., Smith, D.R.
Optical directional coupler using polarization maintaining monomode fibre
Opt. Lett. 8, 10, 1983, p.543

Ok Okoshi, T., Okamoto, K.
Analysis of wave propagation in inhomogeneous optical fibre using a variational method
IEEE, Trans. Microwave Theory Techn. MTT-22, 11, 1974, p.938

Os Ostrowsky, D.B., Poirier, et al.
Integrated optical photodetector
Appl. Phys. Lett., 22, 1973, p.463

Pp Papuchon, M., et al.
Electrically switched optical directional coupler: Cobra
Appl. Phys. Lett. 27, 5, 1975, p.289

Pr Parriaux, O., Gidon, S., Kuznetsov, A.
Distributed coupling on polished single mode optical fibres
Appl. Optics 20, 14, 1981, p.2420

Ps Press, W.H.
Numerical recipes: the art of scientific computation

Rh Rahman, B.M.A., Davies, J.D.
Penalty function improvement of waveguide solution by finite elements
IEEE Trans. Microwave Theory Techn., MTT-32, 1984

Sb Shubert, R., Harris, J.H.
IEEE Appl. Phys. Lett., 14, 1969, p. 291

Sc Schoener, G., et al.
Novel method for making single mode optical fibre directional couplers
Electr. Lett., 18, 13, 1982, p.566

Sf Schiffner, G., Schneider, H., Schoener, G.
Double-core single mode optical fibre as directional coupler
Appl. Phys. 23, 1980, p.41

Sg Seligson, J.
Prism couplers in guided wave optics
Appl. Opt. 26, 13, 1987, p.2609

Sh Sheem, S.K., Giallorenzi
Single mode fiber optical power divider: encapsulated technique
Opt. Lett. 4, 1979, p.29

Sl Snyder, A.W., Love, J.
Optical vaweguide theory
Chapman and Hall, London, New York

Sm Saad M.S.
Review of numerical methods for the analysis of arbitrarily-shaped microwave and optical waveguides
IEEE Trans. Microwave Theory Techn., MTT-33, 10, 1985, p.894

Sn Snyder, A.W.
Asymptotic expressions for eigenfunctions and eigenvalues of a dielectric or optical waveguides
IEEE, Trans. Microwaves Theory Techn. MTT-17, 1969, p.1130

Sn2 Snyder, A.W.
Coupled-mode theory for optical fibers
J. Opt. Soc. Am., 62, 11, 1972, p.1267

St Snitzer, E.,
Cylindrical dielectric waveguide modes
J. Opt. Soc. Am., 51, 1961, p.491

Sv Silvester, P.P., Lowther, C.J., et al.
Exterior finite elements for 2-dimensional field problems, with open boundaries
Proc. Inst. Electr. Eng., 124, 12, 1977, p.1267

Tm Tamir, T
Integrated optics
Springer Verlag 1979

Tn Tien, P.K., Ulrich, R., Martin, R.J.
Modes of propagating light waves in thin deposited semiconductor
Appl. Phys. Lett., 14, 1969, p.291

Ty Taylor, H.F., Yariv, A.
Guided wave optics
Proc. IEEE, 62, 1974, p.1044

Ul Ulrich, R., Tien, P.K.
Modes of propagating waves in thin deposited semiconductor film
Appl. Phys. Lett., 14, 1969, p.291

Ul2 Ulrich, R.
Optimum excitation of optical surface waves
J. Opt. Soc. Am., 60, 1971, p.1337

Ul3 Ulrich, R., Torge, R.
Measurement of thin film parameters with a prism coupler
Appl. Opt., 12, 12, 1973, p.2901

Vc Vanclooster, P., Phariseau, D.
The coupling of two parallel dielectrics fibers, part I and II
Physica, 47, 1970, p.485

Yh Yeh, C., Ha, K., et al.
Single-mode optical waveguide
Appl. Opt., 18, 10, 1979, p.1490

Yr Yariv, A.
Coupled mode theory for guided-wave optics
IEEE, J. Quant. Electron. QE-9, 1973, p.919

Zh Zhang, M., Garmire, E.
Single mode fiber-film directional coupler
J. Lightwave Techn. LT-5, 2, 1987, p.260